Functional characterization of novel mycobacterial zinc metalloprotease *MSMEG3019* and its role in bacterial physiology

Kiara Ramchunder

Submitted in fulfillment of the requirements for the degree of Master of Medical Science in Medical Microbiology in the School of Laboratory Medicine and Medical Sciences, University of KwaZulu-Natal

February 2025

Declaration

I, Ms. Kiara Ramchunder, declare as follows:

1. That the work described in this dissertation has not been submitted to UKZN or other tertiary institution for purposes of obtaining an academic qualification, whether by myself or any other party.
2. That my contribution to the project was as follows:
   Conduct research to obtain a good understanding of the topic, perform all experiments/assays and analyze all the data and results produced by the project.
3. That the contributions of others to the project were as follows:
   My supervisor, Dr. S. Senzani provided guidance, knowledge and assisted with interpretation of results.
   The services of the Microscopy and Microanalysis Unit (MMU) were used to acquire Scanning Electron Microscopy images of the samples used in this project.
4. Signed ___[redacted]_____ Date 30/03/2025
5. Supervisor: _ [redacted] _____ Date 30/03/2025

Dedication

I dedicate this work to my parents, Mr. Niran Ramchunder and Mrs. Mala Ramchunder, and my little brother Nikhiel Ramchunder, for their endless support, motivation, care and love.

I owe everything to them.

Presentations from this research project:

Conference:	College of Health Sciences (CHS) Symposium
Presentation:	Oral
Title:	Characterizing *Mycobacterium tuberculosis* zinc metalloprotease Rv2017 as a novel target for drug discovery
Authors:	Miss. K. Ramchunder, Dr. S. Senzani
Date:	2023
Venue:	South Africa, Durban, UKZN Medical School, K-Rith

Conference:	8th SA TB conference
Presentation:	Poster
Title:	Characterizing Rv2017, an essential *Mycobacterium tuberculosis* zinc metalloprotease, as a potential novel drug target
Authors:	Miss. K. Ramchunder, Dr. S. Senzani
Date:	2024
Venue:	South Africa, Durban, ICC

Conference:	South African Society for Biochemistry and Molecular Biology (SASBMB)
Presentation:	Poster
Title:	Characterizing Rv2017, an essential *Mycobacterium tuberculosis* zinc metalloprotease, as a potential novel drug target
Authors:	Miss. K. Ramchunder, Dr. S. Senzani
Date:	2024
Venue:	South Africa, Limpopo, Polokwane, Protea Ranch Resort

Acknowledgements

I would like to thank my family and friends (shout out to my best friend Shianne) for all of their words of encouragement and support throughout this degree.

I would like to express my gratitude to the National Research Foundation (NRF) for funding this degree.

Thank you to my supervisor, Dr. S. Senzani, not only for the guidance, knowledge and around-the-clock assistance, but also for pushing me to grow as an individual.

Thank you to all the staff and students in the Department of Medical Microbiology for the inspiration, support and comradery.

To all my fellow students who see me cry at campus, thank you for not telling anyone about it.

Thank you to the MMU at UKZN Westville for providing me with imaging of my samples.

Table of contents

List of figures

List of tables

Nomenclature

+6p:	*MSMEG3016* promoter
+p:	*MSMEG3019* promoter
Δ:	Delta
µ:	Micro
µF:	Microfarad
Ω:	Ohm
× g:	Relative centrifugal force
AG:	Arabinogalactan
Amp:	Ampicillin
Amp^R:	Ampicillin resistance
bp:	Base pair
BSL3:	Biosafety Laboratory 3
Ca^{2+}:	Calcium cation
$CaCl_2$:	Calcium chloride
Co^{2+}:	Cobalt cation
CSPD:	Chloro-5-substituted adamantyl-1, 2-dioxetane phosphate
CTAB:	Cetyltrimethylammonium bromide
DC:	Dendritic cells
dH_2O:	Distilled water
DIG:	Digoxigenin
DMSO:	Dimethyl sulfoxide
DNA:	Deoxyribonucleic acid
dNTPs:	deoxynucleotide triphosphates
EDTA:	Ethylenediaminetetraacetic acid disodium salt dihydrate
Erp:	Exported repetitive protein
FAS:	Fatty acid synthase
FBP:	Fibronectin binding protein
FCO:	First Cross Over
g:	Grams
gDNA:	Genomic DNA
GI:	Gastrointestinal
GPL:	Glycopeptidolipids

h:	Hour
HCl:	Hydrochloric acid
HEXXH:	His-Glu-Xaa-Xaa-His
HIV:	Human immunodeficiency virus
Hyg:	Hygromycin
Hyg^R:	Hygromycin resistance
Kan:	Kanamycin
Kan^R:	Kanamycin resistance
kb:	Kilobyte
L:	Liters
LA:	Luria-Bertani Agar
LAM:	Lipoarabinomannan
LB:	Luria-Bertani broth
LF:	Lethal factor
LTBI:	Latent tuberculosis infection
NA:	Nutrient agar
NaCl:	Sodium chloride
NaOH:	Sodium hydroxide
NB:	Nutrient broth
NK:	Natural killer cells
n:	Nano
nm:	Nanometers
NOD1:	Nucleotide-binding oligomerization domain
m:	Meter
M:	Molar
mA:	Milliampere
MA:	Mycolic acid
mAGP:	mycolyl-arabinogalactan-peptidoglycan complex
MDR:	Multidrug-resistant
mg:	Milligrams
MIC:	Minimum inhibitory concentration
mJ:	Millijoule
Min:	Minutes
mL:	Milliliters

Mn^{2+}:	Manganese cation
Mtb:	*Mycobacterium tuberculosis*
OD_{600nm}:	Optical density at 600 nanometer wavelength
OH^-:	Hydroxide ion
OMP:	Outer membrane protein
PBS:	Phosphate Buffered Saline
PCR:	Polymerase Chain Reaction
PE:	Pro-Glu
PEPPI:	Pipeline for the Extraction of Predicted Protein-protein Interactions
PG:	Peptidoglycan
PMN:	Polymorphonuclear neutrophils
PPE:	Pro-Pro-Glu
ROS:	Reactive oxygen species
RPM:	Revolutions per minute
RT:	Room temperature
SCO:	Second Cross over
SDS:	Sodium dodecyl sulfate
Sec:	Seconds
SEM:	Scanning Electron Microscopy
SSC:	Saline-sodium citrate
T7SS:	Type VII secretion systems
TB:	Tuberculosis
TBE:	Tris-Borate-EDTA
TDM:	Trehalose dimycolates
tPA:	Tissue plasminogen activator
UV:	Ultraviolet
V:	Volts
v/v:	Volume per volume percentage
WHO:	World Health Organization
XDR:	Extensive drug resistance
X-Gal:	5-bromo-4-chloro-3-indolyl-β-D-galactopyranoside
Zmp1:	Zinc metalloprotease 1
Zn^{2+}:	Zinc cation

Abstract

Tuberculosis (TB), the infectious disease caused by the pathogenic bacteria *Mycobacterium tuberculosis* (*Mtb*), remains amongst the ten leading causes of death worldwide. Although TB is preventable and curable, approximately 10 million people are diagnosed with TB and 1.5 million TB fatalities are reported annually globally. Complete eradication of TB remains a challenge due to its ability to establish a latent infection and its highly effective virulence mechanisms which facilitates manipulation and colonization of the host, as well as cause subsequent suppression and evasion of the host's immune system. Furthermore, current TB treatment strategies face numerous limitations, such as socio-economic barriers and the emergence of drug resistant TB strains. The pathogenic success of *Mtb* can be attributed to its stellar virulence factors, one of which are zinc metalloproteases, which are proteases that catalyze the hydrolysis of proteins into peptides by the use of an indispensable zinc ion. In mycobacteria, zinc metalloproteases play essential roles in the intracellular survival of *Mtb* in host macrophages. Therefore, investigating other novel zinc metalloproteases, such as *Rv2568c*, is of significant interest. In this study, the *Rv2568c* ortholog *MSMEG3019* was investigated in *M. smegmatis* mc^2155, which is a model organism for TB research. The characterization of *MSMEG3019* involved the creation of a deletion mutant strain, named MΔ3019, which harbored a non-functional version of *MSMEG3019*. The gene deletion method utilized in this study was the two-step allelic exchange method, this was followed by analysis and comparison of the resultant phenotype, to the wild type and complementation strains. Bioinformatics analyses revealed the presence of zinc metalloprotease and zinc ribbon domains in *MSMEG3019* and *Rv2568c*, in addition to predicting protein-protein interactions with transglutaminase genes directly upstream. Bioinformatics were also utilized to identify proteins with structural homology to the target genes. These homologs were involved in pathogenesis of their respective species, which indicates *Rv2568c's* involvement in *Mtb* virulence. MΔ3019 exhibited a reduced capacity to support the exponential phase of mycobacterial growth. Additionally, MΔ3019 cells displayed increased lengths and decreased widths, when compared to mc^2155. *MSMEG3019* was also discovered to be implicated in mycobacterial translocation, as evidenced by MΔ3019's impaired sliding capability. Furthermore, MΔ3019 presented increased susceptibility to the peptidoglycan-targeting drug, Vancomycin. These phenotypic attributes were correlated to the disruption of peptidoglycan synthesis/regulation as the result of *MSMEG3019* deletion. The observations made in this study suggests that *MSMEG3019* is implicated in peptidoglycan-mediated mycobacterial growth, proliferation and dissemination, which represents *Rv2568c's* contribution to pathogenesis in *Mtb*. The findings of this study demonstrated the importance of zinc metalloproteases to mycobacterial viability and physiology, thereby further corroborating that zinc metalloproteases remain an excellent reservoir of drug targets for TB drug development.

1. Introduction

1.1. Pathogenic bacteria

The majority of bacteria that humans encounter either have a neutral or beneficial effect, however a proportion of bacteria possess the capability to negatively affect human health; these bacteria are termed "pathogens" (Balloux & van Dorp, 2017). Originating from Ancient Greek and being popularized in the 1800s, the word "pathogen" refers to an organism that is capable of causing disease to its host (Cunliffe, 2008).

Throughout centuries the world has experienced many pathogenic bacteria, such as *Staphylococcus aureus*, *Vibrio cholerae* and *Streptococcus pneumoniae* which are responsible for a collective death toll exceeding millions (Doron & Gorbach, 2008). However, no other known bacterium has caused a death toll that is as conspicuous as *Mycobacterium tuberculosis* (*Mtb*), the causative agent of tuberculosis (TB). It has been famously dubbed as "the world's deadliest infectious disease" and "the most successful bacterial pathogen" due to its strikingly high annual TB infectious rates and mortality rates (Agyeman & Ofori-Asenso, 2017; Ilic *et al*., 2023).

1.2. TB: the past and present

TB can be traced back to Egypt, exceeding 5 000 years ago, where skeletal abnormalities and Pott's deformities (which were characteristic of TB infections) were found in Egyptian mummies (Cave & Demonstrator, 1939; Daniel, 2006). Modern testing confirmed the presence of *Mtb* DNA in these mummified remains (Crubézy *et al*., 1998). Similar distinctions were later discovered in Peruvian mummies. In addition, there has been written documentation outlining TB infection in India and China as early as 3 300 and 2 300 years ago respectively (Morse, 1967; Daniel, 2006).

The prevalence of TB escalated to epidemic extents during the 18th century and was initially met with widespread misconception. However, modern understanding of TB's virulence can be attributed primarily to three individuals (Daniel, 2006). Unravelling the pathogenesis of TB first occurred at the beginning of the 19th century by Théophile Laennec, who clearly explained TB pathology and symptoms of pulmonary infection in his 1819 book, "D'Auscultation Mediate" (Daniel, 2004). These findings were further enhanced in 1865 by Jean-Antoine Villemin, who demonstrated the infectious status of *Mtb* using a rabbit model. He inoculated a healthy rabbit with a liquid extract from a tuberculous cavity, which resulted in the rabbit developing TB, thus displaying the contagious nature of the infection (Major, 1945). However, the understanding of TB was profoundly impacted by the work of Robert Koch in 1882, who identified the etiological agent of TB as the tubercle bacillus. His presentation, "Die Aetiologie der Tuberculose" paved the way for current infectious etiology, as he also established the Koch-Henle postulates (Daniel, 1997). In 1993, TB was the first infectious disease to be regarded as "a global health emergency" by the World Health Organization (WHO) (Gygli *et al*., 2017). Unfortunately, it remains a global health emergency until today.

TB ranks one of the top ten causes of death worldwide (Churchyard *et al*., 2017). Despite TB being preventable and curable, every year approximately 10 million people are diagnosed with TB (figure 1.1) and 1.5 million TB fatalities are reported (Furin *et al*., 2019).

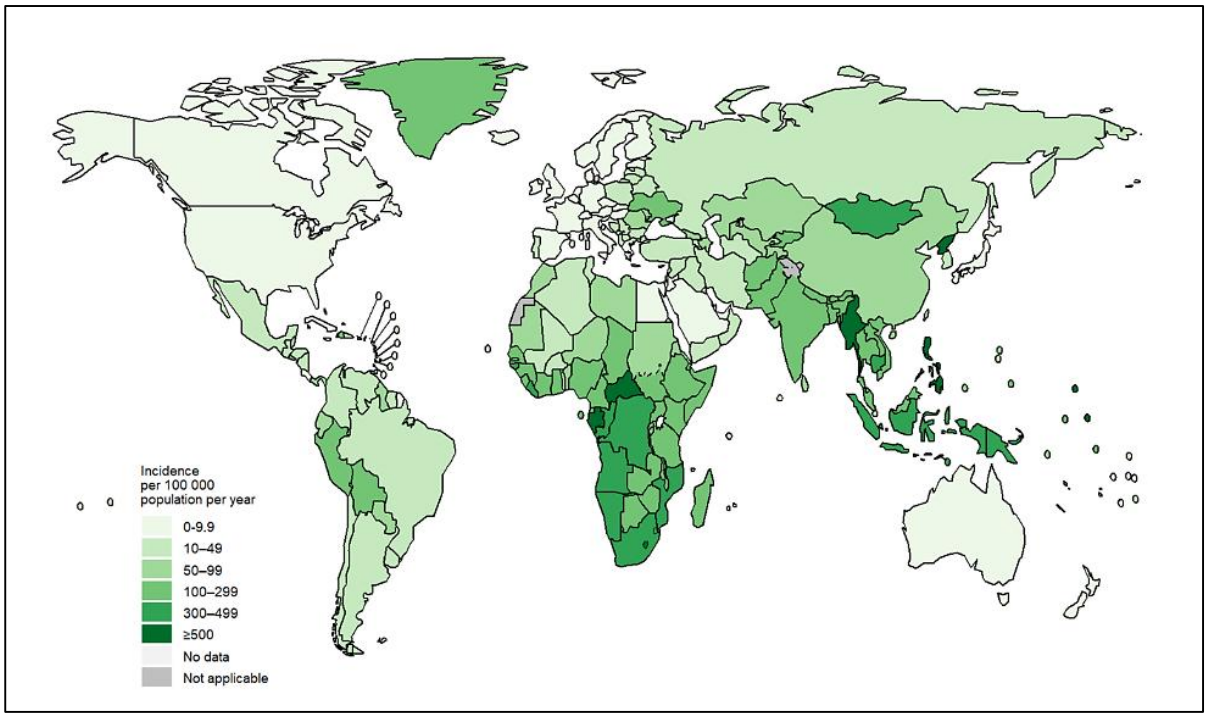

Figure 1.1. Graphical depiction of the estimated global TB incidence rates for 2023. Central Africa and South East Asia are shown to contain the highest burden of TB incidence with exorbitant estimates exceeding 500 new incidents per 100 000 population for 2023. This is closely followed by developing countries in Southern Africa and the south of Asia which amassed estimates of 300-499 (WHO, 2024).

In addition, TB is regarded as the leading cause of death amongst individuals infected with human immunodeficiency virus (HIV) (WHO, 2022). When an individual is co-infected with TB and HIV, each disease speeds up the progression of the other. HIV positive individuals are 18 times more prone to contract active TB (WHO, 2020). The HIV-associated TB cases are highest in the African region where 85% of TB patients were co-infected with HIV (Harding, 2020). This is in keeping with the findings of the Global Tuberculosis Report published by WHO (2024), displayed in figure 1.2, which definitively portrays South Africa and surrounding countries as encompassing the highest prevalence of co-infections.

1.3. TB pathogenesis

1.3.1. Primary infection

TB is transmitted via aerosols which generally originates from the coughing, speaking or sneezing of individuals with active TB (Alzayer & Al Nasser, 2023). Once the aerosols are inhaled, *Mtb* travels through the trachea and into the lungs where it is engulfed by alveolar macrophages (specialized white blood cells that forms part of the immune system) (Master *et al*., 2008).

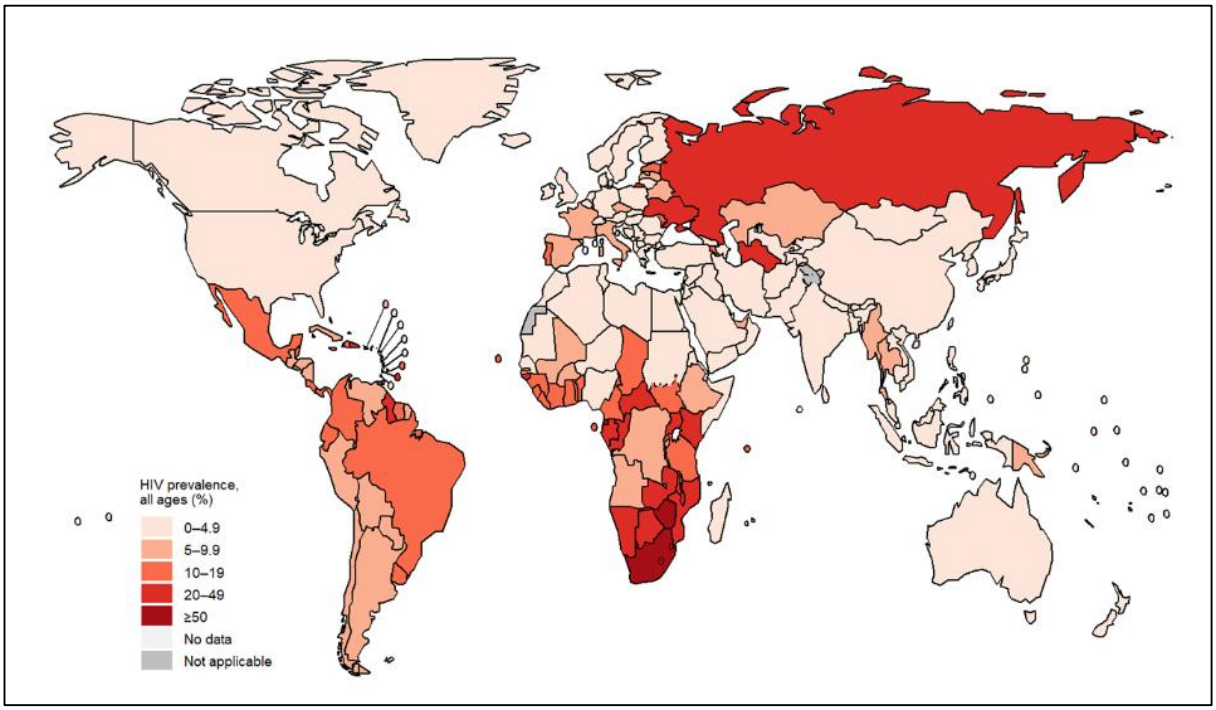

Figure 1.2. Graphical representation of the estimated HIV prevalence with TB co-infections (inclusive of new and relapse TB cases) for 2023. The highest burden of co-infection was seen in developing countries in Southern Africa wherein greater than 50% of the individuals infected with TB were also infected with HIV. The second highest ranking belongs to Northern Asia and Eastern Europe (WHO, 2024).

This process is termed phagocytosis and it results in the formation of a vesicle containing the bacteria (phagosome) (Leseigneur *et al*., 2020). With regard to other pathogenic bacteria, the phagosome fuses with a lysosome in order to enzymatically degrade the pathogen, which is then ejected from the cell as the macrophage matures (Lee *et al*., 2015). However, *Mtb* disrupts this process by inhibiting phagolysosome fusion and preventing the maturation of macrophages which leads to bacterial survival inside the macrophage (Master *et al*., 2008).

In a further attempt to clear *Mtb* and contain it within the infected macrophage to prevent the spread of the infection, the host immune system creates an aggregate of immune cells around the site of infection, called a granuloma (Ehlers & Schaible, 2013). The granuloma consists of multiple strata of dendritic cells (DCs), B and T lymphocytes, natural killer (NK) cells and granulocytes (Chai *et al*., 2018). Majority of healthy individuals possess an innate and adaptive immunity that is capable of clearing *Mtb* within the granuloma, resulting in no symptoms (Chai *et al*., 2018). However, there are two other potential outcomes: active TB or latent TB.

1.3.2. Active TB

Due to *Mtb's* extreme amenability to counteract the host defenses, there is a possibility that the host fails to clear the *Mtb* pathogen in primary infection, causing the patient to develop active TB (Bloom *et al*., 2017). The patient can then present symptoms of TB which include prolonged coughing (sometimes

with blood in the sputum), weakness, chest pain, fatigue, night sweats, fever and weight loss (WHO, 2024). Active TB leads to necrotic damage of the infected macrophages, which releases the intracellularly trapped pathogen, which is now free to disseminate to other sites and infect other host macrophages (Chai *et al*., 2018). Unlike most pathogenic bacteria, the main purpose of *Mtb* is to survive *in vivo*, as opposed to directly attacking the host (Alzayer & Al Nasser, 2023). *Mtb* uses the elicited inflammatory host responses against the host; the multiple sites of infected granulomas lead to extensive tissue damage to the lungs, which is the ultimate cause of death in individuals infected with TB (Smith, 2003).

Although TB predominantly targets the lungs (pulmonary TB), it has the potential to spread to other areas of the body (Alzayer & Al Nasser, 2023). *Mtb* has the ability to disseminate to multiple organs due to its aptitude to adhere and colonize numerous unorthodox immune cells such as neuronal cells, epithelial cells, fibroblasts, endothelial cells and adipocytes (Randall *et al*., 2015). In this way, TB not only causes pulmonary TB, but it has been identified to cause skeletal TB, pleural TB, gastrointestinal (GI) TB, lymphadenitis TB and ocular TB (Shah & Chida, 2017).

1.3.3. Latent TB

If the host is unable to eliminate *Mtb* within the granuloma during the primary infection and provided active TB does not develop, *Mtb* enters a metabolically quiescent state with low activity inside the granuloma, termed latency (Chai *et al*., 2018; Maphasa *et al*., 2021). A quarter of the world's population is estimated to have Latent Tuberculosis Infection (LTBI), which presents as the absence of any clinical signs, symptoms or radiologic detections and only exists as immunoreactivity to TB antigens (WHO, 2020; Maphasa *et al*., 2021). *Mtb* is able to survive inside host macrophages in this persistent state for years and sometimes the entirety of the patient's lifespan. Its survival has been linked to its ability to resist the onslaught of host immune responses coupled with its capability to adapt to host-induced stress conditions (such as hypoxia, low pH and nutrient unavailability) (Deb *et al*., 2009). In order to adapt to the environment and ensure survival, *Mtb* has to modify its gene expression systems, develop alternative mechanisms to scavenge for nutrients and alter its metabolic pathways (Magombedze *et al*., 2013). During latency, *Mtb* utilizes lipids and fatty acids as the substituted source of nutrients and carbon respectively (Ehrt & Schnappinger, 2007).

Unfortunately, in approximately 10% of the cases, latent *Mtb* can be triggered at any point in an individual's life (most commonly by a compromised immunity) and reactivate to an infectious state, where it becomes transmissible (Magombedze *et al*., 2013; Bloom *et al*., 2017). Every year, a significant portion of newly reported active TB cases can be attributed to the reactivation of LTBI. Therefore, it can be discerned that the diagnosis and treatment of LTBI can ease the burden of active TB (Comstock *et al*., 1979). The highest chance of LTBI reactivation occurs within two to three years after primary infection. Added preventative therapy (daily treatment with Isoniazid for 6-9 months) may help

decrease the risk of reactivation in immuno-comprised individuals who may fail to keep the infection contained (Smieja *et al*., 1996). Plans for detection and granting patients the opportunity for preventative therapies are currently lacking in most areas around the world and are urgently required (Magombedze *et al*., 2013).

Despite the advancements in *Mtb* research, very little understanding of LTBI has been gained. Current attempts at prevention, detection and treatment of LTBI are proving to be inadequate, as seen by the ever expanding amount of TB reactivation cases. The development of diagnostic tools and effective therapies have also been severely restricted due to the marginal comprehension of latency in *Mtb* and the factors that favor it (Magombedze *et al*., 2013). Therefore, Latency is considered to be the barricade to total elimination of global TB (Behr *et al*., 2021).

1.4. Shortcomings of current TB treatment

1.4.1. TB treatment regimen

Patients who are infected with drug-susceptible TB are required to take a standard course of 4 first-line antibiotics for six months: Isoniazid, Ethambutol, Rifampicin and Pyrazinamide (Dorman *et al*., 2021). This long treatment regimen requires strict compliance to be fully effective. However, a large proportion of patients discontinue the treatment after just a few months. This could be due to insufficient information being circulated regarding the importance of antibiotic completion (Fiol *et al*., 2010). This could also be due to some side effects which occur occasionally, such as skin rashes, nausea and vomiting (Yee *et al*., 2003). In addition, Isoniazid and Ethambutol administration has been associated with peripheral neuropathy and optic neuropathy respectively, causing irreversible loss of vision (Schaberg *et al*., 2017).

1.4.2. Emergence of drug-resistant TB strains

Due to the adverse side effects, TB treatment has struggled with patient non-compliance resulting in treatment failure (Schaberg *et al*., 2017). This inconsistent conformity has resulted in the development of strains that are resistant to one or more anti-TB drugs and is then spread via community and nosocomial transmission (Seung *et al*., 2015). Drug resistance TB poses an enormous complication in the fight to combat TB (Falzon *et al*., 2011).

The escalation of drug resistant strains has caused current treatments to fail, leaving only second-line and third-line therapies as the alternative (Dartois & Rubin, 2022). Multidrug-resistant (MDR) TB is defined as *Mtb* strains that do not respond to Isoniazid and Rifampicin and require second-line drugs (Harding, 2020; WHO, 2020). The chance of developing MDR TB is approximately 3.8% in developed countries, unfortunately this risk rapidly rises in countries with a high TB burden, such as China and India, wherein it escalates to approximately 20% (Zhao *et al*., 2012). Extensive drug resistance (XDR) TB entails an MDR strain with an additional resistance to fluoroquinolones and injectable second-line medications (Roelens *et al*., 2021). Although there are various second-line drugs for the treatment of

MDR and XDR, the cure rate is much lower than that of drug-susceptible TB (Falzon *et al*., 2011). Treatment success rates of MDR and XDR variants are alarmingly low, with only 54% and 30% respectively (as opposed to the 83% success rate of drug-susceptible TB treatment) (Gygli *et al*., 2017; Seid *et al*., 2018).

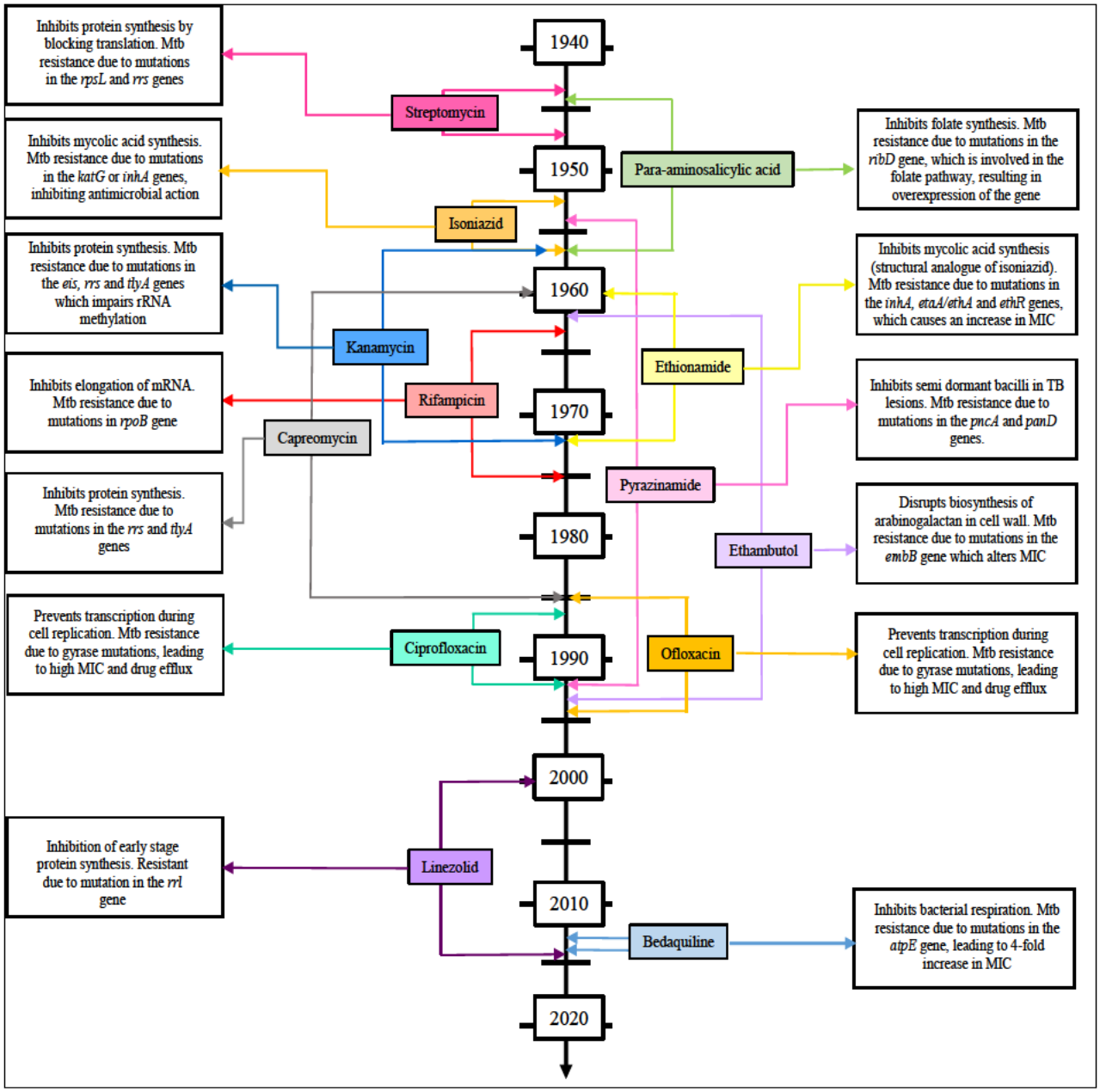

Figure 1.3. Timeline of anti-TB drugs, their mode of action and duration of effectiveness until *Mtb* developed resistance and rendered them ineffective (Illustration conceptualized using information acquired from: Chakraborty & Rhee, 2015; Dookie *et al*., 2018).

This widespread rapid development of drug-resistant TB coupled with the continued failure to create universally efficacious vaccines have emphasized the dire need for new effective therapies (Kieswetter *et al*., 2021). The last few decades have witnessed numerous attempts at creating new antibiotics to aid in the fight against TB. However, drug non-compliance combined with the stellar molecular mechanisms of *Mtb* has always been a cumbersome obstacle that eventually triumphs, leading to drug resistance.

Figure 1.3 showcases the numerous attempts at fixing the global TB burden as well as the extremely fast declination of the drugs after being brought to the market. A contributing factor to drug failure is the use of the same family of compounds to develop different antibiotics. This typically provides similar antimicrobial activity, and therefore decreases its usefulness (Plotniece *et al*., 2023). For example, as seen in figure 1.3, the drugs Isoniazid and Ethionamide are structural analogs which both target mycolic acid synthesis in *Mtb*, which is conferred by the *inhA* gene (Dookie *et al*., 2018). However, mutations to the *inhA* gene causes structural changes to the target of Isoniazid, leading to resistance of the drug. Since Ethionamide targets the *inhA* gene with a similar mode of action, it is also consequently deemed ineffective as treatment, due to the acquired *Mtb* resistance (Tseng *et al*., 2015).

Conversely, creating a variety of antimicrobial compounds may not necessarily progress TB treatment if all the compounds have the same cellular target. Targeting the same cellular processes with many different drugs would render all of them inadequate if the bacterium evolves in a manner that overcomes their mode of action. However, ascertaining new drug targets provides more insight into bacterial physiology. Identifying unique bacterial cellular processes drives drug discovery towards the expansion of targeted therapies with selective toxicity and possibly higher efficacy. Therefore, there is an urgent need, not only for antimicrobial compounds, but also for new drug targets in order to create efficient and sustainable treatment strategies (Plotniece *et al*., 2023).

1.4.3. Socio-economic aspect of eradicating TB

TB is regarded as a socioeconomic problem that is commonly associated with the conditions of developing countries (Houben & Dodd, 2016). Many individuals worldwide have limited access to proper health care facilities and reside in overcrowded areas (Alzayer & Al Nasser, 2023). These conditions stimulate the spread of infectious diseases. There are a total of 197 countries worldwide, of which 152 are developing countries (85.22% of the world's population) (Countries of the world, 2022). The above-mentioned statistics emphasizes the prevalence of TB infections in low-income countries which is substantiated by figure 1.4. Additionally, in South Africa, TB has claimed the title of "leading cause of death" for 3 consecutive years, from 2016 to 2018 (Stats SA, 2021). However, TB is not specific to developing countries; it is globally present (Alzayer & Al Nasser, 2023).

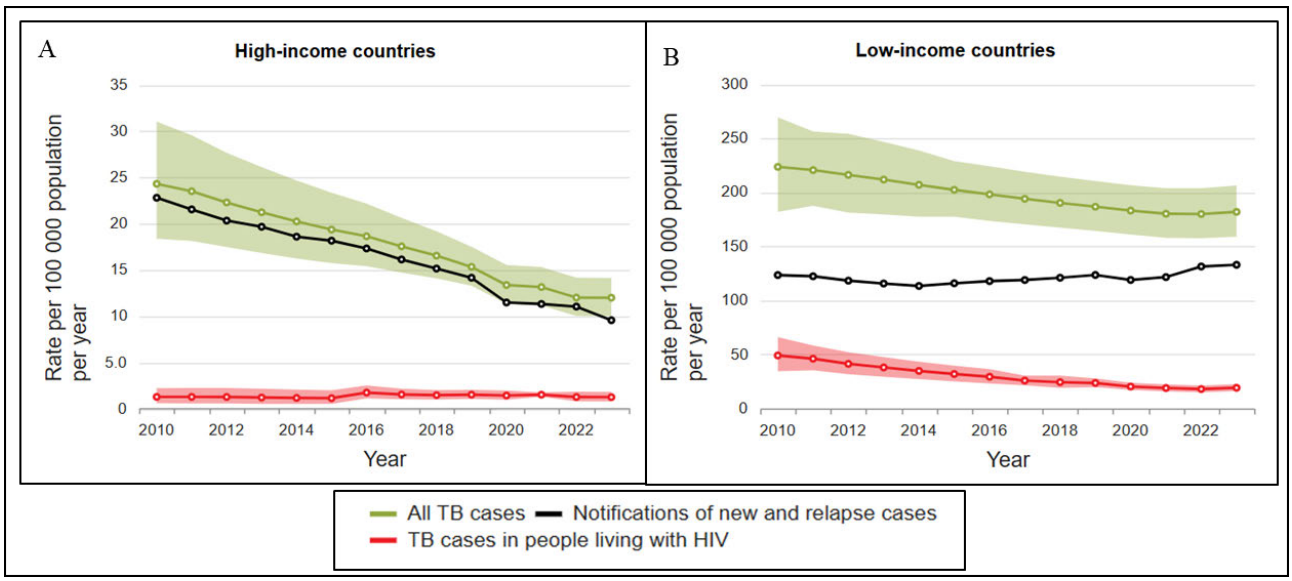

Figure 1.4. (A) and **(B)** depict the trend of estimated TB incidence rates from 2012 to mid-2023 per income group, as an indicator of the role played by socio-economic status on the prevalence of TB. **(A)** High income countries show a steady decrease in the number of all TB cases over the years, along with a constant low rate of TB-HIV co-infection cases, whilst **(B)** low income countries experienced only a minimal decrease in the rate of TB and TB and HIV co-infections. In addition, low income countries experienced a slight increase in the rate of new and relapse TB cases (WHO, 2024).

Drug-resistant *Mtb* strains are more of a burden to low-income countries due to treatment requiring second-line drugs, which are more expensive and less effective. Additionally, sophisticated infrastructure for drug susceptibility testing is not readily available in these resource-limited settings. (Gygli *et al*., 2017; WHO, 2020).

1.4.4. *M. tuberculosis*: the well adapted pathogen

Mtb does not naturally exist in the environment, nor does it naturally infect animals, therefore rendering it an obligate human pathogen. Generally, obligate pathogens are exceedingly well adapted to their hosts due to the molecules and intricate processes that they implement to synchronize their life cycle with their host's behavior, metabolism and immune system, resulting in it being extremely difficult to eradicate (Guinn & Rubin, 2017).

Mtb is able to prevent the macrophagic-clearance of pathogens by obstructing the maturation of phagosomes and the acidification of phagolysosomes, this either leads to latency or progression of infection (Zhai *et al*., 2019). In addition, *Mtb* utilizes the host's immune response against the host, which exacerbates the progression of the infection.

Mtb also inhibits apoptosis and autophagy of immune cells, which permits progression of bacterial replication, infection and tissue damage (Oddo *et al*., 1998). The formation of granulomas also unintentionally provides shelter to *Mtb*, enabling it to survive in a state with low metabolic activity and resume full biological activity under favorable conditions (Ehlers & Schaible, 2013). The reactivation

of *Mtb* infection emphasizes the limitations of the human immune system in overcoming the complexity of *Mtb* (Bloom *et al*., 2017).

Complicated pathogens require clear and concise comprehension of their virulence in order to provide insight on their eradication. Characterizing established virulence factors and identifying new ones could aid in the understanding of *Mtb* pathogenesis and its interactions with the host. This, in turn, brings upon opportunity for the discovery of new drug targets, biomarkers and consequently the development of new drugs, vaccines and diagnostics (Koul *et al*., 2011).

1.5. M. tuberculosis (Mtb)

Mtb is an intracellular pathogen belonging to the phylum Actinobacteria and to the family of Mycobacteriaceae. *Mtb* is an aerobic, slow growing, chemo-organotrophic, non-spore forming and non-motile rod-shaped bacillus (Gordon & Parish, 2018). However, its Gram status, relative to other bacteria, is controversial; *Mtb* has characteristics of both Gram-positive and Gram-negative bacteria (Fu & Fu-Liu, 2002). The bacterium's cell membrane is enclosed by a layer of peptidoglycan (PG) that is nearly as thick as all Gram-positive bacteria. As per figure 1.5, it can be seen that this PG layer is linked to arabinogalactan (AG), which is thereafter linked to the mycolic acids (MA) which comprise the outer membrane of the cell (characteristic of gram negative bacteria) (Maitra *et al*., 2019). In addition, this bacterium also possesses a capsule which surrounds the outer membrane (Alzayer & Al Nasser, 2023).

1.5.1. The mycobacterial cell envelope

It is widely accepted that the convolutions of the mycobacterial cell envelope is one of the principle contributing factors to its prosperous intracellular survival (Kalscheuer *et al*., 2019). The mycolyl-arabinogalactan-peptidoglycan complex is termed the mAGP complex and serves as an essential factor in mycobacterial viability and virulence (Rajni *et al*., 2011). This complex cell envelope contributes to antibiotic impermeability, provides resistance to desiccation, enables evasion of host immune responses and consists of several immunomodulatory molecules (Rajni *et al*., 2011).

1.5.1.1. Peptidoglycan (PG)

The basal layer of the mAGP complex, PG, is comprised of alternating N-acetylglucosamine (GlcNAc) linked to modified N-acetylmuramic acid (MurNAc) residues in a β (1→4) configuration (Lederer *et al*., 1975). Neighboring glycan strands in the PG are joined by short peptide stems with the sequence L-alanyl-γ-D-isoglutamyl-*meso*-diaminopimelate-D-alanyl-D-alanine that are linked to MurNAc via the D-lactoyl residue (Maitra *et al*., 2019). The muric acid residues possess an assortment of N-glycolyl and N-acetyl derivatives which have been oxidized to form MurNGly (Raymond *et al*., 2005). It has been theorized that these glycolyl-modifications contribute to hydrogen bonding which inhibits the lysosome-induced degradation of *Mtb* as well as increases the strength of the mesh-like PG structure (Chatterjee *et al*., 1991; Brennan & Nikaido, 1995). It has also been associated with an increase in the

resistance against β-lactam antibiotics and lastly, it has been implicated in the immunogenicity of *Mtb* and therefore plays a role in inducing the overall host immune response (Raymond *et al*., 2005; Schenk *et al*., 2016). The dynamic, thick and complex architecture of the PG layer can be attributed to the cross-linking of greater than 80% of its peptides, which confers physical protection to the bacilli (Catalão *et al*., 2019; Maitra *et al*., 2019).

The mycobacterial PG layer has been deemed necessary for *Mtb* survival and pathogenesis (Maitra *et al*., 2019). Muropeptides derived from the PG of *Mtb* and released by the action of resuscitation promoting factors (*rpf*) genes, have been annotated as virulence factors due to their involvement in the antibiotic tolerance of vancomycin and β-lactam drugs (Wivagg & Hung, 2012). These muropeptides also have roles in altering the permeability of the outer member (Kana *et al*., 2010). Additionally, PG fragments play roles in inter-bacterial communication and signaling, as witnessed by the function of these muropeptides as messengers to signal the resuscitation of *Mtb* from its metabolically quiescent state (Humann & Lenz, 2009; Nikitushkin *et al*., 2013). Furthermore, mycobacterial PG pentapeptide chains undergo continuous modification (either by glycylation, methylation or amidation) to facilitate cell growth, incorporation of extracellular structures as well as allow the cells to resist the effects of PG hydrolases (Mahapatra *et al*., 2005).

1.5.1.2. Arabinogalactan (AG)

Approximately 10% to 12% of the muric acid residues in PG are covalently linked to the heteropolysaccharide AG (Amar & Vilkas, 1973; Wu *et al*., 2017). The AG layer accounts for approximately 35% of the cell envelope and is composed of arabinose, galactose and a linker unit (responsible for linkage between PG and AG) (Kanetsuna *et al*., 1969). The basic structure of AG has been discovered to exist as a linear 30 alternating β-(1→5)-linked and β-(1→6)-linked D-galactofuranose residues (galactan), to which chains of arabinan (each containing 31 D-arabinofuranose residues) are connected (Bhamidi *et al*., 2011). The hydrophobicity and shape of the cell membrane is heavily influenced by the length of the AG polysaccharides (Justen *et al*., 2020). Additionally, AG is the intermediate that anchors the MA to the PG layer, therefore contributing to the robustness and success of the cell wall as a contributor of bacterial viability (Hett & Rubin, 2008; Li *et al*., 2022).

1.5.1.3. Mycolic acid (MA)

Long chain α-alkyl β-hydroxy fatty acids, MAs, are covalently attached to the AG layer but are also present at other locations in the form of multiple sub-families: the MAs could also be esterified to trehalose and glycerol, giving rise to molecules such as trehalose dimycolates (TDM) (Forrellad *et al*., 2013). MAs are strongly hydrophobic, in this way, the MA layer of the cell envelope provides a protective shell that shields the bacilli from hydrophilic compounds, antibiotics and oxidative damage (Singh *et al*., 2017).

Mycobacteria facilitate the production of these fatty acids via the fatty acid synthase (FAS) system, after which they are transported to their final destination (out of the cell) by use of transport systems such as the *mymA* operon (Forrellad *et al*., 2013). The *kasB* gene encodes one of the β-keto acyl synthetases of the FAS II system and is implicated in the production and elongation of MAs. Deletion of this conditional non-essential *KasB* gene resulted in a change of colony morphology, the loss of acid-fast staining, decreased fatty acid chain length and disrupted TDM function (Bhatt *et al*., 2007). However, the most astounding observation of this deletion was the ability of the mutant mycobacteria to persist in immuno-competent mice for 600 days without causing infection. This not only infers the role of *KasB* in pathogenesis, but also implicates its potential to serve as a model in the study of mycobacterial latency due to its inability to cause a chronic persistent infection (Bhatt *et al*., 2007).

KasA, the essential *Mtb* gene that is part of the FAS II system, catalyzes the 2-carbon elongation of growing fatty acyl chains, a function which is imperative to the synthesis of MAs, ergo the bacterial cell wall (Bhatt *et al*., 2007; DeJesus *et al*., 2017). Its contribution to the composition and integrity of the cell wall highlights the physical protection it confers. Due to MAs providing key elements of mycobacterial survival, it is viewed as an attractive opportunity for treatment therapies and became the target of several drugs, including the first-line anti-TB drugs Isoniazid and Ethionamide (Quémard *et al*., 1992).

MAs also exist as diffusible factors of pathogenesis, such as TDM, which is also referred to as cord factor, a glycolipid that is plentiful in the mycobacterial cell wall (Hunter *et al*., 2006). Cord factor is responsible for the formation of serpentine cords which dictates the chain-like orientation in which the tubercle bacilli grow (Middlebrook *et al*., 1947). It also inhibits migration of polymorphonuclear neutrophils (PMNs) to the site of infection, enabling the infection to persist. It also contributes to mycobacterial survival inside host phagosomes and prompts the formation of granulomas by stimulating the production of proinflammatory cytokines (Asano *et al*., 1993; Indrigo *et al*., 2002).

1.5.1.4. Cell wall lipids

The cell envelope also contains several proteins, lipids, glycoconjugate lipids and secretion systems which have functions in cell signaling and virulence. The upper segment of the cell wall contains lipids such as Lipoarabinomannan (LAM) which acts as an immunomodulator (Rajni *et al*., 2011). LAM inhibits the proliferation of T-cells and prevents the initiation of transcription for gamma-interferon production which interferes with macrophage activation and antibacterial immunity (Knutson *et al*., 1998). LAM also averts the activity of protein kinase C which is a contributor of macrophage killing (Knutson *et al*., 1998). Additionally, LAM contributes to the arrest of phagosomal maturation either by hindering Ca^{2+} concentration in macrophages or obstructing the trafficking pathway between the phagosome and the trans-Golgi network (each of which are key components for phagosome maturation)

(Vergne *et al*., 2003). Furthermore, LAM also possesses the ability to bind to toll receptors and the surfaces of dendritic cells which affects cell signaling (Brennan, 2003).

1.5.1.5. Cell wall proteins

The mycobacterial cell wall contains upwards of 500 hundred proteins, inclusive of outer membrane proteins (OMPs) (Mawuenyega *et al*., 2005; Forrellad *et al*., 2013). Approximately 144 OMPS have been identified, some of which may be involved in efflux processes and the transport of nutrients and hydrophobic compounds across the membrane (Song *et al*., 2008). The cell-wall-associated surface protein, Exported repetitive protein (Erp), contributes to bacterial virulence due to its implication in bacterial replication whilst in macrophages (Berthet *et al*., 1998). Additionally, the ability of mycobacteria to adhere to the host mucosal surface is conferred by three surface proteins: FbpA, FbpB and FbpC2, which are collectively referred to as the complex of Fibronectin binding protein (FBP) (Wiker & Harboe, 1992). Its effect on the cell surface promotes the virulence of the bacteria by providing it with the basis for entry into the host (Wiker & Harboe, 1992). The FBP complex also possesses mycolyltransferase activity which enables it to catalyze the transfer of mycolates to trehalose which contributes to the creation of TDM (Forrellad *et al*., 2013).

1.5.1.6. Mycobacterial secretion systems

The translocation of proteins, enzymes and toxins across a bacterial cell membrane is considered to be a benefactor of pathogenesis (Ly & Liu, 2020). Secretion of these substances allows the bacteria to acclimatize to changing/unfavorable environments (Ly & Liu, 2020). Mycobacteria transport folded proteins across the inner bacterial membrane using the twin-arginine transporter pathway. Whereas the translocation of unfolded proteins with an N-terminal signal sequence across the cell membrane is on account of the Sec secretion systems (Feltcher *et al*., 2010). *Mtb* contains five of the type VII secretion systems (T7SS) in its plasma membrane, three of which (namely, ESX-1, ESX-3 and ESX-5) are essential to bacterial virulence, whilst ESX-2 does not play a role in pathogenesis and ESX-4 is yet to be characterized (Abdallah *et al*., 2007; Roy *et al*., 2020).

The ESX-5 system was found to be crucial for the secretion of several Pro-Glu (PE)/Pro-Pro-Glu (PPE) family proteins (Wang *et al*., 2020). These PE/PPE proteins, in turn, play roles in virulence, outer membrane localization, the transport of nutrients across the membrane barrier and host-cell interactions (Cole *et al*., 1998; Wang *et al*., 2020). ESX-5 is vital for the secretion of PPE41, EsxN and the integrity of the cell wall (Bottai *et al*., 2012). It also facilitates modification of the cell wall permeability for nutrient uptake, as well as contributes to the spread of infection amongst macrophages (Abdallah *et al*., 2006; Ates *et al*., 2015). ESX-3 was shown to transport PE5/PPE4 and EsxG/EsxH across the membrane (Roy *et al*., 2020). PE5/PPE4 is associated with mycobactin-mediated iron acquisition which contributes to cell growth, while EsxG/EsxH interferes with phagosome maturation and antigen processing by engaging with the host endosomal sorting complexes (Siegrist *et al*., 2009; Portal-Celhay

et al., 2016). The *exs-1* locus encodes the genes *Rv3875* and *Rv3874* which produces the proteins EsxA and EsxB respectively (Clemmensen *et al*., 2017). These were found to be crucial for normal bacterial growth in host macrophages and for the stimulation of proinflammatory immune responses from the host (Guinn *et al*., 2004; Clemmensen *et al*., 2017). Additionally, ESX-1 secretes the EspA/EspC heterodimer, which is contingent on EsxA/EsxB (Fortune *et al*., 2005). EspC is responsible for the formation of surface filaments which are thought to facilitate the transport of EsxA to the host membrane via contact dependent delivery (Lou *et al*., 2017). EspB orients into heptameric ring-like structures and exhibits its membranolytic activity which promotes macrophagic necrosis (Solomonson *et al*., 2015).

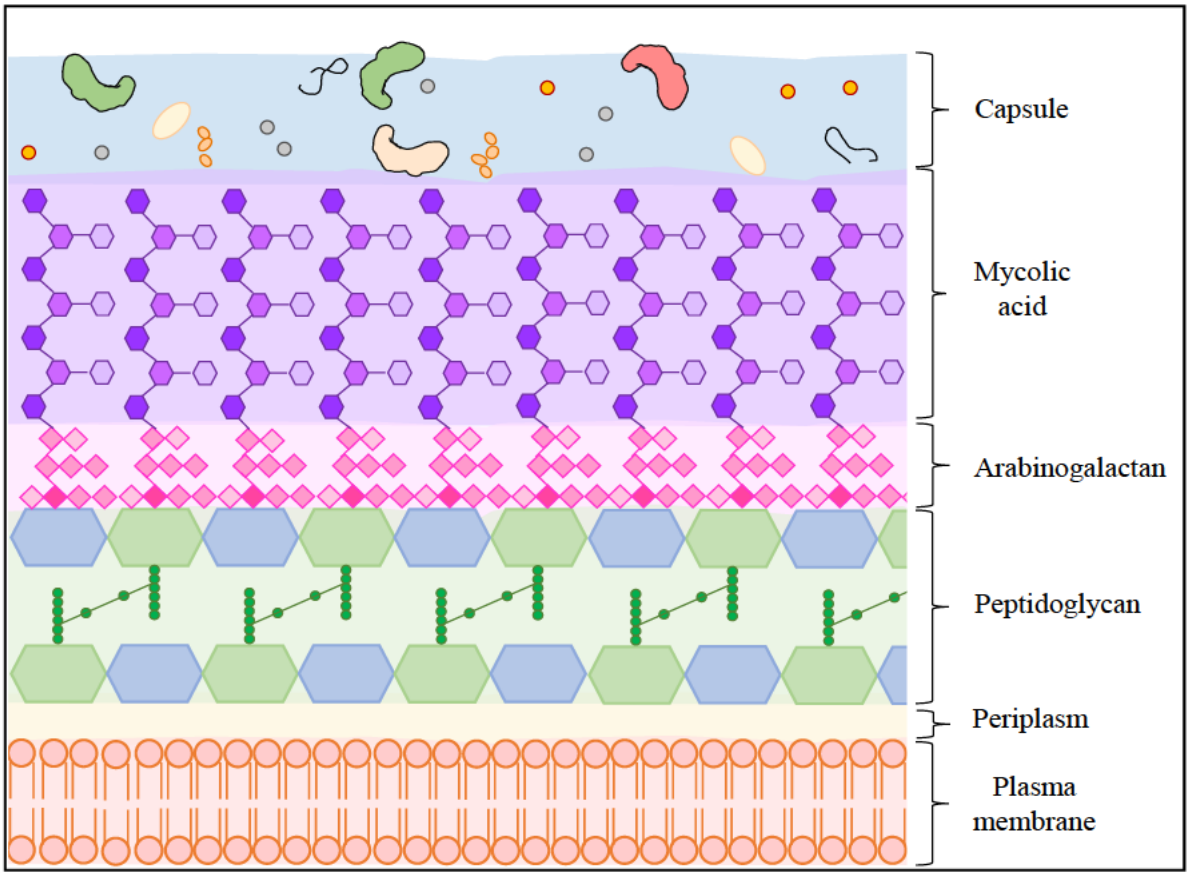

Figure 1.5. Schematic illustration of mycobacterial cell envelope depicting the bacterium's phospholipid bilayer in orange, the periplasm layer in yellow, the PG layer in green and blue, the AG layer in pink and the MA layer in purple. These layers are all encased within the outer blue layer, the capsule, which contains an array of proteins and lipids (adapted from Daffé & Marrakchi, 2019).

1.5.1.7. The mycobacterial capsule

The outermost layer of the bacterial cell, the capsule, is a form of survival strategy that confers protection and viability. The *Mtb* capsule is abundant with proteins, lipids and primarily polysaccharides and is weakly bound to the cell wall with the capacity to detach under unfavorable circumstances (e.g. agitation) (Ortalo-Magne *et al*., 1995; Kalscheuer *et al*., 2019). The *Mtb* capsule

contains three main polysaccharides: α-D-glucan, D-mannan and D-arabino-D-mannan (Kalscheuer *et al*., 2019). These not only modulate the uptake of *Mtb* by immune cells but also facilitate survival of *Mtb* whilst captured by them (Kalscheuer *et al*., 2019). The presence of the mycobacterial capsule also enhances the proinflammatory response of the host, which is beneficial for the spread of *Mtb* (Sani *et al*., 2010).

1.5.2. *Mtb* virulence factors

In addition to cell wall constituents, bacteria produce an arsenal of substances that they capitalize on to achieve host colonization (Finlay & Falkow, 1997). A pathogen's ability to establish infection in a host can be attributed to its virulence factors. Virulence factors are molecules which are required to manipulate and colonize the host, as well as cause subsequent suppression and evasion of the host's immune system (Peterson, 1996). Virulence factors can include cell wall constituents, cellular structures, secretory proteins, toxins, factors promoting biofilm formation, immune response inhibitors and any molecules that support bacterial invasion and colonization (Wu *et al*., 2008). These substances/molecules can either directly or indirectly disrupt host homeostasis, cause infection within host tissues and occasionally even shield the pathogen from the host's defense mechanisms (Finlay & Falkow, 1997)

Mtb contains an abundance of enzymes and proteins that enriches its pathogenicity. PMNs generate reactive oxygen species (ROS), which induces lipid peroxidation and damage to pathogenic DNA and proteins in an attempt to clear pathogens. Unfortunately, this activity is not specific as it also targets human host cells and tissues, resulting in tissue damage (Romero *et al*., 2012). However, *Mtb* has developed strategies to address this oxidative stress, such as its production of the enzyme KatG, which is a virulence factor with catalase and peroxidase activity, which shields *Mtb* from the effects of ROS (Zhai *et al*., 2019). This results in the immune system negatively impacting only the host, with minimal effect against the target pathogen (Zhai *et al*., 2019).

Another example of virulence factors implemented by *Mtb* is the Secreted Acid Phosphatase (SapM) enzyme which is integral for the interference of phagosome maturation as it dephosphorylates the phosphotidylinositol 3-phosphate (PI3P) which is present on phagosomes (Puri *et al*., 2013). SapM also contributes to bacterial growth and survival in the lung and spleen of guinea pig models (Puri *et al*., 2013).

Proteases are proficient executors of bonds within peptides (López-Otín & Bond, 2008). Their function in protein demolition results in the formation of new protein products (a process termed proteolysis) (Britannica, 2020). In this regard, they coordinate multiple biological processes in all lifeforms, including but not limited to: regulating cellular maintenance, activation/termination of signal transduction, apoptosis and cell cycle control, as well as function as virulence factors in microorganisms (Theron & Divol, 2014).

1.6. Proteases

Proteases, also known as proteinases or proteolytic enzymes, occur universally and are commonly found in humans, animals, plants and microorganisms such as bacteria (López-Otín & Bond, 2008). The degradative function of bacterial proteases tasks them with the responsibility to produce new bioactive molecules, regulate the activity of many proteins, engage in the processing of cellular information as well as modulate protein interactions (López-Otín & Bond, 2008)

Proteases are subdivided into two groups: endoproteases and exoproteases (Rao *et al*., 1998). The former referring to proteases which cleave sites within proteins, whilst the latter cleaves proteins at the terminal ends (Britannica, 2020). Endoproteases are further categorized according to their catalytic activity into the following groups: serine, aspartic, metallo-, cysteine, threonine and glutamic (Rao *et al*., 1998).

Metalloproteases, the most substantial proportion of proteases, are a heterogeneous group of proteases which perform hydrolytic reactions by using an indispensable metal ion, present at the core, to catalyze the degradation of proteins (Rahman *et al*., 2022). The metal ions that are most commonly used include: cobalt (Co^{2+}), manganese (Mn^{2+}) and most substantially, zinc (Zn^{2+}) (Crichton, 2012).

1.6.1. Zinc metalloproteases

A zinc metalloprotease is a protease with an indispensable zinc ion at its active site that is responsible for its catalytic activity (McCall *et al*., 2000). Zinc ions lack redox activity and instead function as a Lewis acid to accept a pair of electrons (McCall *et al*., 2000). This is due to its fully filled *d* orbital (d^{10}), which makes it a stable ion, ergo an ideal metal cofactor to participate in reactions such as proteolysis (Williams, 1987; Butler, 1998). In addition, the filled *d* orbital also provides the zinc ion with a ligand-field stabilization energy of zero (Huheey *et al*., 2006). The absence of this energy tax required for the rearrangement of the coordination geometries around the central zinc atom is beneficial to zinc metalloproteases, as it promotes ease of alteration of reactivity, therefore improving its ability to catalyze chemical transformations (McCall *et al*., 2000). Despite this capacity, zinc metalloproteases most frequently occur as "a slightly distorted tetrahedral with the metal ion coordinating three or four protein side chains" (McCall *et al*., 2000).

Further classification of zinc metalloproteases can be conducted based on the zinc binding motif and the core function of the metalloprotease. Generally, zinc metalloproteases comprise the zinc binding motif consisting of two histidine residues as zinc ligands that may be identified as the His-Glu-Xaa-Xaa-His (HEXXH) motif (Zastrow & Pecoraro, 2014). Furthermore, the role of the zinc ion in metalloproteases varies between catalytic, structural and regulatory (Zastrow & Pecoraro, 2014).

Zinc ions enhance protein function through orienting and stabilizing active site residues and structures as well as transducing signals across the protein to maintain structural three-dimensional conformity

(Vallee & Auld, 1990; Dutta & Bahar, 2010). Additionally, zinc metalloproteases with structural zinc ions facilitate protein-protein interactions between surfaces of both proteins involved in order to promote stability, specificity and functionality (Lin *et al*., 2016). Zinc ions also play regulatory roles in metalloproteases, as shown by their involvement in mediating cellular interactions, cellular signaling and overall protein activity (Thompson, 2022).

A zinc ion is considered to be catalytic when it is located at the active site of an enzyme and directly interacts with the substrate molecules involved in the reaction, wherein it is responsible for polarizing a water molecule with intent to increase its nucleophilicity, to promote hydrolysis which facilitates a nucleophilic attack on the peptide bond (McCall *et al*., 2000). In addition to polarization, catalytic zinc ions also function by methods such as ionization and displacement (figure 1.6). The zinc ion could ionize the zinc-bound water molecule which results in the formation of a hydroxide ion (OH^-), a nucleophile, which executes proteolysis by cleaving the bond within the peptide (McCall *et al*., 2000). The zinc-bound water could also be displaced by the substrate (which instead binds to the zinc ion at the active site) for catalytic activity to commence (McCall *et al*., 2000).

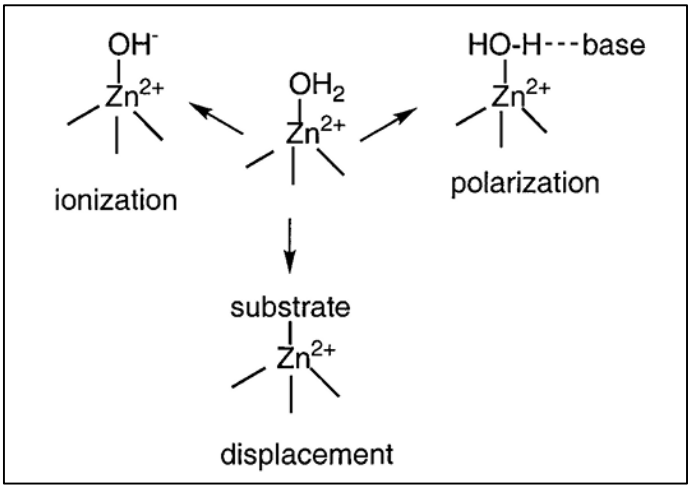

Figure 1.6. The three mechanisms by which zinc ions at the active site of zinc metalloproteases bring about proteolytic activity (McCall *et al*., 2000).

1.6.2. Zinc metalloprotease's contribution to bacterial virulence

Extracellular zinc metalloproteases are universally present and a substantial amount of them function as toxins in pathogenic bacteria. Zinc metalloproteases often contribute to invasion, infection and evasion of host immune responses, often enabling progression of infection to severe or lethal magnitudes (Peterson, 1996). This is seen in zinc metalloproteases present in *Clostridium difficile* and Enterohemorrhagic *Escherichia coli*, which function in invasion of host cells by catalyzing degradation of protective molecules (extracellular matrix constituents and mucin respectively) that are secreted by the host in order to facilitate colonization (Angel *et al*., 2012; Wade *et al*., 2020). Zinc metalloproteases also contribute to a pathogens capability to forage for nutrients within a host as witnessed by Thermolysin from *Bacillus thermoproteolyticus*, pseudolysin from *Pseudomonas aeruginosa* and

aureolysin from *Staphylococcus aureus* which catalyze extracellular proteins and peptides of the host for bacterial nutrition as well as to contribute to bacterial biofilm formation (Miyoshi & Shinoda, 2000; Rawlings *et al*., 2018; Rahman *et al*., 2022). Some other bacterial zinc metalloproteases play roles in migration, mammalian cell adhesion, extracellular matrix remodeling as well as cell-to-cell interactions, ergo conferring virulence (Kearns *et al*., 2002).

The widespread presence of zinc metalloproteases in nearly all pathogenic bacteria, despite their diverse respective physiologies, suggests that these enzymes provide a significant advantage to the organisms that produce them. Investigating them further may, therefore, be very worthwhile.

1.6.3. *Mtb* zinc metalloproteases

Despite the numerous zinc metalloproteases encoded within the genome of *Mtb*, only a selected few have been identified and even less have been characterized. The *Mtb* gene *Rv0198c* codes for Zinc metalloprotease 1 (Zmp1), which is annotated as an immunomodulatory metalloprotease, due to its imperativity for *Mtb* survival in host macrophages (Vemula *et al*., 2016). Macrophages contain the inflammosome, which is a multi-protein complex containing the nucleotide-binding oligomerization domain (NOD1) and the inactive pro-caspase-1 (Ferraris *et al*., 2011). The inflammosome is activated by pathogen-associated molecules, which drives the transformation of the inactive proform pro-caspase-1 into caspase-1, which subsequently utilizes the precursor pro-IL-1β as a substrate to proteolytically activate the proinflammatory cytokine IL-1β (Dinarello, 2005). Secreted IL-1β is responsible for coordinating the inflammatory response such as formation of the phagolysosome, phagosome maturation, stimulating other proinflammatory cytokines and the production of reactive oxygen and nitrogen intermediates (Master *et al*., 2008). Phagosome maturation is crucial for the successful clearance of bacteria (Ferraris *et al*., 2011). However, Zmp1 is able to inhibit inflammosome activation which prevents secretion of IL-1β, therefore obstructing phagosome maturation (Master *et al*., 2008). This allows progression of the infection as well as hinders antigen processing and eradication of the bacteria (Kaufmann, 2001; Pieters, 2008; Johansen *et al*., 2011).

Infection of macrophages with Zmp1-deletion mutants of *Mtb* exhibited production of IL-1β, in addition to full maturation of the phagosome into phagolysosome and subsequent clearance of the pathogen (Ferraris *et al*., 2011). This is indicative of Zmp1's essentiality for *Mtb's* intracellular survival inside host macrophages and highlights its role in bacterial virulence, however "the exact details of how the Zmp1 gene product acts are not known" (Master *et al*., 2008).

Conventionally, the recruitment of immune cells to an infected site is advantageous to the host as it promotes pathogen clearance. However, *Mtb* has manipulated this host defense mechanism and "hijacked" this process for its own dissemination. Secretion of Zmp1 in granuloma induces necrotic damage of the immune cells, stimulates migration of these infected/damaged cells to other areas and thereafter stimulates the release of chemotactic factors which attracts uninfected immune cells

(lymphocytes, macrophages, monocytes and dendrites) to the inflammatory site (Vemula *et al*., 2016). These newly attracted cells get infected by the *Mtb* bacteria that gets released from the necrotic infected cells; ergo assisting mycobacterial dissemination (Vemula *et al*., 2016).

Sigma factors modulate gene expression in response to stress-inducing stimuli (Raman *et al*., 2004). This is done in an attempt to activate stress response genes to facilitate adaptation to hostile environments and maintain virulence (Raman *et al*., 2004). The lesser known and partially characterized *Mtb* secretory zinc metalloprotease, Rip (encoded within the *Rv2869c* gene), was shown to be activated under hypoxic conditions and during the mycobacterial stationary phase (Calamita *et al*., 2005). Upon activation, Rip catalyzes the degradation of anti-sigma substrate RsdA which releases the sigma factor SigD, enabling it to transcribe specific SigD stress-response genes, thus promoting bacterial survival and virulence (Sklar *et al*., 2010).

Additionally, Rip regulates intramembrane proteolysis of several lipid biosynthetic pathways by targeting membrane bound transcriptional regulators, which contributes to mycobacterial growth and persistence *in vivo* (Makinoshima & Glickman, 2005; Forrellad *et al*., 2013). Mutants with defective *Rv2869c* lead to changes in the composition of MAs and phosphatidylinositol mannosides, which is a lipid present in the cell wall (Makinoshima & Glickman, 2005).

Considering the impact of only two zinc metalloproteases on the success of *Mtb* as a pathogen, it would be extremely advantageous to explore the functions of the remaining zinc metalloproteases as they have strong but unrealized potential to be contenders as drug targets.

1.6.4. The suitability of zinc metalloproteases as candidates for drug targets

Metalloproteases comprise one third of all known enzymes in prokaryotes and eukaryotes (Chen *et al*., 2018). However, those present in bacteria differ significantly compared to those contained within eukaryotes (Plotniece *et al*., 2023). Exploiting these functional and structural differences provides an opportunity for the design of drugs with reduced off-target effects due to toxic specificity (Plotniece *et al*., 2023). The discovery of drugs targeting zinc metalloproteases could propel, not only *Mtb* treatment, but also the treatment of other bacterial infections, as zinc metalloproteases are conserved amongst certain bacterial species.

In addition, bacterial zinc metalloproteases often play central/essential roles in virulence and parasitic processes, inhibiting these functions offers an appealing solution as the ramifications could be detrimental to bacteria (Moianos *et al*., 2023). Furthermore, impairment of zinc metalloproteases makes pathogens incapacitated and therefore possibly more susceptible to current treatment therapies thereby presenting a synergistic approach to enhance treatment efficacy. It can therefore be asserted that the identification and elucidation of bacterial zinc metalloproteases and their involvement in virulence paves the way for the development of novel antibacterial drugs, potentially revolutionizing therapeutic strategies (Plotniece *et al*., 2023).

1.7. Use of model organism *Mycobacterium smegmatis* for *Mtb* research

Mtb is amongst the most notorious pathogenic species belonging to the genus *Mycobacterium*. This can be accredited to its centuries-long dominance of the global public health sectors. Despite its prolonged period of anguish upon humanity, latest advancements on deciphering *Mtb's* genetic composition and molecular mechanisms have only scratched the surface of full comprehension.

The answer to eradicating TB can only be found by unravelling *Mtb*. The dire need for research in this field is unfortunately met with equally dire complications. The pathogenicity and slow growing characteristics of *Mtb*, coupled with the requisites of a Biosafety Laboratory 3 (BSL 3) and accompanied safety requirements presents a significant challenge to study the pathogen (Sparks *et al*., 2023).

Fortunately, the implementation of "model organisms" in *Mtb* research resolves almost all of the above-mentioned predicament. A model organism is a species (chosen on account of its convenience) which is extensively studied with the intent to apply all acquired information to another species (Müller & Grossniklaus, 2010). The ideal model organism should share biological traits and the genetic make-up of the target species (Müller & Grossniklaus, 2010). Interestingly, the *Mycobacterium* genus also consists of non-pathogenic microbes which naturally occur in environmental habitats, including soil and water (Ranjitha *et al*., 2020). One such bacterium is *Mycobacterium smegmatis*, which is universally acclaimed for pioneering mycobacterial research by functioning as a model organism (Sparks *et al*., 2023). *Mtb* research attained a milestone advancement when *M. smegmatis* was utilized to create the transformable derivative strain, named mc^2155 (Sparks *et al*., 2023).

Mtb and *M. smegmatis* mc^2155 contain the same physiology, cell structures and are susceptible to the same anti-TB drugs (Sparks *et al*., 2023). Furthermore, greater than 70% of the protein-coding genes in *Mtb* have orthologs in *M. smegmatis* with an average protein identity surpassing 70% (Malhotra *et al*., 2017; Judd *et al*., 2021). The core proteins and genetic organization of both species are very well conserved, as seen by similar patterns of gene co-localization around the chromosome (Sparks *et al*., 2023). The inference of conserved gene regulation and function between both species is further supported by transposon mutagenesis studies, which revealed that 90% of essential genes in *Mtb* are also present and essential in *M. smegmatis* (Dragset *et al*., 2019).

By contrast, the non-pathogenic state of this bacterium negates the necessity of a BSL3 facility and safety requirements for its experimentation. This provides a more cost effective alternative which also doubles as a safer option for researchers due to the non-infectivity of the bacterium (Sparks *et al*., 2023). Additionally, mc^2155 is a fast growing strain which is capable of forming colonies in 2 days as compared to *Mtb* which requires weeks (Sparks *et al*., 2023). This characteristic is especially beneficial for the study of cell architecture and growth of single cells which mandates the use of specialized equipment (Sparks *et al*., 2023). This strain is also capable of growing at temperatures up to 55°C

(which enables isolation of temperature-sensitive mutants, allowing targeted mutagenesis) (Pope *et al*., 2011).

The use of *M. smegmatis* in *Mtb* research over the last few decades has yielded substantial and transformative results. *M. smegmatis* research has aided in identifying the mode of action of Isoniazid and Ethambutol (Forbes *et al*., 1965; Zhang *et al*., 1992). It is also utilized in preliminary screening and optimization of antimicrobial compounds in drug development, e.g. Bedaquiline (Andries *et al*., 2005). Therefore, it has remarkable application in characterizing targets of TB drugs and biological processes. It has the prospect to decipher mycobacterial metabolic reactions at cellular levels, identify protein-protein interactions as well as expedite the determination of unannotated proteins (Sparks *et al*., 2023).

1.8. Hypothesis

It is hypothesized that the *Rv2568c* zinc metalloprotease is a contributor of bacterial virulence in *Mtb* and shall therefore pose as a novel target for drug discovery.

1.9. Aim

The aim of this research project is to investigate the role of zinc metalloproteases in mycobacteria. The zinc metalloprotease *MSMEG3019* from the model organism *M. smegmatis* mc^2155 will be characterized in order to elucidate the function of its ortholog, *Rv2568c*, in the physiology of *M. tuberculosis*.

1.10. Objectives

The following objectives have been established:

- Conduct bioinformatics analysis to identify genes with similar sequences or crystal structures to that of the target gene, in order to aid in inferring possible function.
- Construct a knockout mutant strain of *M. smegmatis* mc^2155 containing an inactive version of the *MSMEG3019* gene, using the two-step allelic exchange method.
- Conduct phenotypic characterization of the mutant and wild type strains in order to determine the role of *MSMEG3019* in bacterial growth, physiology and antimicrobial tolerance.

2. Methods and Materials

2.1. Plasmids and bacterial strains

All bacterial strains and plasmids created and/or utilized for this study are listed in tables 2.1 and 2.2. All bacterial strains were grown in their appropriate media and thereafter supplemented with 30% (v/v) glycerol in a ratio of 1:1 and stored at – 80°C.

Table 2.1. Plasmids created and/or used in this study

Plasmid	**Genotype**	**Source**
p2NIL	Suicide vector utilized for cloning in *Escherichia coli*; Kan^R	(Parish & Stoker, 2000)
pGOAL17	Cloning vector containing a *PacI* cassette consisting of l*acZ* and *sacB* genes; Amp^R	(Parish & Stoker, 2000)
p2Δ3019	Derivative of p2NIL carrying inserts of the upstream and downstream regions of *MSMEG3019* (with an internal deletion of 964 base pairs (bp)); Kan^R	This study
p2Δ3019pac	Derivative of p2Δ3019 carrying the *PacI* cassette from pGOAL17; Kan^R	This study
pMV306h	Complementation vector which integrates into the mycobacterial genome at the *attB* attachment site; Hyg^R	(Stover *et al*., 1991)
pMV3019+6p	Derivative of pMV306h carrying the promoter region of the *MSMEG3016* gene incorporated upstream the entirety of the *MSMEG3019* gene; Hyg^R	This study
pMV3019p	Derivative of pMV306h carrying the *MSMEG3019* gene and its hypothesized promoter region (400 bp upstream the gene); Hyg^R	This study

Kan^R: Kanamycin resistance, Hyg^R: Hygromycin resistance, Amp^R: Ampicillin resistance

Table 2.2. Bacterial strains created and/or used in this study

Bacterial strain	Genotype	Source
Escherichia coli DH5α	F^- φ80*lac*ZΔM15 Δ(*lac*ZYA-*arg*F)U169 *rec*A1 *end*A1 *hsd*R17(r_K^- ,m_K^+) *pho*A *sup*E44 λ^-*thi*-1 *gyr*A96 *rel*A1	Thermo Scientific
Mycobacterium smegmatis mc^2155	Laboratory-created strain designed for efficient plasmid transformation.	Snapper *et al*., (1990)
MΔ3019FCO	Derivative of mc^2155, merodiploid state, carrying the plasmid p2Δ3019pac integrated at either the upstream or downstream region of *MSMEG3019* homology; Kan^R	This study
MΔ3019	Derivative of MΔ3019FCO, carrying an in-frame deletion of *MSMEG3019*	This study
MComp9+6p	Derivative of MΔ3019 carrying the pMV3019+6p complementation vector integrated into the mycobacterial genome at the *attB* site; Hyg^R	This study
MComp9	Derivative of MΔ3019 carrying the pMV3019p complementation vector integrated into the mycobacterial genome at the *attB* site; Hyg^R	This study

Kan^R: Kanamycin resistance, Hyg^R: Hygromycin resistance, Amp^R: Ampicillin resistance

2.2. Growth of bacterial strains

2.2.1. *E. coli* DH5α and derivatives

E. coli DH5α cells (ThermoScientific, United States) were grown in nutrient broth (NB) or Luria-Bertani broth (LB) (Merck, Germany) at 37ºC with shaking at 180 Revolutions per minute (RPM), using the Apex scientific incubated shaker ISS-7100. The cells were grown on nutrient agar (NA) or Luria-Bertani Agar (LA) (Merck, Germany) at 37ºC. The broth and agar were supplemented with the following antibiotic concentrations where applicable: Kanamycin (Kan): 50 µg/mL, Hygromycin (Hyg): 200 µg/mL and Ampicillin (Amp): 100 µg/mL (Merck, Germany).

2.2.2. *M. smegmatis* mc^2155 and derivatives

Mycobacterial cells were grown at 37ºC with shaking at 180 RPM in Middlebrook 7H9 liquid media (broth) supplemented with glycerol, 20% tyloxapol and 100 × glucose-salt (Merck, Germany). The strains were grown on Middlebrook 7H11 agar supplemented with glycerol and 100 × glucose-salt at 37ºC (Merck, Germany). The broth and agar were supplemented with the following appropriate antibiotic concentrations where applicable (refer to tables 2.1 and 2.2): Kan: 25 µg/mL and Hyg: 50 µg/mL.

2.3. DNA extraction

2.3.1. *M. smegmatis* genome extraction

2.3.1.1. Cetyltrimethylammonium bromide (CTAB) genomic DNA extraction

One hundred microliters of an overnight *M. smegmatis* culture was spread onto 7H11 agar and incubated at 37°C for 2 days. The colonies were scraped off and resuspended in 500 µL Tris-EDTA (TE) buffer. The bacterial cells were heat killed by incubation at 65°C for 35 min. After being cooled to room temperature (RT) (20°C to 22°C), 50 µL of 10 mg/mL lysozyme (Merck, Germany) was added and the mixture underwent incubation at 37°C for 1 h. Thereafter, 70 µL of 10% Sodium dodecyl sulphate (SDS) and 6 µL of 10 mg/mL proteinase K were added and this was incubated at 65°C for 2 h. Subsequently, 100 µL of 5 M Sodium chloride (NaCl) and 80 µL of pre-warmed Cetyltrimethylammonium bromide (Merck, Germany) was added to the sample, mixed by pipetting and incubated at 65°C for 10 min. Equal volumes of chloroform: isoamyl alcohol (24:1) (Merck, Germany) was added to the sample, mixed by inverting and centrifuged at 12 000 rpm for 10 min. The resultant top layer was transferred to a sterile microfuge tube (Eppendorf) and 0.6 × volume equivalent of isopropanol (Merck, Germany) was added to the solution, mixed by inverting and centrifuged at 12 000 rpm for 20 min. The supernatant was discarded and the pellet was washed using 70% ethanol. Afterwards, the pellet was dried, using the Genevac miVac DNA Concentrator and thereafter resuspended in 50 µL of sterile distilled water (dH_2O). The resulting genomic DNA (gDNA) was stored at 4°C (Somerville *et al*., 2005).

2.3.1.2. Small scale colony boil for gDNA extraction

Half of a selected colony was scrapped off the 7H11 agar plate and resuspended in 50 µL dH_2O. This cell suspension was incubated at 65°C for 20 min. Thereafter, 50 µL of chloroform was added, mixed by inverting and subsequently centrifuged at 13 000 RPM for 5 min. The upper aqueous layer that formed was transferred into a sterile microfuge tube and stored at 4°C. Two microliters of this DNA was utilized as a template for Polymerase Chain Reaction (PCR) screening (Ruiz-Barba *et al*., 2005).

2.3.2. *E. coli* plasmid extraction

2.3.2.1. Plasmid extraction using GeneJet kit

Plasmid DNA extractions were conducted using the GeneJet Plasmid Midiprep Kit (Thermo Scientific, United States) as per the manufacturer's protocol. Briefly, a 50 mL overnight bacterial culture of DH5α containing the plasmid was grown and centrifuged for 10 min at 4 000 × g. The supernatant was discarded and the harvested cells were resuspended in 2 mL Resuspension Solution. Thereafter 4 mL of Solution II was added and the mixture was then allowed to sit at RT for 5 min. Thereafter, 3 mL of Solution III was added, the centrifuge tube was inverted 5-6 times and incubated on ice for 10 min. The cell suspension was centrifuged at 4 000 × g for 40 min in order for the cell debris and chromosomal

DNA to pellet. The supernatant was transferred to a clean 15 mL centrifuge tube, to which 3 mL of 96% ethanol was then added and immediately mixed by inverting 5-6 times. Approximately 5.5 mL of the sample was transferred to the supplied pre-assembled collection tube with column. The sample was centrifuged at 2 000 × g for 3 min. The flow-through was discarded and the column was placed back into the collection tube. This step was repeated until all of the sample had been processed through the column. Four milliliters of Wash Solution I was added to the purification column and centrifuged at 3 000 × g for 2 min, after which the flow-through was discarded. Thereafter 4 mL of Wash Solution II was added to the purification column, centrifuged at 3 000 × g for 2 min and the resultant flow-through was discarded. This column wash step using Wash Solution II was repeated. In order to remove any remaining wash solution, the empty column was centrifuged for an additional 5 min at 3 000 × g. The purification column was then transferred into a sterile 15 mL collection tube and 0.35 mL of sterile dH_2O was added to the center of the membrane in the column. This was incubated at RT for 2 min and subsequently centrifuged at 3 000 × g for 5 min. The purified DNA was stored at – 20°C.

2.3.2.2. Plasmid miniprep extractions for colony screening

A single colony was picked using a sterile loop and inoculated into 2 mL of LB broth and grown in a 14 mL polypropylene round-bottom falcon tube (Lasec, South Africa). This was supplemented with the appropriate antibiotics and incubated at 37°C overnight with shaking at 180 RPM. Following this, 1 mL of the culture was transferred to an Eppendorf tube and centrifuged at 4 000 RPM for 10 min. The pellet was resuspended in 100 µL of Solution I, after which 200 µL of Solution II was added to the mixture. This was allowed to incubate at RT for 5 min, thereafter 150 µL of cold Solution III was added and the contents of the tube was mixed by inverting the tube 5-6 times. The mixture was then incubated on ice for 10 min, followed by centrifugation at 10 000 RPM for 10 min. The supernatant was transferred into Eppendorf tubes containing 2 µL of 10 mg/mL RNase and this was incubated at 37°C for 30 min. Thereafter, 150 µL of chloroform was added and the contents were mixed by inverting the tube 5-6 times. The mixture was centrifuged at 10 000 RPM for 10 min and the resultant top layer was transferred into a fresh Eppendorf tube, to which 300 µL of isopropanol was added, mixed and centrifuged at 10 000 RPM for 20 min. The supernatant was discarded and 500 µL of 70% ethanol was added to the tube and centrifuged at 12 000 RPM for 5 min. The supernatant was discarded and the pellet was dried using the Genevac miVac DNA Concentrator, after which the pellet was resuspended in 20 µL of sterile dH_2O and stored at – 20°C (Birnboim & Doly, 1979).

2.3.2.3. Sodium acetate DNA precipitation

A $\frac{1}{10}$ volume equivalence of 3 M sodium acetate and a 2 × volume equivalence of 100% ethanol was added to the eluted DNA solution. The solution was mixed by inverting and incubated at – 80 ° C for 30 min to facilitate DNA precipitation. The solution was thereafter centrifuged at maximum speed for 20 min. The supernatant was discarded and the pellet was washed with 500 µL of ice cold 70% ethanol.

The solution was centrifuged at 12 000 rpm for 5 min. The pellet was dried and resuspended in 100 µL of sterile dH_2O. The purified DNA sample was stored at – 20°C (Qiagen, 2024).

2.3.3. Nucleic acid quantification

All DNA samples were quantified using the Nanodrop 2000c spectrophotometer, manufactured by Thermo Scientific, using a baseline correction of 340 nm. The 260/280 and 260/230 ratios of all samples were analyzed prior to storage at their respective conditions. Genomic DNA was stored at 4°C, whilst plasmid DNA was stored at – 20°C.

2.4. Polymerase Chain Reaction (PCR)

2.4.1. Phusion PCR

PCR amplification of gDNA was conducted using Phusion high-fidelity DNA polymerase (Thermo Scientific, United States). Fifty microliter reactions were set up in 0.2 mL flat cap tubes (Thermo Scientific, United States). The reaction mixture consisted of 10 µL of 5 × GC buffer, 1 µL of 10 mM deoxynucleotide triphosphates (dNTPs), 0.25 µL of forward primer (100 µM), 0.25 µL of reverse primer (100 µM), 50 ng *M. smegmatis* mc^2155 gDNA, 1.5 µL of dimethyl sulfoxide (DMSO) and 0.5 µL of Phusion enzyme. The reaction was made up to 50 µL using sterile dH_2O. A reaction containing all components except DNA was utilized as a negative control. The reactions were run in a Bio-rad T100 thermal cycler (Lasec, South Africa) as per the manufacturer's protocol stipulated below.

The initial denaturation step was conducted at 98°C for 3 min. This was followed by 35 cycles of the following successive steps: 10 sec of denaturation at 98°C, 30 sec of annealing and 1 min of extension at 72°C. The annealing temperatures varied depending on the respective primer sequences. A final extension step was then performed for 5 min at 72°C. The reactions were then held in the thermal cycler at 4°C, after which they were stored at – 20°C until use.

2.4.2. DreamTaq PCR

PCR amplification using DreamTaq (Thermo Scientific) was utilized for PCR screening of recombinant/mutant DNA. Fifty microliter reactions were set up in 0.2 mL flat cap tubes. The reaction mixture consisted of 5 µL of 10 × DreamTaq buffer, 0.75 µL of 10 mM dNTPs, 0.2 µL of forward primer (100 µM), 0.2 µL of reverse primer (100 µM), 50 ng *M. smegmatis* genome DNA and 0.75 µL of DreamTaq DNA polymerase. The reaction was made up to 50 µL using autoclaved dH_2O. A reaction containing all components except DNA was utilized as a negative control. The reactions were run in a Bio-rad T100 thermal cycler with slight modification to the manufacturer's protocol.

The initial denaturation step was conducted at 95°C for 3 min. This was followed by 34 cycles of the following steps: 30 sec of denaturation at 95°C, 25 sec of annealing and 45 sec of extension at 72°C. The annealing temperatures varied depending on the respective primer sequences. A final extension

step was then carried out for 5 min at 72°C. The reactions were then immediately held in the thermal cycler at 12°C and thereafter stored at – 20°C until use.

2.4.3. PCR cleanup

The PCR amplicons were cleaned up using the GeneJet Gel Extraction and DNA Clean Up micro kit (Thermo Scientific, United States) as per manufacturer's protocol. Briefly, the volume of the PCR reaction was increased to 200 µL using sterile dH_2O. One hundred microliters of binding buffer was added to the solution and this was mixed thoroughly by pipetting. Thereafter, 300 µL of 96% ethanol was added to the solution and mixed by pipetting. The solution was transferred to the supplied pre-assembled column with collection tube and centrifuged at 12 000 RPM for 60 sec. The flow-through was discarded. Thereafter, 200 µL of pre-wash buffer was added to the column and centrifuged at 12 000 RPM for 1 min. After the flow-through was discarded, 700 µL of wash buffer was added to the column, centrifuged at 12 000 RPM for 1 min and the resultant flow-through was discarded. The column was washed with 700 µL of wash buffer and centrifuged for 30 sec at 12 000 RPM twice. After the supernatant was discarded, the tube was centrifuged for an additional 1 min at 12 000 RPM. The column was transferred to a clean 1.5 mL microfuge tube where 25 µL of sterile dH_2O was added. This tube was centrifuged for 1 min at 12 000 rpm and the eluted DNA was stored at – 20°C.

2.5. Agarose gel electrophoresis

For separation of high molecular weight DNA, 0.8% agarose gels were made by dissolving agarose (manufactured by SeaKem) in 1 × Sodium borate buffer. Separation of low molecular weight DNA was accomplished by 2% gels. Generuler 1 kb and Generuler 1 kb plus were procured from Merck (Germany) and utilized as molecular weight markers. All DNA samples (including markers) were mixed with 2 µL of loading dye (Thermo Scientific, United States), diluted with dH_2O and thereafter loaded onto the gel. Gel electrophoresis was conducted in 1 × Sodium borate buffer in Bio-rad Sub Cell GT Tanks and were run at 100 V for 1 h using the Hoefer PS300-B power pack. The gels were thereafter viewed using the Syngene G:Box gel imaging system along with the GeneSys software.

2.6. Cloning

2.6.1. DNA restriction digestion

Restriction digestion reactions were conducted using enzymes procured from Thermo Scientific (United States). The reactions were set up according to the manufacturer's protocol unless stated otherwise. Twenty microliter reactions were set up, containing 2 µL of the recommended buffer, 1 µg DNA, 1 µL restriction enzyme and made up to 20 µL using sterile dH_2O. The restriction digestions were mixed by pipetting and incubated at 37°C overnight. Following the incubation period, the restriction enzymes were heat inactivated at 60°C for 10 min.

The amount of DNA required for the reaction was calculated using the following formula:

$$\textit{Volume of required DNA (µl)} = \frac{Mass\ required\ (1\ 000\ ng)}{Concentration\ of\ extracted\ DNA\ (ng/\mu l)}$$

2.6.2. DNA dephosphorylation

DNA was dephosphorylated using the enzyme Fast AP Alkaline Phosphatase (Thermo Scientific, United States). This enzyme serves to remove single phosphate groups from the 5´-ends of restricted (linear) vectors in order to prevent re-circularization. Thirty microliter reactions were set up using 3 µL of 10 × Buffer AP, 1.5 µL of Fast AP alkaline phosphatase enzyme, 20 µL of restricted vector DNA and made up to 30 µL using sterile dH_2O. The reaction was mixed thoroughly by pipetting, briefly spun at 8 000 RPM for 30 sec in the centrifuge and incubated at 37°C for 1 h. Subsequent to incubation, the enzyme was heat inactivated on a heating block (FMH electronics, ABH2) at 75°C for 5 min.

2.6.3. DNA phosphorylation

DNA was phosphorylated using the enzyme T4 Polynucleotide Kinase (T4 PNK) (Thermo Scientific, United States). This enzyme transfers ATP's gamma-phosphates to the 5'-OH end of the DNA; aiding in downstream DNA manipulations (i.e. ligations). Thirty microliter reactions were set up using 3 µL of 10 × Buffer A, 2 µL of 10 mM ATP, 1.5 µL of T4 PNK enzyme, 20 µL of restricted insert DNA and made up to 30 µL using sterile dH_2O. The reaction was mixed thoroughly by pipetting, briefly spun at 8 000 RPM for 30 sec in the centrifuge and incubated at 37°C for 20 min. After incubation, the enzyme was heat inactivated on a heating block at 75°C for 10 min.

2.6.4. Ligation

Ligation reactions were conducted using T4 DNA Ligase (Thermo Scientific, United States). All ligation reactions utilized a constant amount of vector DNA, 50 ng, and were set up using the vector: insert molar ratios of 1:1, 1:3 and 1:5. The amount of insert DNA required for each ligation ratio was calculated using the following formula:

$$\frac{insert\ size\ (kb)}{vector\ size\ (kb)} \times \frac{insert\ ratio}{vector\ ratio} = \frac{amount\ of\ insert\ required\ (ng)}{amount\ of\ vector\ (50\ ng)}$$

Twenty microliter reactions were set up containing 2 µl of 10 × T4 DNA ligase buffer, 50 ng vector DNA, insert DNA (1, 3 and 5 molar ratio equivalents), 2 µl of T4 DNA ligase and sterile dH_2O. The reactions were incubated at 22°C for 2 h, followed by heat inactivation at 65°C for 10 min. All reactions also contained a vector only control, in which no insert DNA was added to the reaction. This was done in order to estimate the likelihood of vector recircularization.

2.6.5. Competent cells

2.6.5.1. *E. coli* DH5α competency using the Calcium chloride ($CaCl_2$) method

One milliliter of DH5α freezer stock (Thermo Scientific, United States) was added to 10 mL of LB broth and incubated at 37°C overnight with shaking at 180 RPM. Thereafter, 1 mL of the overnight culture was added to 30 mL of LB broth and incubated at 37°C for 1 h with shaking at 180RPM. The culture was then transferred to a 50 mL falcon tube, incubated on ice for 10 min and centrifuged at 4 000 RPM for 10 min. The supernatant was discarded, the pellet was resuspended in 10 mL of 50 mM $CaCl_2$ and subsequently centrifuged at 4 000 RPM for a further 10 min. The resultant pellet was resuspended in 10 mL of 50 mM $CaCl_2$ and incubated on ice for 20 min. The cell suspension was centrifuged at 4 000 RPM for 10 min, after which the pellet was resuspended in 2.5 mL of 50 mM $CaCl_2$ supplemented with 15% glycerol. The cell suspension was split into 100 µL volumes and aliquoted into microfuge tubes and stored at -80°C until required (Chang *et al*., 2017).

2.6.5.2. *M. smegmatis* competency using the 10% glycerol method

A 50 mL culture of *M. smegmatis* mc^2155 was grown to an OD_{600nm} of 0.8 (optical density determined by use of spectrophotometer (Jenway, 7205 UV)). The culture was transferred to a 50 mL centrifuge tube and centrifuged at 4 000 RPM for 10 min. The supernatant was discarded and the pellet was resuspended in 45 mL of 10% glycerol (Merck, Germany). The cell suspension was centrifuged at 4 000 RPM for 10 min, the resultant supernatant was discarded and the pellet was resuspended in 20 mL of 10% glycerol. The cell suspension was centrifuged at 4 000 RPM for 10 min, the resultant supernatant was discarded and the pellet was resuspended in 10 mL of 10% glycerol. The cell suspension was centrifuged at 4 000 RPM for 10 min, the resultant supernatant was discarded and the pellet was resuspended in 5 mL of 10% glycerol. The cell suspension was centrifuged once more at 4 000 RPM for 10 min, the resultant supernatant was discarded and the pellet was resuspended in 2 mL of 10% glycerol. The cells could either be used immediately or stored at – 80°C (Yamazaki *et al*., 2006; Viljoen *et al*., 2018).

2.6.6. Transformation

2.6.6.1. *E. coli* heat shock

One hundred microliters of competent DH5α cells were thawed on ice and thereafter supplemented with 1 µg of plasmid DNA and incubated on ice for 20 min. This cell suspension and DNA mixture was then heat shocked for 90 sec at 42°C by submerging the microfuge tube in a water bath (FMH electronics), this was immediately followed by incubation on ice for 2 min. The cells were rescued by promptly adding 750 µL of 2 × TY broth, followed by a 1 h incubation period at 37°C with shaking at 120 RPM. The cells were briefly centrifuged at 4 000 RPM for 5 min and the pellet was resuspended in 200 µL of 2 × TY broth. The cell suspension was plated on NA containing the appropriate antibiotics and incubated for 1 or 2 days at 37°C or 30°C respectively, depending on the plasmid size (plasmid sizes <

8 kilobyte (kb) require the former incubation conditions; plasmid sizes >8 kb require the latter incubation conditions) (Chang *et al*., 2017).

2.6.6.2. *M. smegmatis* electroporation

Four hundred microliters of competent *M. smegmatis* cell suspension was transferred to electroporation cuvettes 5 times (Thermo Scientific, United States). Each of these cuvettes were supplemented with 1 µg, 3 µg and 5 µg of clone DNA respectively. The 4th cell suspension contained 1 µg of control plasmid DNA and the 5th cell suspension served as a competent cell only control. Each of these samples were electroporated at 2.5k V, 25 µF and 1 000 Ω using the BTX Electro Cell Manipulator 630. Following electroporation, the cells were immediately rescued with 800 µL of warm 2 × TY broth and incubated at 37°C for minimum 3 h. Thereafter, the cell suspension was centrifuged at 8 000 RPM for 10 min. The pellet was resuspended in 100 µL of 2 × TY broth and this was plated onto 7H11 containing the appropriate antibiotics/ supplements. These plates were thereafter incubated at 37°C for 3-7 days (Viljoen *et al*., 2018).

2.7. Ultraviolet treatment of DNA prior to mycobacterial electroporation

DNA (1, 3 and 5 µg) and control plasmid DNA (1 µg) was transferred to a 96-well plate (Lasec, South Africa) and placed into the UVP CL-100 Ultraviolet Crosslinker and exposed to 100 mJ/cm^{-2} of ultraviolet (UV) radiation. This treated DNA was used immediately for electroporation into competent mycobacterial cells (Parish *et al*., 1999).

2.8. Southern blotting

2.8.1. Labelling of probe

Digoxigenin (DIG)-labelled experimental probes were created using the PCR DIG Probe Synthesis Kit (Merck, Germany). The protocol was conducted as per manufacturer's instructions. Briefly, a 50 µL DIG-labelled experimental probe reaction was set up, consisting of 5 µL of 1 × PCR buffer, 5 µL of PCR DIG probe synthesis mix, 1 µM forward primer, 1 µM reverse primer, 0.75 µL of enzyme mix, 50 ng gDNA and dH_2O. Two control reactions were also made: unlabelled control probe and DIG-labelled tissue plasminogen activator (tPA) control probe. The unlabelled control contained dNTPs instead of the PCR DIG probe synthesis mix whereas the labelled control contained supplied primers instead of experimental primers. The reactions were mixed and incubated in a thermal cycler according to conditions stipulated in the manufacturers protocol. Briefly, initial denaturation was conducted at 95°C for 2 min. This was followed by 30 cycles of the following steps: pre-incubation at 95°C for 30 sec, annealing at 60°C for 30 sec and thereafter elongation at 72°C for 40 sec. A final elongation step was then carried out at 72°C for 7 min. Thereafter, 5 µL of each reaction underwent gel electrophoresis in order to verify formation of the correct product. After confirmation, the labelled probe was stored at -20°C until required.

2.8.2. Blotting

Southern blotting was conducted by use of the reagents provided in the DIG-High Prime DNA Labelling and Detection Starter Kit II (Merck). Restriction digestions of 2 µg of wild type and mutant gDNA were set up using the selected restriction enzyme. The restrictions were incubated overnight and thereafter heat killed. The DNA was separated by means of gel electrophoresis, using a 0.8% agarose gel comprised of 1 × Tris-Borate-EDTA (TBE) buffer and ran at 80 V for 2-3 h. The DNA separation on the gel was viewed using the SYNGENE G:BOX. The DNA was depurinated by soaking the gel in 0.2 M Hydrochloric acid (HCl) for 15 min with gentle shaking at 100 RPM on the Eins Sci E-OS7.5-P shaker (White Sci, South Africa). The depurination solution was decanted and the gel was gently rinsed in 1 × TBE buffer. The gel was then soaked in denaturation solution for 30 min with gentle shaking. Thereafter the denaturation solution was discarded and the gel was rinsed in 1 × TBE buffer. The Amershan Protran Premium 0.2 µm nitrocellulose blotting membrane was cut into a 9 × 6 cm rectangle and pre-soaked in 1 × TBE buffer. The membrane was overlaid on the gel (DNA side facing up). This was sandwiched between two Immobilon Blotting Filter Paper and thereafter encased within two Mini Trans-Blot Foam sponges (Biorad). The sandwich constituents were all pre-soaked as well as assembled in 1 × TBE buffer. The sandwich was inserted into a Mini Trans-Blot Gel Holder Cassette (Biorad), which was thereafter placed inside the Mini Trans-Blot Replacement Module (Biorad). This was positioned inside the Mini-Protean tetra system tank (Biorad) containing 1 × TBE buffer and run at 600 mA for 2 h. The DNA was then crosslinked to the membrane by UV irradiation twice by use of the UVP CL-100 Ultraviolet Crosslinker at 250 mJ/cm^2. The membrane was transferred to a hybridization bottle, to which 10 mL of DIG EASY HYB solution was added and incubated at 42°C for 30 min in the Hydrization oven/Shaker (Stuart scientific) with rotation. The DIG-labelled probe was denatured by incubation at 100°C for 5 min and then immediately placed on ice. After denaturing, the probe was added to the hybridization bottle, into the solution, and incubated overnight at 42°C with shaking.

The following day, the probe-hybridization solution was decanted into a 50 mL falcon tube and stored at – 20°C for future use. The membrane was then gently rinsed with a 2 × SSC and 0.1% SDS solution for 5 min at RT and thereafter rinsed twice with the 0.5 × SSC and 0.1% SDS solution for 15 min at 68°C. Thereafter, the membrane was washed with wash buffer for 5 min at RT, followed by a 30 min incubation at RT with 30 mL of 1 × blocking solution. The solution was decanted and thereafter replenished with 20 mL antibody solution for 30 min at RT. The membrane was then washed twice in wash buffer for 15 min and placed inside a hybridization bag (Thermo Scientific, United States) (DNA side facing up). One milliliter of Chloro-5-substituted adamantyl-1, 2-dioxetane phosphate (CSPD) was added to the bag and this was incubated for 10 min at RT. After which, the CSPD was wiped off the membrane, the bag was sealed and incubated at 37°C for 5 min (Lepp *et al*., 2010).

2.8.3. Developing X-Ray film

The hybridization bag containing the membrane was taped onto a hypercassette, on top of which an Hyperfilm X-Ray film (Amershan, South Africa) was laid. The hypercassette was closed and placed inside a darkroom (in which the entirety of the X-Ray development process was conducted). After 30 min, the film was removed and immersed in Developer (AGFA) for 2 min. The film was removed, rinsed in water and thereafter immersed in Fixer (AGFA) for 2 min. The film was then rinsed with water, air dried and viewed using a red light.

2.9. Growth kinetics analysis

2.9.1. Growth curve analysis

A growth curve examining the growth rates of the wild type and mutant *M. smegmatis* strains was established to determine if the *MSMEG3019* gene is implicated in mycobacterial growth. Ten milliliter starter cultures were set up for all strains/conditions, these were used as inoculum to start 50 mL cultures, each at an OD_{600nm} of 0.05 (using the 7205 UV/ Visible spectrophotometer (Jenway, United Kingdom)). These cultures were incubated at 37°C with shaking at 100 RPM, from which OD_{600nm} readings were taken every 3 h for a period of 24 h to monitor bacterial growth. The experiment was conducted in triplicates and the mean data was displayed as a scatter plot using GraphPad Prism 10. Unpaired student's t-tests were conducted to obtain p-values for the data to determine its significance.

2.9.2. Bacterial spotting assay

In order to observe the colony morphology and the effect of the target gene on bacterial growth, wild type and mutant strains were spotted onto solid agar in triplicates and qualitatively observed. Briefly, cultures were grown, with their respective antibiotics, to an OD_{600nm} of 0.8. Ten-fold serial dilutions of 10^0- 10^{-6} were made of each culture, from which 10 µL of each dilution was plated on 7H11 agar containing the appropriate supplements. Theses plates were incubated at 37°C for 2-3 days until bacterial growth was visible.

2.9.3. Biofilm formation

All mycobacterial strains were grown to an $OD_{600nm} > 2$ to ensure that the cells were in the stationary phase. The cells were harvested by centrifugation at 4 000 RPM for 10 min and they were thereafter washed twice with Sauton's media. The optical densities of the cultures were measured, and subsequently adjusted to an OD_{600nm} of 2. A ten-fold serial dilution of each of these cultures were made from 10^0 -10^{-5}. One hundred microliters of each dilution was added to a respective well in a 6-well plate, each well already containing 10 mL of Sauton's media. The plates were closed, sealed with parafilm and placed into a plastic bag sealed. This was placed into the incubator at 37°C for 5 days until the formation of a pellicle on the surface of the media was witnessed (Kulka *et al*., 2012).

2.9.4. Sliding motility

All mycobacterial strains were streaked on 7H11 plates (supplemented with the appropriate antibiotics) using the 4-way streak method in order to isolate individual colonies. These colonies were picked and placed at the center of a 7H9 agar plate, which was made using 7H9 media containing 0.25% agar and 0.5% glycerol. These plates were sealed with parafilm and incubated upright at 37°C for 1 week. Thereafter, bacterial growth was viewed and imaged (Martínez *et al*., 1999).

2.9.5. Scanning Electron Microscopy (SEM)

Fifty milliliters of all mycobacterial cultures were grown in 7H9 to an OD_{600nm} of 0.8. The cells were centrifuged at 4600 RPM for 10 min, the resultant supernatant was discarded and the harvested cells were washed twice with 1 mL Phosphate Buffered Saline (PBS). The cells were then centrifuged and resuspended in 500 µL of 2.5% glutaraldehyde in PBS and incubated overnight at 4°C. The cells were harvested by centrifugation at 8 000 RPM for 5 min, thereafter washed twice with 1 mL PBS and subsequently resuspended in 100 µL of 2% osmium tetroxide (diluted in PBS), followed by incubation at RT for 1 h. Thereafter, the cells were washed twice with 1 mL PBS, this was superseded by successive submersions for 2 min each in ethanol solutions of increasing concentrations: 30%, 50%, 70% and twice at 100%. This was conducted with intent to dehydrate the cells and was followed by storage of the cells at 100% ethanol at RT until use. The cells were then spotted on a filter and coated twice with carbon. The prepared cells were then viewed using the Zeiss Ultra Plus FEG SEM (Germany), at a magnification of 5 000 X, 10 000 X and 20 000 X, wherein the length and width of 100 cells were measured (Senzani *et al*., 2017). The cell measurements were analyzed and the mean data was displayed as a box and whisker plot using GraphPad Prism 10. Unpaired student's t-tests were conducted to obtain p-values for the data to determine if the difference in cell sizes were significant.

2.10. Antimicrobial susceptibility testing

The minimum inhibitory concentration (MIC) of various mycobacterial antibiotics was determined by use of the microbroth dilution assay conducted in 96-well plates. Antibiotic stocks of anti-TB drugs were formulated to be 4 × the initial concentration required as inoculum for the first row. One hundred microliters of these stocks were inoculated into row 1. Fifty microliters of 7H9 broth was added into each well from rows 2-12. Thereafter, 50 µL of the antibiotic stock from row 1 was aspirated, aliquoted into row 2 and mixed. Fifty microliters from row 2, was then aspirated, aliquoted into row 3 and mixed. This method of diluting the antibiotic stock continued sequentially until row 12 was reached, from which the extra 50 µL was aspirated and discarded. Overnight bacterial cultures of each strain was grown to an OD_{600nm} of 0.8 and thereafter diluted to an OD_{600nm} of 0.05 in 7H9 broth. Fifty microliters of each culture was added to their respective wells. Each dissolving solvent utilized to constitute the antibiotics served as negative controls, while the positive control entailed using 7H9 media only. The

susceptibility of each strain per antibiotic/control was conducted in triplicates, each with two independent replicates per condition. The plates were placed in a plastic bag and incubated at 37°C for 3 days. After incubation, 30 µL of 0.01% resazurin was added to each well and further incubated overnight to allow for colour change to occur. Colour change to pink can be interpreted as insufficient antibiotic to inhibit growth, whilst colour change to blue implies growth inhibition (Bento *et al*., 2021).

2.11. Bioinformatics analysis

Bioinformatics analysis was conducted using several online tools/websites:

M. tuberculosis H37Rv *Rv2568c* and *M. smegmatis* mc^2155 *MSMEG3019* gene sequences were obtained from Mycobrowser (https://mycobrowser.epfl.ch/). Biocyc, a genome database, was utilized to obtain the cistronic position of *MSMEG3019* (https://biocyc.org/). The domain of *MSMEG3019* was identified by use of KEGG (Kyoto Encyclopedia of Genes and Genomes) (https://www.genome.jp/kegg/). iTasser (Iterative Threading ASSEmbly Refinement) and D-I-Tasser (Deep learning-based Iterative Threading ASSEmbly Refinement) were the online tools utilized to predict *MSMEG3019* and *Rv2568c* protein function and crystal structure as well as identify crystal structures of other proteins similar to that of the query sequence (https://zhanggroup.org/I-TASSER/) (https://zhanggroup.org/D-I-TASSER/). PEPPI (Pipeline for the Extraction of Predicted Protein-protein Interactions) is an online program which was used to predict protein-protein interactions between genes present in the *MSMEG3019* operon (https://zhanggroup.org/PEPPI/).

2.12. Knockout mutants

In order to study gene function, the target gene needs to be deleted or suppressed, thus creating a mutant strain. This non-functional version of the gene needs to be examined and compared to the functional version which is present in the wild type strain. Provided that the site-directed mutations were correctly executed, any observable differences in the mutant strain can be attributed to the target gene. The gene deletion method utilized in this study was the two-step allelic exchange system which capitalizes on homologous recombination to replace the target endogenous gene with a mutant allele (Gordhan & Parish, 2001)

To facilitate allelic replacement, firstly, a suicide vector is genetically engineered to harbor a copy of the gene of interest with the intended mutation encased within flanking regions of DNA. This vector also contains selection markers and conditional lethal genes in order to enable selection and counter selection respectively (as per figure 2.1). The selection markers utilized in this study were the Kan^R gene and the *lacZ* gene. This facilitates uptake of the plasmid when grown in/on media containing Kan. Additionally, the *lacZ* gene, originating from *E. coli*, produces β-galactosidase, which cleaves X-Gal (5-bromo-4-chloro-3-indolyl-β-D-galactopyranoside), leading to the formation of a blue pigment. This blue-white selection aids in tracking the vector. This construct is incorporated into the genome of the

wild type bacteria and gives rise to the first cross over (FCO) event, as per figure 2.2. This results in a merodiploid state, in which the bacterium contains both the wild type and mutant alleles (Hmelo *et al*., 2015).

The counter selection is implemented to eject the plasmid along with the native gene. This is brought upon by employing the *sacB* gene, which is the counter selection gene present on the suicide vector, as per figure 2.1. The *sacB* gene encodes the enzyme levansucrase which is responsible for the hydrolysis of sucrose, which produces a toxic byproduct, thus killing the cells which express it. Therefore, this sucrose sensitivity renders *sacB* the ideal conditional lethal gene. The second cross over (SCO) event is achieved by plating the FCO merodiploid strain on media containing sucrose and anticipating the formation of a white colony. As per figure 2.2, the resultant colony will contain either only the wild type allele or the mutant allele; this is dependent on which genomic location the second crossover occurred (Hmelo *et al*., 2015).

2.13. Construction of knockout clone

2.13.1. Amplification of inserts

The *MSMEG3019* gene sequence, including upstream and downstream regions, were obtained from the online tool Mycobrowser and analyzed on Clone Manager Version 9 software. Primers were designed using the Primer3Plus website in order to amplify the upstream and downstream regions of *MSMEG3019* (Table 2.3). The primers contain restriction sites which correspond to the identified restriction enzymes required for the cloning process. Fusion of the upstream and downstream regions creates an inactive version of the gene which comprises only 6% of the original gene. Expasy Translate Tool was utilized to conclude that the gene deletion is in-frame as well as to confirm the absence of the initially identified domain and zinc binding motif, rendering the gene inactive. It is currently unconfirmed if *MSMEG3019* is a monocistronic gene or if it belongs to a four-gene-operon, of which it is the last gene. However, regardless of its cistronic layout, no interference with any downstream genes are expected.

M. smegmatis mc^2155 was grown on 7H11 plates for 2 days. The resultant mycobacterial lawn was scraped and utilized to conduct a CTAB gDNA extraction for subsequent amplification of target regions. PCR amplifications of the upstream and downstream fragments were conducted using Phusion high-fidelity DNA polymerase, with an optimized annealing temperature of 68.3°C. The PCR amplicons thereafter underwent gel electrophoresis using a 0.8% agarose gel in order to confirm amplification of correct regions. The reactions containing the correct amplicons were thereafter purified using the GeneJet Gel Extraction and DNA Clean Up micro kit. This resulted in clean upstream and downstream DNA, free of impurities and primer dimers. The DNA was quantified and stored at – 20°C until required.

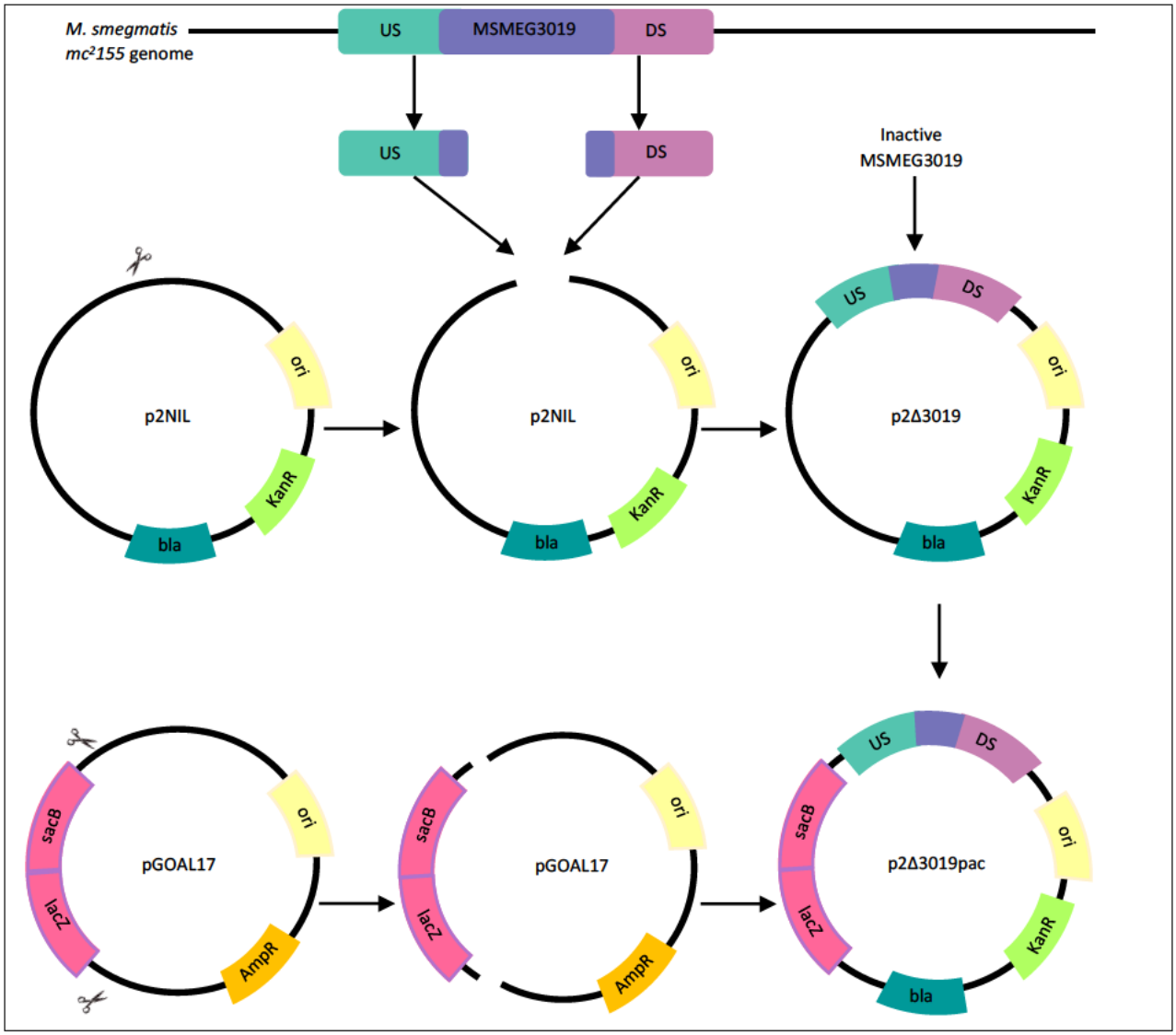

Figure 2.1. Illustrative representation of the steps taken towards the creation of the knockout vector. The process begins with obtaining the upstream (US) and downstream (DS) inserts, followed by insertion of them into a digested p2NIL vector (containing a *Kan*^{R} gene, an origin of replication in *E. coli* gene (*ori*) and a *bla* gene which encodes beta-lactamase). This gives rise to the plasmid p2Δ3019, into which the *PacI* cassette (containing the *sacB* and *lacZ* genes) is thereafter inserted, constructing the final knockout plasmid, p2Δ3019pac.

Table 2.3. Primers designed for amplification of upstream and downstream region of *MSMEG3019*

Region	Primer	Sequence	Properties of amplicon
Upstream	Forward	GCGCGCAAGCTTTCGCTGATCTACCAACTGGA	1228 bp amplicon of upstream region of *MSMEG3019* comprising 25 bp of the 5' region of *MSMEG3019*. Amplicon contains *HindIII* and *BglII* restriction sites on forward and reverse primers respectively.
	Reverse	GGGCCCAGATCTAGTTCGGGCACGTGAAGT	
Downstream	Forward	GCGCGCAGATCTGTTCGTGCACACCGTGAT	1010 bp amplicon of downstream region of *MSMEG3019* comprising 40 bp of the 3' region of *MSMEG3019*. Amplicon contains *BglII* and *PmlI* restriction sites on forward and reverse primers respectively.
	Reverse	GGGCCCCACGTGGATCAGTGCAGGCTCCAGAT	

2.13.2. Three-way cloning

Using the GeneJet Plasmid Midiprep Extraction Kit, the plasmid/vector p2NIL was extracted and thereafter quantified. One microgram of p2NIL vector plasmid DNA was digested with *PmlI* and *HindIII*. One microgram of the upstream insert DNA was double digested with *HindIII* and *BglII* and lastly, 1 µg of the downstream fragment was double digested with *BglII* and *PmlI*. These reactions were mixed by pipetting and incubated at 37°C overnight, followed by heat inactivation at 80°C for 20 min.

The digested vector p2NIL underwent dephosphorylation, whereas the digested insert fragments underwent phosphorylation. These reactions were thereafter heat killed at 75°C for 5 and 10 min respectively. Ligation ratios of vector: upstream insert: downstream insert used were 1:1:1, 1:3:3, 1:5:5 and lastly 1:0:0 wherein no insert DNA was added to the ligation reaction. This served as a digested vector only control and was utilized to examine the efficiency of the vector restriction digestion and dephosphorylation i.e. as an estimate of how many colonies form as a result of vector recircularization instead of insert uptake.

The ligation reactions were incubated for 2 h at 22°C and thereafter heat inactivated at 65°C for 10 min, in order to improve transformation efficiency. Simultaneously, chemically competent *E. coli* DH5α cells were prepared using the calcium chloride method and were stored on ice until ready to use. The entirety of every ligation reaction was each added to 100 µL of competent cells. A competent cell only control was generated, in which no DNA was added, this served as a negative control for the transformation protocol. The positive control was created by adding 1 µg of unrestricted p2NIL plasmid DNA. All experimental DNA samples and control samples underwent transformation via heat shock at

42°C for 90 sec followed by incubation on ice for 2 min. The cells were rescued and thereafter plated on NA containing Kan and were incubated at 30°C for 2 days.

Resultant colonies were selected on the basis that the control plates were as expected (negative control contained no colonies, positive control contained a substantial amount of colonies and the vector only control contained little to no colonies). The most well established single colonies on the experimental plates were selected for screening using a sterile loop and inoculated into 2 mL of nutrient broth containing 2 µL of Kan and incubated at 37°C overnight with shaking at 180 RPM. Using these overnight cultures of individual colonies, plasmid miniprep extractions were conducted. All of the resultant DNA underwent screening via restriction digestion using the enzymes *SmaI* and *PvuI*. The restriction reactions were then run on a 0.8% agarose gel. Provided the expected bands (determined on clone manager V9 to be 2384, 2348, 2171 and 94 bp) corresponded to the bands obtained on the gel, the three-way-cloning could be deemed successful and this recombinant p2NIL plasmid carrying the *MSMEG3019* deletion was named p2Δ3019.

2.13.3. Insertion of *PacI* cassette

Using the GeneJet Plasmid Midiprep Extraction Kit, the DNA of the plasmid pGOAL17 was extracted and thereafter quantified. One microgram each of pGOAL17 and p2Δ3019 plasmid DNA was digested with *PacI* restriction enzyme. This was incubated at 37°C overnight. Subsequently, the restriction digestions were heat killed, the p2Δ3019 vector was dephosphorylated and the liberated *PacI* cassette from pGOAL17 (containing the *lacZ* and *sacB* genes) was phosphorylated. The *PacI* cassette was ligated to the p2Δ3019 vector at 22°C for 2 h in the ratios of 1:1, 1:3 and 1:5 (by use of a thermal cycler (Biorad, T100)). A vector only control was also conducted to determination the proportion of self-circularization. The ligations were transformed into chemically competent *E. coli* DH5α cells via heat shock at 42°C for 90 sec. Subsequent to rescuing the cells, they were plated on NA containing Kan and 80 µg/mL X-Gal and incubated at 30°C for 2 days.

A positive clone was determined by the formation of a blue colony, as it would present a blue coloured phenotype if uptake of the *PacI* cassette occurred and would only be present if conferred the Kan resistance gene present in p2Δ3019. Blue colonies were picked using a sterile loop and used as inoculum for overnight cultures, which underwent DNA miniprep extractions and successive restriction digestion screening to confirm the genotype of the plasmid as well as determine orientation of the insert. The clones were screened using *EcoRI* and displayed the correct bands which resembled the *in silico* expectations (7133, 3594, 1863 and 766 bp). This recombinant p2NIL plasmid carrying the *MSMEG3019* deletion allele and *PacI* cassette was named p2Δ3019pac.

2.13.4. Sucrose sensitivity of clone

Prior to using the *sacB* gene for allelic exchange, it requires to be tested while still present in *E. coli* to ensure lethality of the gene to corroborate reliability of the system when creating the mutant. The plasmid p2Δ3019pac was grown overnight in nutrient broth supplemented with Kan. The sucrose sensitivity of the plasmid was thereafter tested by conducting the spotting assay, using different dilution factors of the culture (10^0- 10^{-6}) and plating 10 µL of each dilution onto three types of agar: (1) LA containing X-Gal and Kan, (2) LA containing X-Gal, Kan and 5% sucrose and (3) LA containing X-Gal and 5% sucrose. The plates were then placed into a plastic bag, sealed and incubated at 30°C for 2 days. The result was deemed positive if bacterial growth on plate (1) was blue and plate (3) was white and the growth on plate (2) was white and formed little/no colonies. Once sucrose sensitivity of the plasmid was confirmed, p2Δ3019pac plasmid DNA was extracted using the GeneJet Plasmid Midiprep Extraction Kit and thereafter quantified and stored at -20°C.

2.14. Creation of knockout mutant strain

2.14.1. FCO event

Fifty milliliters of an mc^2155 culture was grown overnight at 37°C with shaking at 180 RPM. Upon reaching log phase (OD_{600nm} 0.6-0.8), the cells were subjected to a series of successive washes in 10% glycerol in order to induce competency. Simultaneously, p2Δ3019pac DNA was UV treated in preparation for electroporation. Differing amounts of this DNA (1 µg, 3 µg, 5 µg) was added to the competent cells, electroporated and thereafter incubated at 37°C on 7H11 agar supplemented with Kan and X-Gal until the formation of blue colonies. The blue phenotype present is indicative of the FCO event, as the colonies shall only appear blue if the cells incorporate p2Δ3019pac into their genome and as a result, express the *lacZ* gene. This merodiploid strain was labelled MΔ3019FCO.

2.14.2. SCO event

The resultant blue MΔ3019FCO colonies were picked and grown overnight at 37°C with shaking at 180 RPM in 10 mL of 2 × TY broth supplemented with Kan. One milliliter of this culture was inoculated into 10 mL of fresh 2 × TY broth (without antibiotics), which was grown overnight at 37°C with shaking. This culture was used to create a 10-fold serial dilution (10^0-10^{-6}), of which 100 µL of each dilution factor was plated onto (1) 7H11 agar containing X-Gal, Kan and 2% sucrose and (2) 7H11 agar containing X-Gal and 2% sucrose. The plates were incubated at 37°C for 3-5 days, until the emergence of blue and white colonies on plate (2). The white phenotype witnessed is indicative of the SCO event, resulting in the loss of the plasmid, ergo loss of *lacZ* gene function, and consequential reversion to a wild type state or the desired knockout mutant state.

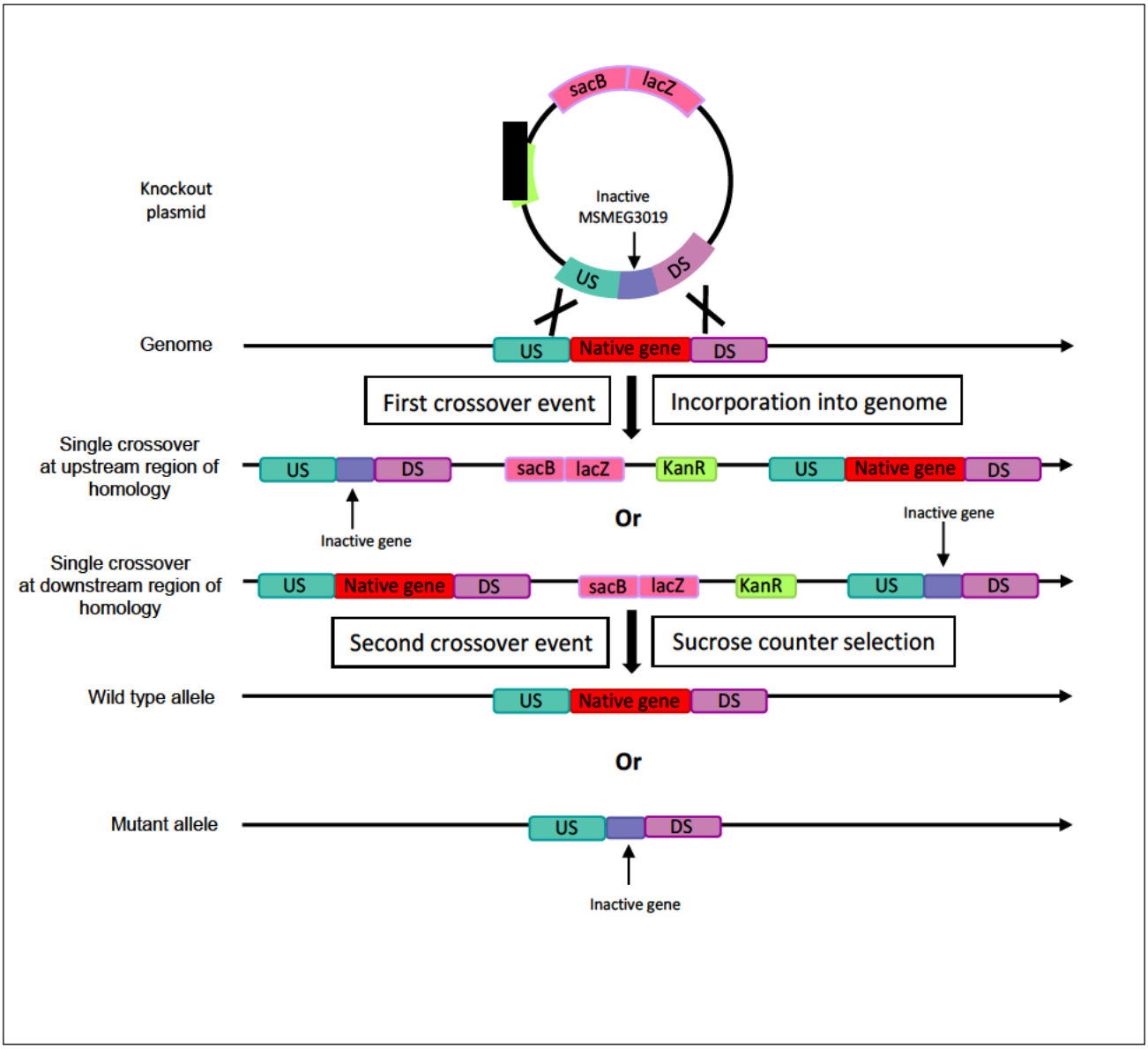

Figure 2.2. Depiction of the first and second crossover events leading up to the creation of the mutant strain. The knockout plasmid integrates into the *M. smegmatis* mc^2155 genome via homologous recombination at either flanking site, facilitating the first crossover. The sucrose counter selection gives rise to the second crossover event, which produces a mutant strain or causes reversion to a wild type state.

2.14.3. Confirmation of knockout genotype

2.14.3.1. PCR screening

White colonies were picked and plated on 7H11 agar with and without Kan, using the gridded streak plating method. This was done to eliminate any strains that retained the plasmid (selection conferred by the Kan resistance gene present on the plasmid) yet still appeared white, which is representative of a mutation in the *lacZ* gene. Colonies that grew on the plain 7H11 plates but not on the 7H11 + Kan plates were picked and thereafter underwent gDNA extraction using the colony boil method. The DNA was utilized for DreamTaq PCR wherein primers were designed in order to differentiate between a wild type

and mutant genotype. As per table 2.4, the forward primer for both genotypes is the same and binds upstream *MSMEG3019*, therefore the binding site shall be present in spite of successful gene deletion.

However, the reverse primers bestow the differentiation: one primer is designed to bind within the target gene and one primer is designed to bind after the gene. The reverse primer which binds within the gene shall only produce a PCR product if that specific complementary sequence is present; provided successful gene deletion has occurred, the sequence would not be present. Accordingly, a wild type strain would contain that specific complementary sequence and would facilitate formation of that PCR product, whereas a mutant strain would only contain the binding site which occurs downstream the target gene. Both reverse primers were added to all PCR reactions and PCR was conducted at an annealing temperature of 63.8°C. The resultant amplicons were run on a 0.8% agarose gel and analyzed to infer which strains were present.

Table 2.4. Screening primers designed for detection of either mutant or wild type strain

Strain	**Forward primer**	**Reverse primer**	**Amplicon properties**
Wild type	GACGTGGCACCG TACGAG	ATGACACCGTT CTCGTGACC	492 bp amplicon signifying presence of wild type gene due to reverse primer binding within the *MSMEG3019* gene sequence.
Mutant		GATCCTAGGA ACGCCTTCGG	277 bp amplicon signifying gene deletion due to reverse primer binding after the *MSMEG3019* gene sequence.

2.14.3.2. Southern blotting

Once PCR screening confirmed deletion of the target gene, Southern blotting was the subsequent step to confirm if integration of the knockout construct is at the correct genomic position. Genomic DNA extraction of the wild type and mutant strains were conducted using the CTAB DNA extraction method. This gDNA was thereafter restricted with the enzyme *BglII*, and used for Southern blotting. The probe was created using the downstream forward and reverse primers as per table 2.3. Clone manager v9 was utilized to determine *in silico* expected band sizes for the wild type and mutant strain. Verification attained from the Southern blot implied successful creation of a knockout mutant strain, harboring an inactive version of the *MSMEG3019* gene. This mutant strain was named MΔ3019 and stored at – 80°C for further analysis.

2.15. Complementation

Accurate and proper characterization of a gene goes beyond simply creating a knockout mutant strain. Further analysis is required to verify that any phenotypic differences observed can be attributed to only the deleted target gene and not any unintended repercussions due to off-target effects (Arras *et al*., 2015). This is accomplished by "complementing" the mutant strain. Complementation of a knockout mutant strain entails reintroducing the active/native form of the gene into the genome of the mutant strain with the intent to reinstate gene function. The complementation strain thereafter undergoes phenotypic and growth kinetics analysis alongside the wild type and mutant strains in order to confirm restoration of the target gene, which is indicative of successful mutagenesis (Arras *et al*., 2015). Complementation may also aid in identifying if the target gene interacts with other genes, in its vicinity, in order to bring about phenotypic change, however, since *MSMEG3019* is either a single gene or the last gene of an operon, no second site polar effects are expected.

The complementation system utilized in this study involved the use of an integrating plasmid vector (pMV306h) harboring a wild type copy of the target gene (the entirety of the gene and its native promoter). Integration of this plasmid into the genome of the mutant strain results in the creation of the complement strain.

To account for the uncertainty surrounding *MSMEG3019's* cistronic status and therefore its promoter region, two complementation strains were created, each containing different promoter regions. It is hypothesized that the promoter regions are present either at 400 bp upstream *MSMEG3019* or 400 bp upstream the first gene of the operon (*MSMEG3016*) that *MSMEG3019* is presumed to be a part of. The construction of the two complementation alleles involved amplifying the respective promoters (*MSMEG3019* and *MSMEG3016*) and fusing it upstream *MSMEG3019*, giving rise to the corresponding plasmids and strains named "p" and "+6p".

2.15.1. Complement plasmid 1 (pMV3019+6p): *MSMEG3016* promoter

Phusion PCR was conducted using the primers specified in table 2.5 to amplify the promoter region of *MSMEG3016* and the *MSMEG3019* gene, using an annealing temperature of 62°C and 67.8°C respectively. The PCR reactions were run on a 0.8% agarose gel to confirm amplification of the correct product. The PCR reactions were thereafter purified using the GeneJet Gel Extraction and DNA Clean Up micro kit.

One microgram of pMV306h DNA was doubled digested with *NotI* and *EcoRV*. In addition, the *MSMEG3016* promoter amplicon was digested with *NotI* and *HindIII* and lastly, the *MSMEG3019* gene was digested using *EcoRV* and *HindII*. All reactions were mixed by pipetting and incubated at 37°C overnight, followed by heat inactivation at 80°C for 20 min.

The digested vector was dephosphorylated while the two inserts were phosphorylated. The inserts were ligated to the vector using molar rations of 1:1:1, 1:3:3 and 1:5:5. After incubation at 22°C for 2 h, the ligation reactions were transformed into chemically competent *E. coli* DH5α using the heat shock method. The cells were then plated on NA containing Hyg and incubated at 37°C overnight.

Resultant colonies were picked, underwent miniprep DNA extraction and successive restriction digestion screening using the enzyme *HindIII*. Successful complementation plasmid 1 clone DNA would display 4621 bp and 1024 bp bands when run on an agarose gel and was then called pMV3019+6p.

Table 2.5. Primers designed for amplification of components for the creation of the different complementation plasmids

Region	**Primer**	**Sequence**	**Properties of amplicon**
MSMEG3016 promoter	Forward	GCGCGCGCGGCCGCATGGGTATCAAAGTGGCGCT	400 bp amplicon of promoter region of *MSMEG3016* gene. Amplicon contains *NotI* and *HindIII* restriction sites on forward and reverse primers respectively.
	Reverse	GGGCCCAAGCTTACAGTTCACCCGGACCCGAG	
MSMEG3019	Forward	GCGCGCAAGCTTATGCGTGACTTCACGTGCCC	1029 bp amplicon containing entirety of *MSMEG3019* gene. Amplicon contains *HindIII* and *EcoRV* restriction sites on forward and reverse primers respectively.
	Reverse	GGGCCCGATATCTCAGGCCGAGGTCACCTCGT	
MSMEG3019 + respective promoter	Forward	GCGCGCGCGGCCGCTCCGGTTCGACGACGATTTC	1429 bp amplicon of *MSMEG3019* gene inclusive of promoter region 400 bp upstream. Amplicon contains *NotI* and *EcoRV* restriction sites on forward and reverse primers respectively.
	Reverse	GGGCCCGATATCTCAGGCCGAGGTCACCTCGT	

2.15.2. Complement plasmid 2 (pMV3019p): *MSMEG3019* promoter

Phusion PCR was conducted using the primers specified in table 2.5 to amplify *MSMEG3019* and its promoter region (400 bp upstream) with an annealing temperature of 72°C. The PCR reactions were thereafter purified using the GeneJet Gel Extraction and DNA Clean Up micro kit.

One microgram of pMV306h DNA and 1 µg of the *MSMEG3019+p* amplicon was doubled digested with *NotI* and *EcoRV* and incubated at 37°C overnight, followed by heat inactivation at 80°C for 20 min.

The digested vector was dephosphorylated and the insert was phosphorylated. The insert was ligated to the vector using molar rations of 1:1, 1:3 and 1:5 and thereafter transformed into competent *E. coli* DH5*α* cells which were plated on NA containing Hyg and incubated at 37°C overnight.

Resultant colonies were picked, underwent miniprep DNA extraction and successive restriction digestion screening using the enzyme *PstI*. Successful complementation plasmid 2 clone DNA would display 4932 bp and 753 bp bands when run on an agarose gel and was labelled pMV3019p.

2.15.3. Creation and screening of complementation strains

Plasmid extractions were conducted on the complementation plasmids pMV3019+6p and pMV3019p. The resultant DNA was thereafter subjected to sodium acetate DNA precipitation. These plasmid DNA samples were UV treated and thereafter added to the knockout mutant strain, MΔ3019, which had already been made competent using the 10% glycerol method. The DNA was added in respective amounts of 1, 3 and 5 µg and was then electroporated into the cells. After the cells were rescued and incubated, a ten-fold serial dilution from 10^{0}-10^{-4} was conducted in order to obtain individual colonies after incubation. One hundred microliters of the 10^{-4} dilution was plated on 7H11 agar supplemented with Hyg and incubated at 37°C for 3 days, giving rise to the complementation strains MComp9+6p (containing plasmid pMV3019+6p) and MComp9 (containing the plasmid pMV3019p).

Colonies for each of the two strains were picked and streaked onto 7H11 with Hyg plates. After incubation for 2 days at 37°C, the bacterial growth was scraped and used as inoculum for the CTAB gDNA extraction protocol. The gDNA for both strains was thereafter screened for the presence of the *MSMEG3019* gene by use of DreamTaq PCR at an annealing temperature of 60°C. The forward primer (TTCACGTGCCCGAACTGC) and reverse primer (ATGACACCGTTCTCGTGACC) was designed to produce a 452 bp product. The amplicons were run on a 0.8% agarose gel and visualized for presence of the gene, which provided genotypic confirmation that the two complementation strains were correctly constructed.

3. Results

3.1. Bioinformatics analysis of *MSMEG3019* and *Rv2568c*

Due to the lack in research of mycobacterial zinc metalloproteases, many basic aspects of its biological data remain unexplored, thus creating obstacles when interpretation of genomic data is required. Therefore, in order to identify potential gene function, extensive bioinformatics analyses were conducted using multiple platforms.

The first step of gene characterization is to obtain biological context provided by the gene layout within the genome (Alberts *et al*., 2002). An operon is a cluster of consecutive genes that contains genetic information that may code for functionally related proteins (Wang *et al*., 2021). Genes in close proximity/genes that comprise an operon could be co-regulated and functionally related, ergo, identification and analysis of neighboring genes provides insight on the expression and biological role of the target gene (Alberts *et al*., 2002). Additionally, evaluation of operons/surrounding genes allows for identification of the promoter region of the target gene. In the case of operons, the promoter may be located at the beginning of the operon and may be accountable for the transcription of multiple genes downstream. However, internal promoters may also be present upstream individual gene/s within an operon (Wang *et al*., 2021).

To obtain a schematic representation of the target genes *MSMEG3019* in mc^{2}155 and *Rv2568c* in *Mtb* and their corresponding neighboring genes and promoter regions, the online tool Biocyc was utilized to display the transcriptional units containing the genes. Figure 3.1 shows the Biocyc output for *Rv2568c* and *MSMEG3019* respectively.

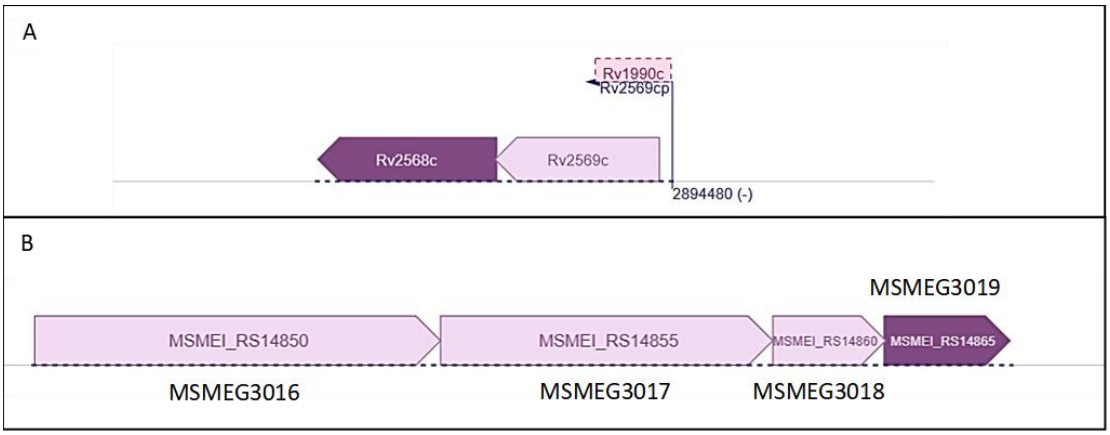

Figure 3.1. Biocyc analysis hypothesizing the location of target genes **(A)** *Rv2568c* and **(B)** *MSMEG3019* in relation to surrounding genes, in addition to displaying their promoter regions (presented as a red dashed-line box above an arrowhead).

Figure 3.1 (A) shows that the *Rv2569c*'s promoter regulates both genes: *Rv2569c* and *Rv2568c*. This implies that *Rv2568c* belongs to a two-gene operon, of which, it is the second gene. However, due to the uncharted nature of mycobacterial zinc metalloproteases, there is no annotated promoter for

MSMEG3019 nor is there concise determination if its surrounding genes are operonic or simply neighboring (figure 3.1 (B)). Therefore, to account for both possibilities, it is hypothesized that the promoter is present either upstream *MSMEG3019* or upstream *MSMEG3016*.

Neighboring genes often function collectively to produce a specific phenotype, therefore it is important to study the interaction between genes in close proximity (Rao *et al*., 2014). This could be especially helpful if the neighboring genes are well characterized, as it can aid in refining the target gene's regulation, expression and function. Due to the possibility of protein-protein interactions between the target genes and their corresponding adjacent genes, Kegg and PEPPI were utilized to identify their annotations and to predict protein-protein interactions respectively (table 3.1)

Table 3.1. Kegg and PEPPI analyses predicting the annotations and protein-protein interactions between target genes and their respective neighboring genes

Organism	**Target gene**	**Neighboring genes**	**Annotation**	**Log(LR)**	**Interaction**
M. smegmatis	*MSMEG3019*	*MSMEG3016*	Transglutaminase	-0.719	No
		MSMEG3017	ATP-grasp enzyme	-0.249	No
		MSMEG3018	Transglutaminase	0.065	Yes
M. tuberculosis	*Rv2568c*	*Rv2569c*	Transglutaminase	0.048	Yes

The neighboring genes of *MSMEG3019* and *Rv2568c* have annotations that insinuate their functions, but are uncharacterized in mycobacteria (table 3.1). A negative Log(LR) value returned by PEPPI implies no interaction between the two query genes, therefore it can be said that *MSMEG3016* and *MSMEG3017* do not interact with *MSMEG3019*. However, *MSMEG3018* and its genetic ortholog *Rv2569c* (both of which are transglutaminases and located upstream the target genes *MSMEG3019* and *Rv2568c* respectively) present a positive Log(LR) value. Log(LR) values of 0.065 and 0.048 are relatively low, however its mere presence suggests potential relevance and should not be disregarded (Bell *et al*., 2022).

The next step of gene characterization is domain identification. A domain refers to a specific sequence of amino acids that correspond to a particular function (Liu *et al*., 1999). Therefore, identification of domains in unknown proteins/enzymes could help elucidate their function. The domains present in *MSMEG3019* and *Rv2568c* were identified using the online tool Kegg and are listed in table 3.2.

Table 3.2 dictated that both orthologs consist of zinc ribbons and zinc-binding metalloprotease domains. All four results contain low E-values, indicating that the results are reliable and significant (Smith & Pease, 2017). It is probable that both domains contribute to different functions of each enzyme.

Table 3.2. Identification of functional domains within the zinc metalloprotease orthologs *MSMEG3019* and *Rv2568c* (Kegg)

Orthologs	Functional Domain	E-value
Rv2568c	Zinc-binding metalloprotease	1.5e-101
	Zinc ribbon	5.8e-17
MSMEG3019	Zinc-binding metalloprotease	3.2e-102
	Zinc ribbon	1e-26

In table 3.2, it can be seen that the zinc-binding metalloprotease domain displays a higher degree of conservation in *MSMEG3019* and is therefore more of a principal feature of the enzyme. However, this finding does not disregard the functionality of the zinc ribbon present in *MSMEG3019*; it is, however, not the focus of this study.

In addition to domain identification, bioinformatics analysis of the crystal structure of an unknown protein could help identify its function. This is due to protein structural homology corresponding to functional homology (Ogura *et al*., 2001). This implies that functional identification could be narrowed down by generating a crystal structure of the unknown protein and searching for similar crystal structures of other established proteins in a database. The function of the resultant protein matches could be similar to that of the target protein. The online tool iTasser was utilized to render the crystal structures of *MSMEG3019* and *Rv2568c*, which was thereafter utilized as a query to search for pre-existing crystal structures in the PDB database: these results are displayed in figure 3.2.

Figures 3.2 (A) and (B) depict the well-folded, compacted crystal structures of *MSMEG3019* and *Rv2568c* respectively. The structures mainly consist of α-helices with the slight occurrence of β-sheets. The loops that are present on both structures could possibly contain the active site residues of the zinc metalloproteases i.e. the catalytic zinc ion that catalyzes the hydrolysis of peptides (Heinemann *et al*., 2021). Additionally, the unstructured regions with minimal folding (such as red ends of the structures) could potentially be involved in signaling or interactions, such as that with the substrate (Wright & Dyson, 2009).

Figure 3.2 (C) reveals the proteins with highest structural homology to that of *Rv2568c* and *MSMEG3019*. *MSMEG3019* is closest related to a zinc metalloprotease present in *Bacteroides caccae*, with a TM alignment score of 0.63. Interestingly, *Rv2568c* is also structurally similar to this gene. *B. caccae* is an opportunistic pathogen of the intestine, seldomly causing anaerobic bloodstream infection (Nakjang *et al*., 2012). The second highest hit of *MSMEG3019* is the human oxireductase, which is involved in redox reactions wherein it facilitates the transfer of electrons to detoxify compounds (Boichot *et al*., 2023). Lastly, *MSMEG3019* is structurally similar to dicer hydrolases from the intestinal parasite *Giardia intestinalis*. Both catalytic zinc metalloproteases and hydrolases belong to the category of hydrolytic enzymes, implicating a similar function but with varying substrates and active sites (Liao *et al*., 2014).

Rv2568c has the highest alignment score with anthrax lethal factor, a zinc metalloprotease produced by *Bacillus anthracis*, which is a fatal disease (Quinn *et al*., 2004). Additionally, the homolog mu1, is an outer capsid protein, which generally confers protection and viability to viruses, such as the orthoreovirus, which causes disease of the upper respiratory tract and gastroenteritis (Liemann *et al*., 2002). Unfortunately, the only shared protein between *MSMEG3019* and *Rv2568c* is unknown, and its annotation could have clarified the function of these zinc metalloproteases.

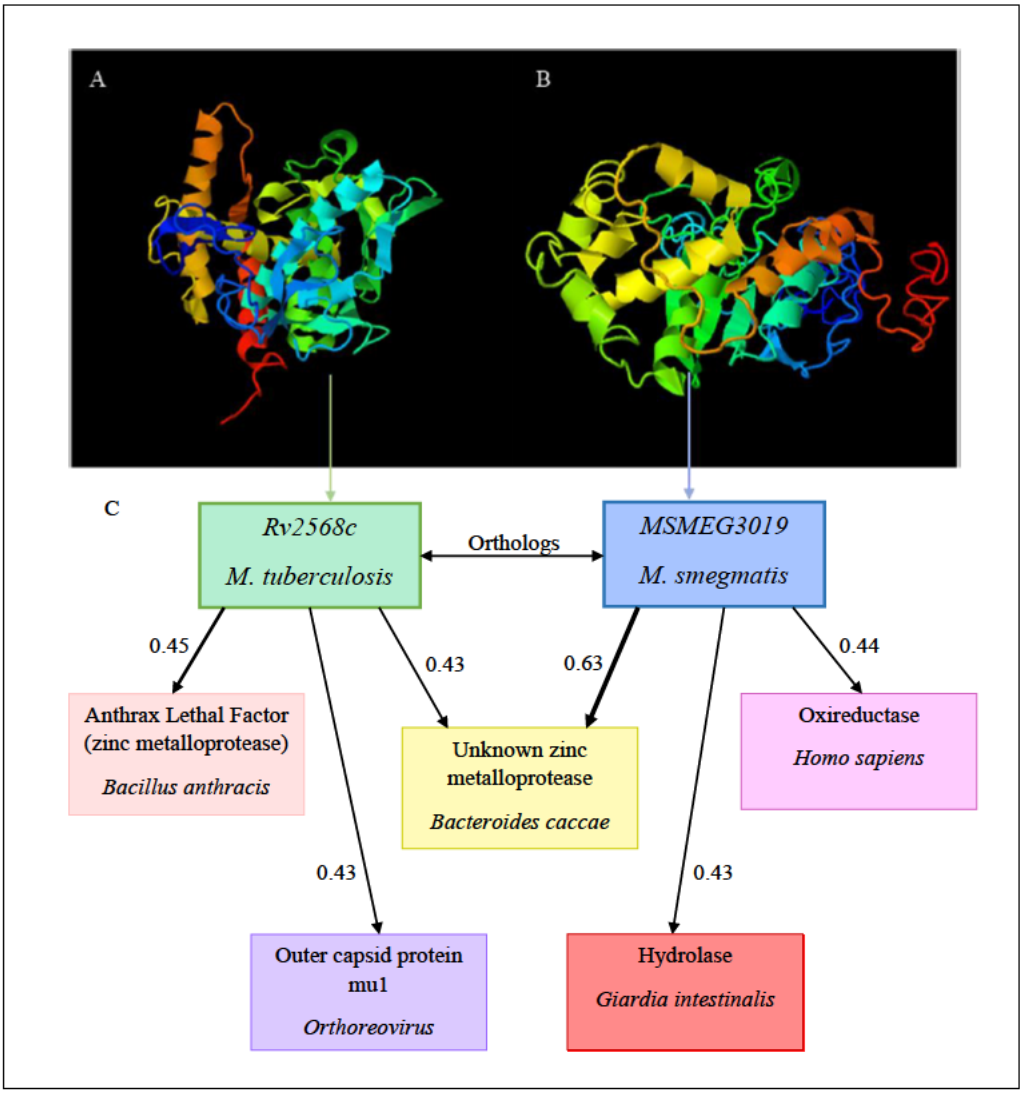

Figure 3.2. iTasser results depicting predicted protein crystal structures and other identified related proteins with structural homology. **(A)** Crystal structure of *MSMEG3019*. **(B)** Crystal structure of *Rv2568c*. **(C)** Identification of structurally similar proteins in relation to the target gene orthologs, inclusive of the TM-score of the structural alignment and the respective organisms containing the related protein (Yang & Zhang, 2015).

3.2. Construction of deletion mutant

Bioinformatics analysis suggests that *Rv2568c* could hypothetically contribute to *Mtb* virulence (due to its structural homologs being mediators of pathogenesis). *Rv2568c's* potential implication in virulence would make it the subject of future *Mtb* studies in order to elucidate its function. If evidence supporting the hypothesis of its virulence is found, it would render *Rv2568c* a possible drug target. Therefore, the

first phase of research would be to investigate its ortholog *MSMEG3019* in the model organism *M. smegmatis* as a faster, cheaper and safer alternate (Sparks *et al*., 2023). Characterization of unknown genes involves substituting the native gene with a truncated version of the gene. The gene deletion system utilized in this study was the two-step allelic exchange system, which entails constructing an inactive version of the gene on a plasmid and capitalizing on bacterial homologous recombination for incorporation of this construct into the genome. Subsequently, the use of conditional lethal genes on the plasmid facilitate removal of the native gene (Gordhan & Parish, 2001).

3.2.1. Construction of cloning vectors

Using Clone manager v9, the zinc-binding motif (amino acid sequence of HEXXH) of the zinc-binding metalloprotease domain in *MSMEG3019* was identified and PCR primers were designed to amplify flanking upstream and downstream regions, which excluded the identified motif. These upstream and downstream regions were cloned into the plasmid p2NIL, as stipulated in sections 2.13.1 and 2.13.2, giving rise to the truncated version of *MSMEG3019*. Preliminary restriction digestion screening was conducted using *SmaI* and *PvuI* (data not shown) to identify a correct clone. This selected knockout recombinant plasmid thereafter underwent multiple restriction digestions (restriction profiling) in order to validate its accuracy in comparison to its *in silico* model, as depicted in figure 3.3.

A

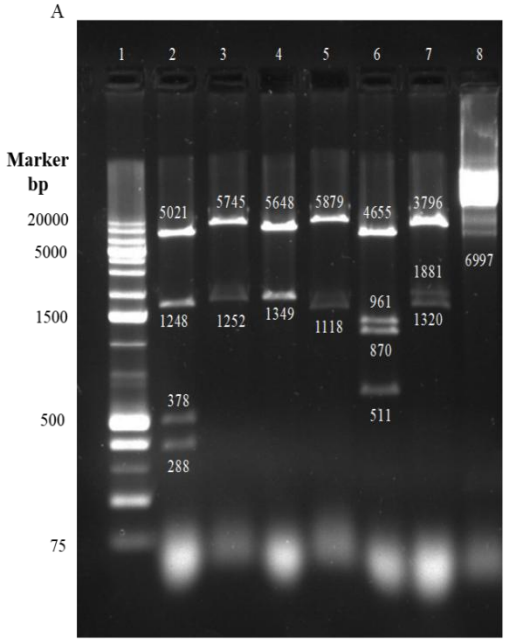

B

Lane on gel	Restriction enzymes	Expected sizes (bp)
2	*BamHI*	5021, 1248, 378, 288, 62
3	*EcoRI, EcoRV*	5745, 1252
4	*BglII, EcoRI*	5648, 1349
5	*BsrGI, BglII*	5879, 1118
6	*EagI*	4655, 961, 870, 511
7	*NotI, PstI*	3796, 1881, 1320

C

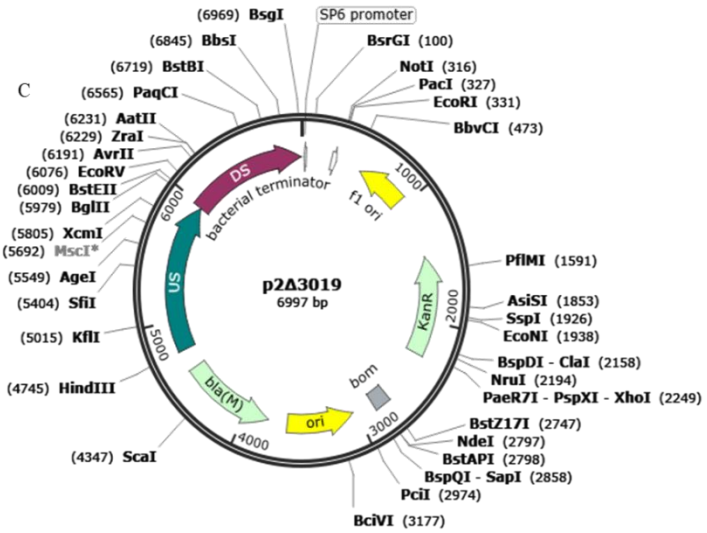

Figure 3.3. Restriction profile of recombinant plasmid p2Δ3019. **(A)** Agarose gel depicting the result of p2Δ3019 restriction profiling, **[lane 1]** GeneRuler 1 kb plus marker, **[lane 8]** uncut plasmid DNA and **[lanes 2-7]** the result of various restriction digestions as outlined in table **(B)**, which includes the expected fragment sizes and their respective restriction enzymes. **(C)** Plasmid map of p2Δ3019 exhibiting the fused upstream (US) and downstream (DS) flanking regions, forming the mutant allele, which was cloned into the p2NIL backbone.

Restriction profiles of p2Δ3019 shown in figure 3.3 (A) corresponded to the expected fragment sizes stipulated in figure 3.3 (B). This provided evidence to substantiate the genetic congruency between the created recombinant plasmid and its *in silico* model.

Subsequently, selection markers and conditional lethal genes from the plasmid pGOAL17 were incorporated into p2Δ3019 in order to facilitate the allelic exchange. The *PacI* cassette in pGOAL17, which contains the genes *sacB* and *LacZ*, was excised by restriction digestion using the enzyme *PacI*. This insert was cloned into the plasmid p2Δ3019 as per section 2.13.3. Preliminary restriction digestion screening was conducted using *EcoRI* (data not shown) to identify a correct clone. The resultant recombinant plasmid containing the inactive allele, the *PacI* cassette and the Kan^R gene was termed p2Δ3019pac and underwent restriction profiling, as seen in figure 3.4.

B

Lane on gel	Restriction enzymes	Expected sizes (bp)
2	*PstI*	5696, 4298, 2042, 1320
3	*BsrGI*	6997, 4611, 1748
4	*EcoRI*	7133, 3594, 1863, 766
5	*KpnI*	5375, 5197, 1622, 1132, 30
6	*HindIII*	9910, 3680, 739
7	*BglII, EcoRI*	5648, 3594, 1863, 1485, 766

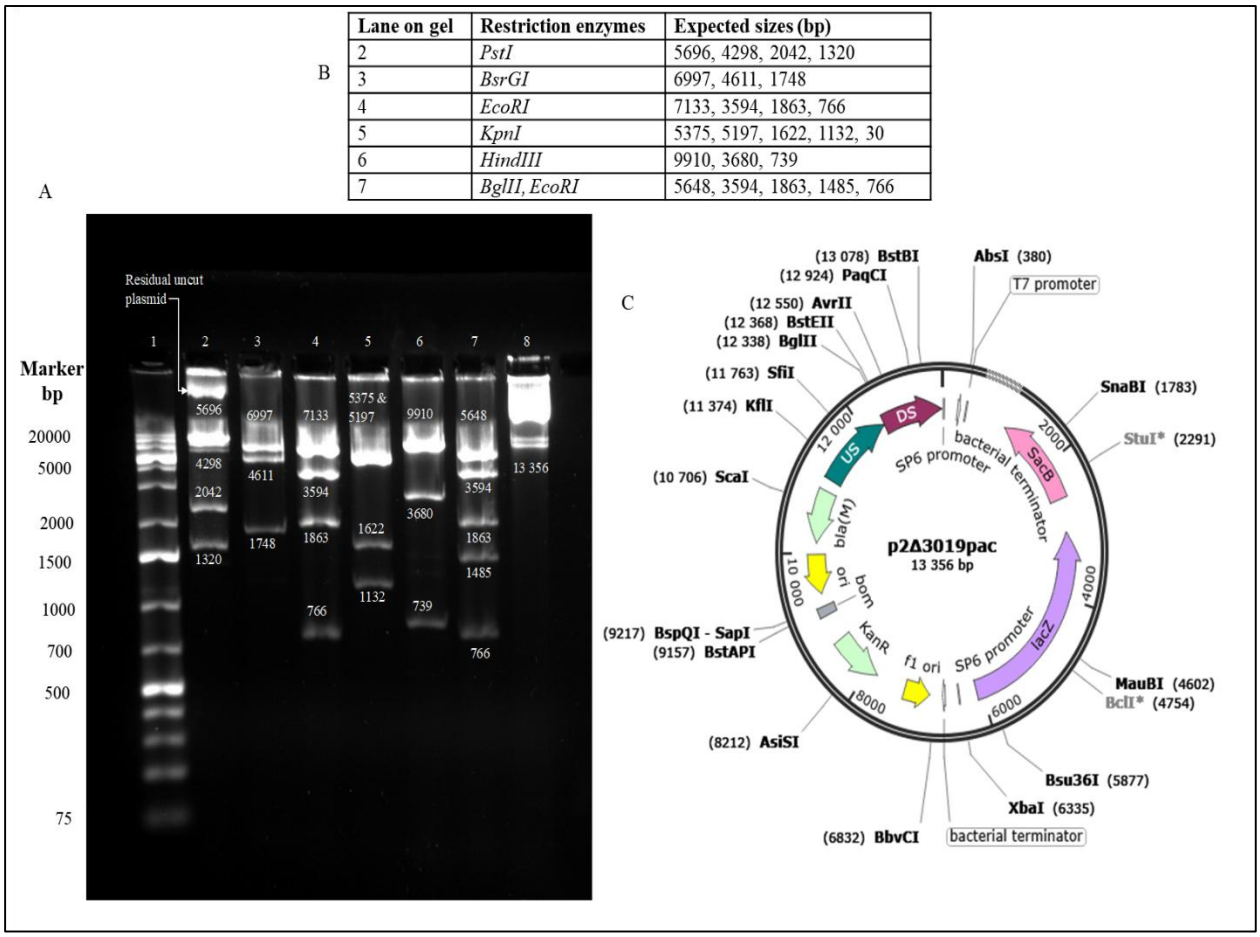

Figure 3.4. Restriction profile of plasmid p2Δ3019pac. **(A)** Agarose gel depicting the result of p2Δ3019pac restriction profiling, **[lane 1]** GeneRuler 1 kb plus marker, **[lane 8]** uncut plasmid DNA and **[lanes 2-7]** the result of various restriction digestions as outlined in table **(B)**, which includes the expected fragment sizes and their respective restriction enzymes. **(C)** Plasmid map of p2Δ3019pac exhibiting insertion of *sacB* and *lacZ* genes into the p2Δ3019 plasmid which contains the knockout mutant *MSMEG3019* allele.

The restriction profile of p2Δ3019pac displayed in figure 3.4 (A) corresponded to the expected fragment sizes stipulated in figure 3.4 (B). Lane 2 of the agarose gel in figure 3.4 (A) shows some undigested plasmid DNA, however, that is potentially due to suboptimal restriction digestion of the particular enzyme utilized (*PstI*) and does not reflect the genetic accuracy of the plasmid construct. Since the recombinant plasmid was confirmed to be constructed as per its *in silico* model, the plasmid thereafter underwent testing to ensure proper functioning of the genes encoded within it.

The *E. coli* DH5α cells containing the plasmid p2Δ3019pac were plated on NA with differing supplements (sucrose, X-Gal and Kan) to test the sensitivity of the s*acB* gene to sucrose as per section 2.13.4, the results of which are displayed in figure 3.5. Testing this system in *E. coli* allows for examination of the effect that the selection markers and conditional lethal genes have on bacterial growth, as this would indicate if the genes present on p2Δ3019pac are functional.

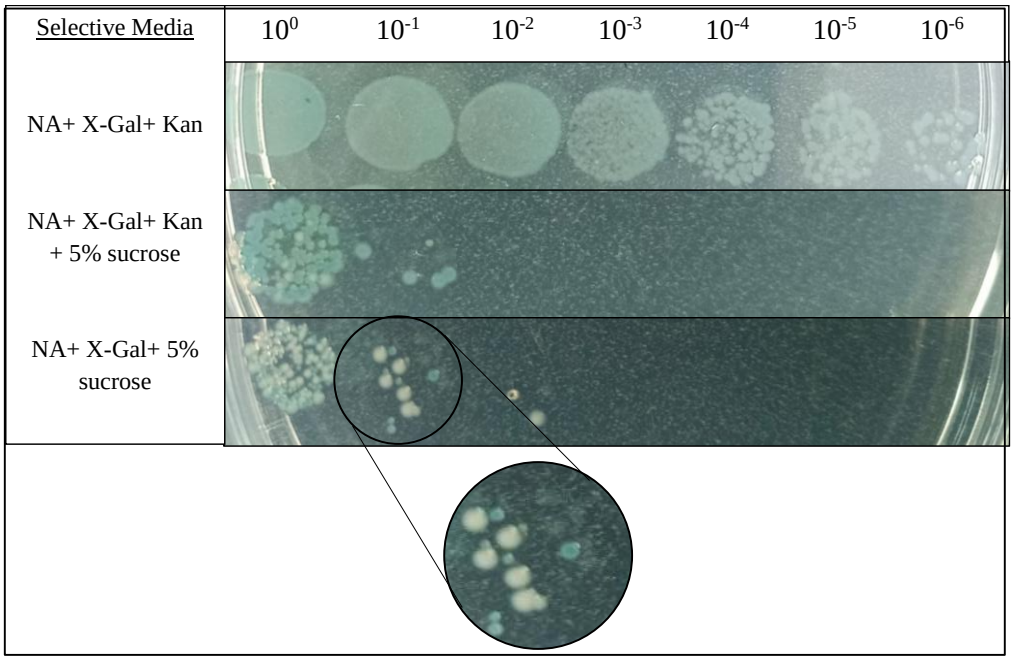

Figure 3.5. Sucrose sensitivity test of the *E. coli* DH5α strain carrying the knockout construct p2Δ3019pac. Decreasing dilutions of the strain was spotted onto three different types of agar in order to assess the effect of plasmid retention on bacterial growth.

As per figure 3.5, it can be seen that when no selective pressure is present (NA+ X-Gal+ Kan), the cells exhibit normal growth in blue, as expected. However, the introduction of sucrose results in the production of the toxic byproduct, which causes growth inhibition due to the introduction of cellular pressure to eject the plasmid. Conversely, when Kan is present in the media, it pressures the cells into keeping the plasmid due to the Kan^R gene. These cellular responses to varying substrates causes growth variations and respective colour changes, which represents different plasmid retention states. Therefore, the presence of sucrose, but not Kan, results in inhibited growth of white colonies, representing the loss of p2Δ3019pac. The results obtained from the sucrose sensitivity test exhibit the sensitivity of the *sacB*, *lacZ* and Kan^R genes to their respective substrates. Proper functioning of these genes confirms that

p2Δ3019pac shall be able to facilitate the allelic exchange and can therefore be introduced into the mycobacterial genome.

3.2.2. Two-step homologous recombination

Allelic exchange was accomplished (as per section 2.14) by electroporating the plasmid p2Δ3019pac into competent mc^2155 cells, leading to the formation of blue colonies when plated on X-Gal, due to expression of the *lacZ* gene present on the construct (FCO). The sucrose-induced SCO on agar containing X-Gal and sucrose resulted in the formation of white colonies. These white colonies could either be the desired mutant strain or a reverted wild type strain. However, it is also possible for the plasmid to obtain a mutation in its *lacZ* or *sacB* gene and cause the formation of a white colony which still retained the plasmid. Fortunately, plasmid retention would confer resistance to Kan and this mechanism was utilized as the first phase of screening. To capitalize on the growth characteristic provided by the presence of Kan^R, all the produced white colonies were streaked onto 7H11 agar with and without Kan to assess the plasmid retention state, the result of which is depicted in figure 3.6.

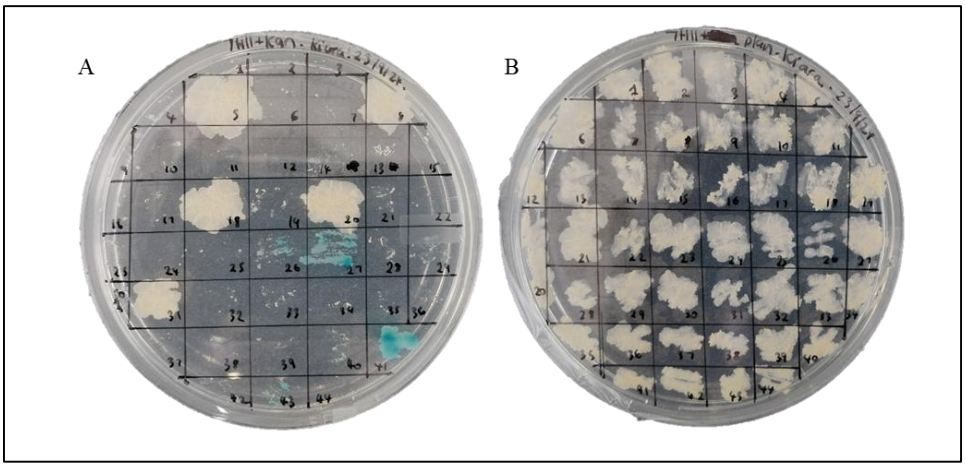

Figure 3.6. Gridded streak plate method as the first stage of mutant screening to identify incorrect mutants based on mutated *lacZ* and/or *sacB* gene. **(A)** 7H11 agar containing Kan and X-Gal which only supports the growth of cells which contain the plasmid. **(B)** Plain 7H11 agar supporting the growth of all mycobacterial cells.

The colonies that formed on the 7H11 agar supplemented with Kan (figure 3.6 (A)) represent strains which still contain the plasmid and possibly incurred a mutation in its *lacZ* or *sacB* gene. Therefore, a mutant or wild type strain was narrowed down to colonies that grew on the plate shown in figure 3.6 (B) but not on the plate shown figure in 3.6 (A). This newly refined pool of colonies were utilized for gDNA extraction via the colony boil method. This gDNA then underwent PCR screening to differentiate between wild type and mutant genotypes by the use of different reverse primers with specialized binding sites (displayed in figure 3.7).

Figure 3.7 (B) displays the PCR screening outcome. Lanes 3 and 7 display a 277 bp band which represents the presence of only the mutant allele in the mycobacterial genotype. Lanes 2 and 4, which display only a 492 bp band, indicate reversion to wild type state. Two colonies which retained the

plasmid after the SCO event (colonies formed in figure 3.6 (A)) were included in the PCR (Lanes 5 and 6) as a control to determine if both the native and inactive alleles were present as expected, in order to track the recombination events and validate the theoretic accuracy of the exchange system.

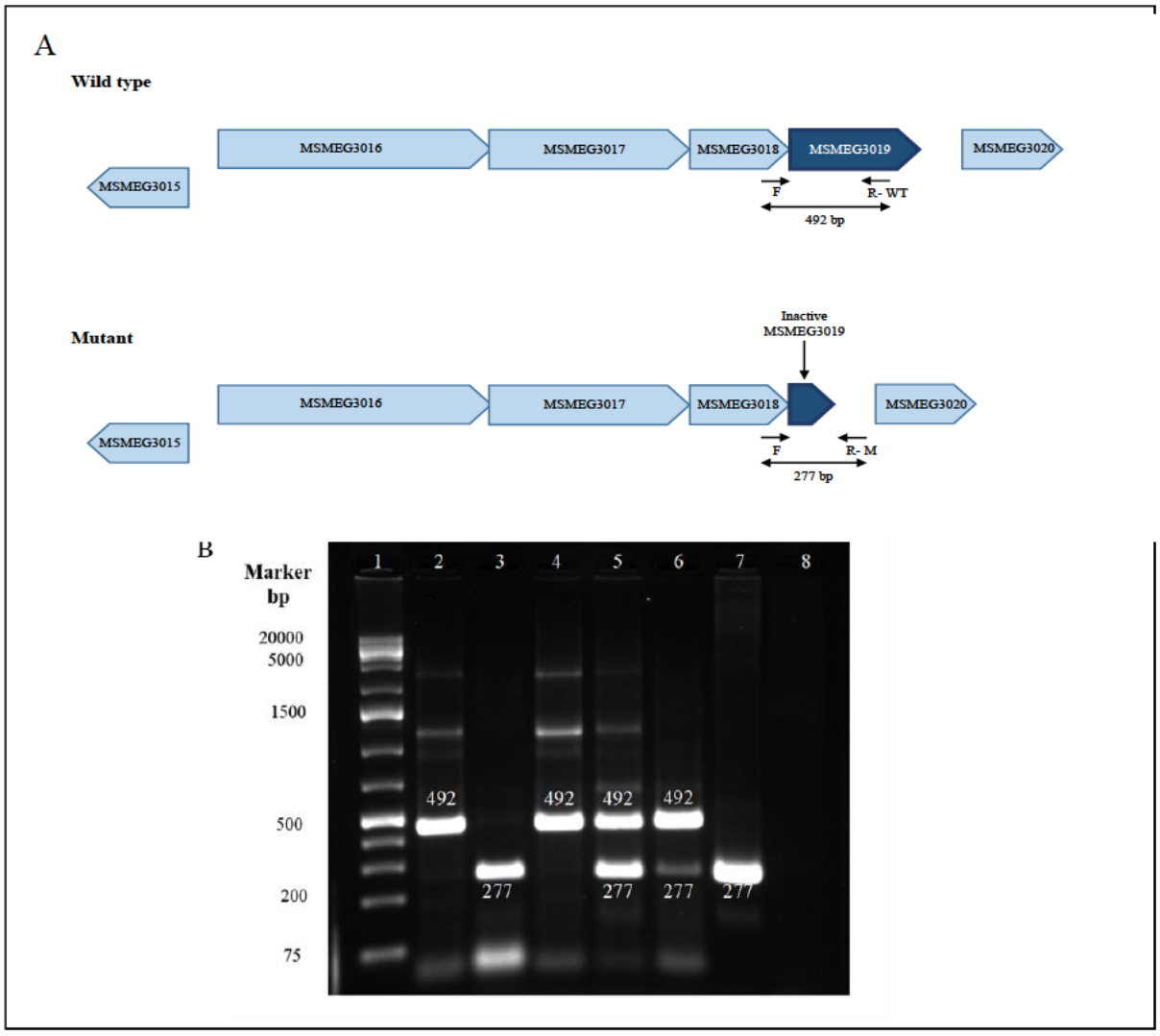

Figure 3.7. PCR screening to differentiate between wild type and mutant strains. **(A)** Diagram of the wild type and mutant alleles surrounded by neighboring cells displaying the primer binding sites. The forward primer binds to sequences before the target gene on both genomes, whereas the mutant reverse primer (R-M) and wild type reverse primer (R-WT) have different complementary sequences within and after the gene respectively. **(B)** Agarose gel showing PCR screening of a few prospective colonies. [**Lane 1**] GeneRuler 1 kb plus marker, [**lane 2**] wild type genotype, [**lane 3**] mutant genotype, [**lane 4**] wild type genotype, [**lane 5**] merodiploid state, [**lane 6**] merodiploid state, [**lane 7**] mutant genotype and lastly, [**lane 8**] contains a no-template control PCR reaction.

The colonies that presented the mutant allele were further screened to ensure incorporation of the mutant allele at the correct genomic location. This was accomplished by Southern blotting as per sections 2.8 and 2.14.3.2 and displayed in figure 3.8.

Figure 3.8 (B) displays the southern blot of the five potential mutant strains. Lanes 1-5 all contain the correct genotype, as stipulated by figure 3.8 (A), confirming the site-specific integration of the mutant

allele, without any interference of surrounding genes. Additionally, the gDNA of the wild type strain produced a distinct 9970 bp band, as expected. Screening for a correct mutant strain was deemed successful due to figures 3.7 (B) and 3.8 (B). The mutant strain was named MΔ3019 and was thereafter subjected to complementation and subsequent phenotypic examination.

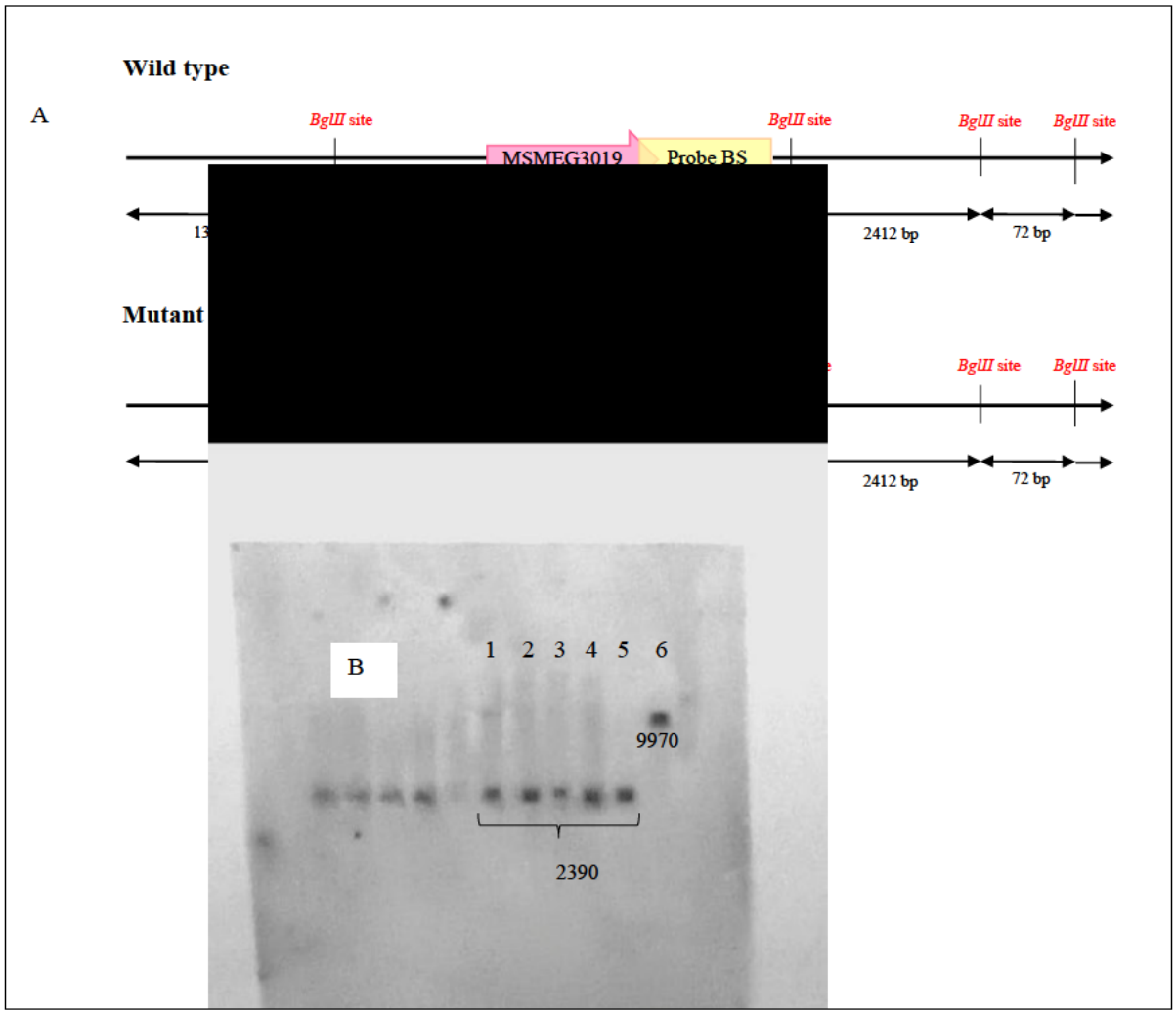

Figure 3.8. Southern blot analysis of the mutant strain **(A)** Visualization of the wild type and mutant alleles along with their respective genomic maps, digested fragments using *BglII* and the Probe Binding Site (Probe BS). Circled in red is the expected size of the radioactive labelled fragments for both genotypes (9970 bp fragment represents a wild type genome, while a 2390 bp fragment represents a mutant) **(B)** Southern blot displaying the fragments bound by the probe, **[lanes 1-5]** display 2390 bp bands (mutant genotype), whereas **[lane 6]** is the wild type control showing a 9970 bp band.

3.3. Complementation

Complementation of MΔ3019 was achieved by the use of the integrating vector, pMV306h. The *MSMEG3019* gene along with its hypothesized promoter regions (*MSMEG3016* promoter and *MSMEG3019* promoter) were reintroduced into the mutant strain. This was conducted with the intent of reinstating gene function to confirm that the mutant phenotype can be attributed to the loss of the target gene, instead of any off-target effects.

3.3.1. Construction of complementation plasmids

The first complement plasmid was constructed using the promoter region of *MSMEG3016* and the *MSMEG3019* gene, which was amplified by PCR and subsequently cloned into the plasmid pMV306h as per the section 2.15.1. The resultant colonies were subjected to preliminary restriction digestion screening using *HindIII* (data not shown) to identify a correct clone. The resultant recombinant plasmid, containing the *MSMEG3016* promoter region upstream the target gene was termed pMV3019+6p and underwent restriction profiling, as per figure 3.9, in order to confirm sequence accuracy.

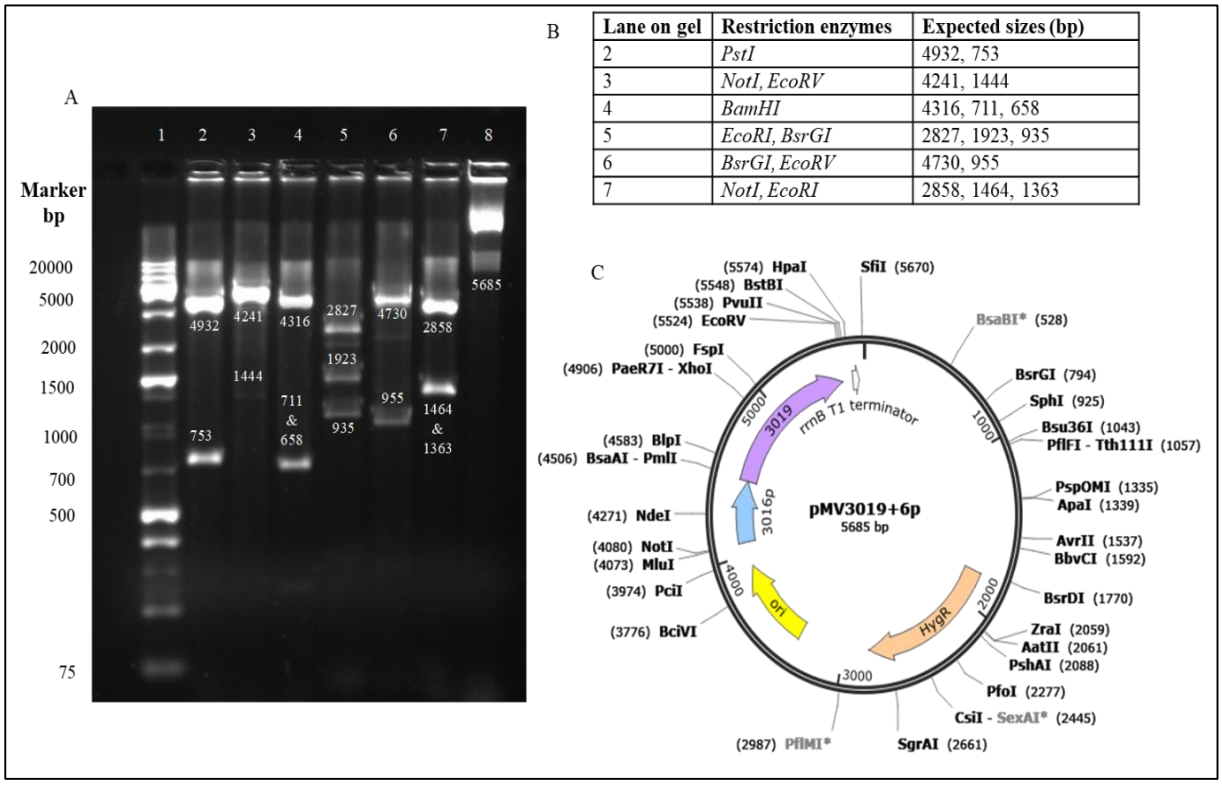

Lane on gel	Restriction enzymes	Expected sizes (bp)
2	*PstI*	4932, 753
3	*NotI, EcoRV*	4241, 1444
4	*BamHI*	4316, 711, 658
5	*EcoRI, BsrGI*	2827, 1923, 935
6	*BsrGI, EcoRV*	4730, 955
7	*NotI, EcoRI*	2858, 1464, 1363

Figure 3.9. Restriction profile of plasmid pMV3019+6p. **(A)** Agarose gel depicting the result of pMV3019+6p restriction profiling, **[lane 1]** GeneRuler 1 kb plus marker, **[lane 8]** uncut plasmid DNA and **[lanes 2-7]** various restriction digestions as outlined in table **(B)**, which includes the expected fragment sizes and their respective restriction enzymes. **(C)** Plasmid map of pMV3019+6p exhibiting the promoter region of *MSMEG3016* (3016p) fused upstream *MSMEG3019* (3019) and cloned into the plasmid pMV306h.

Restriction profiles of pMV3019+6p shown in figure 3.9 (A) corresponded to the expected fragment sizes stipulated in figure 3.9 (B). This provided evidence to substantiate the genetic fidelity of the recombinant plasmid and confirmed that the plasmid was constructed as per its *in silico* model.

The second complementation plasmid was created using *MSMEG3019* and the region 400 bp directly upstream (its second hypothesized promoter region). These regions were amplified by PCR and subsequently cloned into the plasmid pMV306h as per the section 2.15.2. The resultant colonies were subjected to initial restriction digestion screening using *PstI* (data not shown) to identify a correct clone. The resultant recombinant plasmid, containing the *MSMEG3019* gene and its respective promoter

region was named pMV3019p and underwent restriction profiling, as per figure 3.10, in order to confirm its genetic integrity.

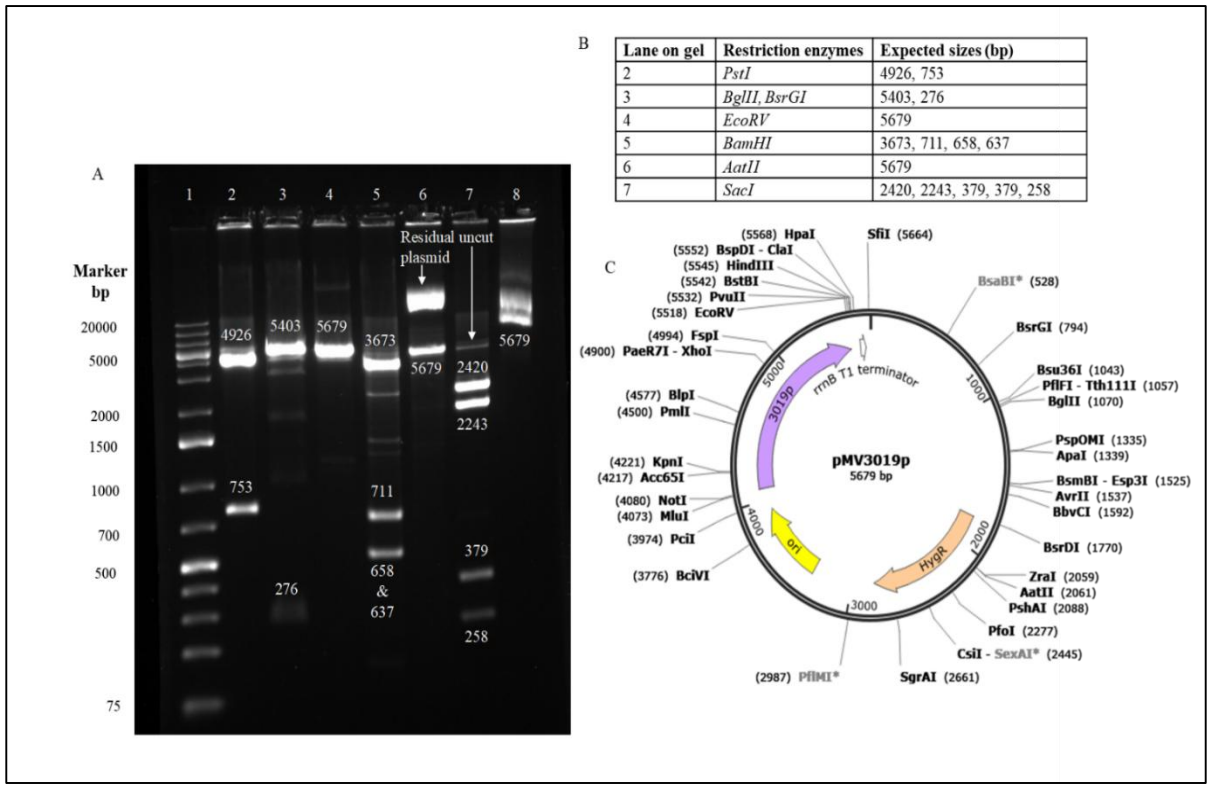

Lane on gel	Restriction enzymes	Expected sizes (bp)
2	*PstI*	4926, 753
3	*BglII, BsrGI*	5403, 276
4	*EcoRV*	5679
5	*BamHI*	3673, 711, 658, 637
6	*AatII*	5679
7	*SacI*	2420, 2243, 379, 379, 258

Figure 3.10. Restriction profile of pMV3019p. **(A)** Agarose gel depicting the result of pMV3019p restriction profiling, **[lane 1]** GeneRuler 1 kb plus marker, **[lane 8]** uncut plasmid DNA and **[lanes 2-7]** various restriction digestions as outlined in table **(B)**, which includes the expected fragment sizes and their respective restriction enzymes. **(C)** Plasmid map of pMV3019p exhibiting *MSMEG3019* and its promoter region (3019p) cloned into the plasmid pMV306h.

Restriction profiles of pMV3019p shown in figure 3.10 (A) resembled the expected band sizes specified in figure 3.10 (B). This provided evidence to support the genetic accuracy of the recombinant plasmid and confirmed that it was constructed as per its *in silico* model. Lanes 6 and 7 display some unexpected bands, which are the result of partial digestion by the enzymes *AatII* and *SacI* respectively.

3.3.2. Complementation of MΔ3019 strain

The complementation vectors pMV3019+6p and pMV3019p were electroporated into competent MΔ3019 cells, as outlined in section 2.15.3. Resultant colonies were picked and underwent gDNA extraction via the colony boil method. The gDNA was utilized for PCR screening using primers designed to amplify a region within the *MSMEG3019* gene. The agarose gel depicting the PCR amplicons are shown in figure 3.11.

PCR screening of the complementation strains were confirmed by the amplification of the desired 452 bp product, as seen in lanes 2 and 3 of figure 3.11. This implied incorporation of the native gene into

the genome of the mutant, therefore complementing it. The complementation strains, named MComp9+6p and MComp9 (signifying incorporation of pMV3019+6p and pMV3019p respectively) were thereafter examined for a variety of phenotypic attributes in conjunction with the wild type and mutant strain.

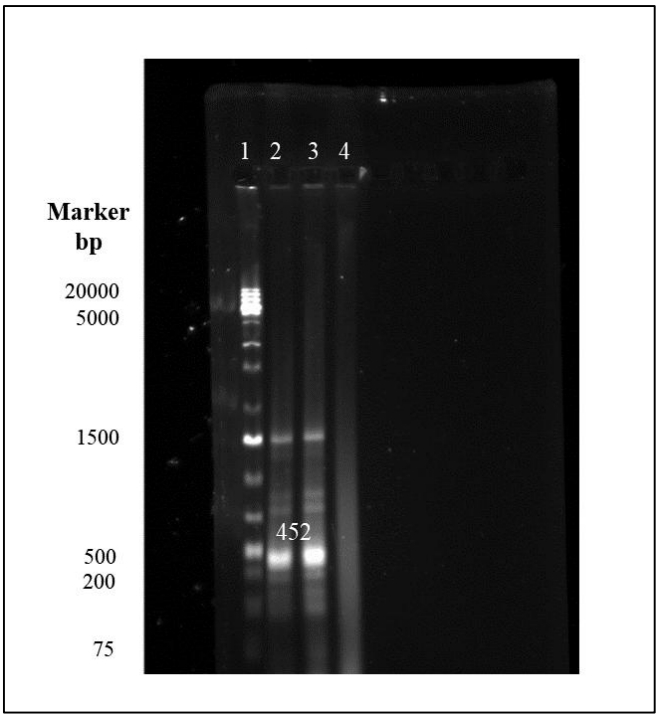

Figure 3.11. PCR screen for the presence of *MSMEG3019* in the gDNA of the two complementation strains. A 452 bp amplicon signifies amplification of the correct region.

3.4. The role of *MSMEG3019* on mycobacterial growth

In order to elucidate the function of *MSMEG3019* on mycobacterial physiology, the wild type mc^{2}155, the deletion mutant MΔ3019 and complement strains (MComp9+6p and MComp9) were subjected to a series of assays, in which the growth, motility, response to unfavorable conditions and antimicrobial tolerance was examined.

3.4.1. *MSMEG3019* does not significantly affect growth rate

Analyzing mutant bacterial growth rates enables the extrapolation of the target gene's role in vital cellular functions (Krishnamurthi *et al*., 2021). This evaluation can provide key insights and serve as a foundational step in determining whether *MSMEG3019* is involved in cellular metabolism, biosynthesis, nutrient uptake or other processes which are critical for bacterial growth (Hall *et al*., 2014). Growth rate analysis of the mycobacterial strains were conducted as per section 2.9.1, the results of which are shown in figure 3.12.

The growth curves (figure 3.12) depict a unanimous growth rate amongst all four strains during lag phase, until approximately 9 h. Thereafter, MΔ3019 and mc^{2}155 grow at a steady, common pace until

18 h, after which the growth rate of mc^{2}155 surpasses MΔ3019. Both of these strains thereafter reached stationary phase, as depicted by the plateau in the amount of cells present during 21-24 h. Despite being considered non-significant, the p-value dictating the difference between MΔ3019 and mc^{2}155 at 21 h was very low. This finding, in conjunction, with the result of stationary phased being induced at a lower OD_{600nm} for MΔ3019, compared to mc^{2}155, may implicate *MSMEG3019* in bacterial growth during the latter part of exponential phase and stationary phase, however not significantly. The two complementation strains, MComp9+6p and MComp9, grew at a slower rate compared to MΔ3019 and mc^{2}155. While the calculated p-value determined this slower growth non-significant, it is visible that these complementation strains were still in exponential growth while MΔ3019 and mc^{2}155 had reached the stationary phase.

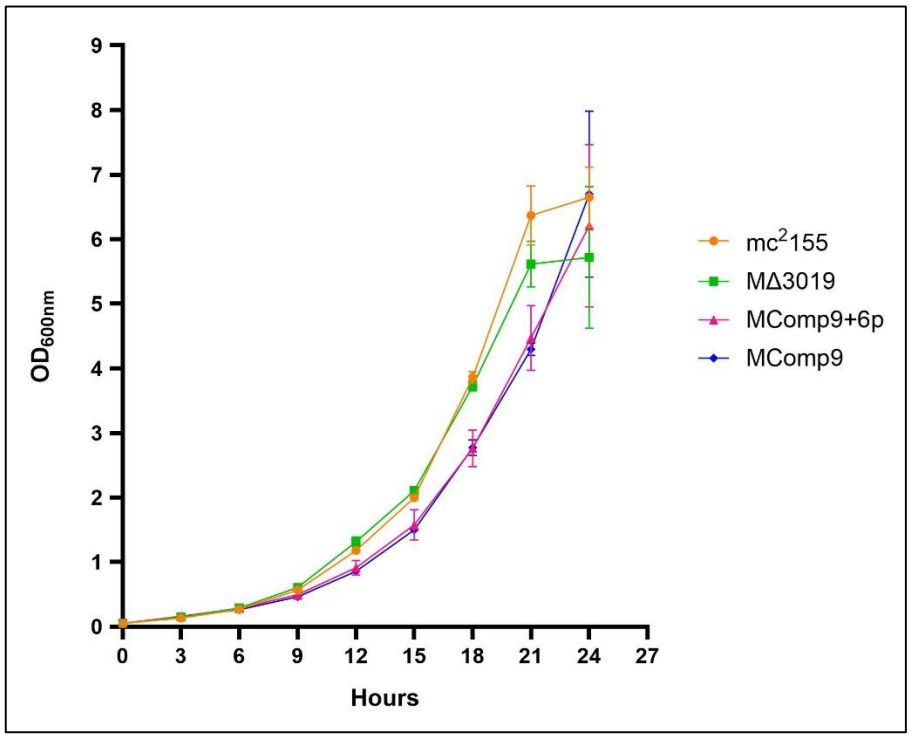

Figure 3.12. Growth rate analysis of MΔ3019 in comparison to mc^{2}155, MComp9+6p and MComp9 over a period of 24 h. Although there is no significant difference in the growth rates, MΔ3019 appears to reach stationary phase at a lower OD_{600nm}.

3.4.2. *MSMEG3019* influences the length and width of mycobacterial cells

Microscopy offers observation of bacterial cell morphology and structural features such as shape, size, orientation and cellular division (Salton & Kim, 1996). Examination and comparison of the phenotypic characteristics between the wild type and mutant strain may help relate *MSMEG3019* to functions involved in determining cellular structure. Therefore, SEM analysis of the four mycobacterial strains was conducted. The strains were grown to exponential phase, harvested and prepared using the method stipulated in section 2.9.5. The cells were thereafter transported to a microscopy facility (The MMU at

UKZN Westville) for imaging using the Zeiss Ultra Plus FEG SEM microscope, the resultant images are shown in figure 3.13

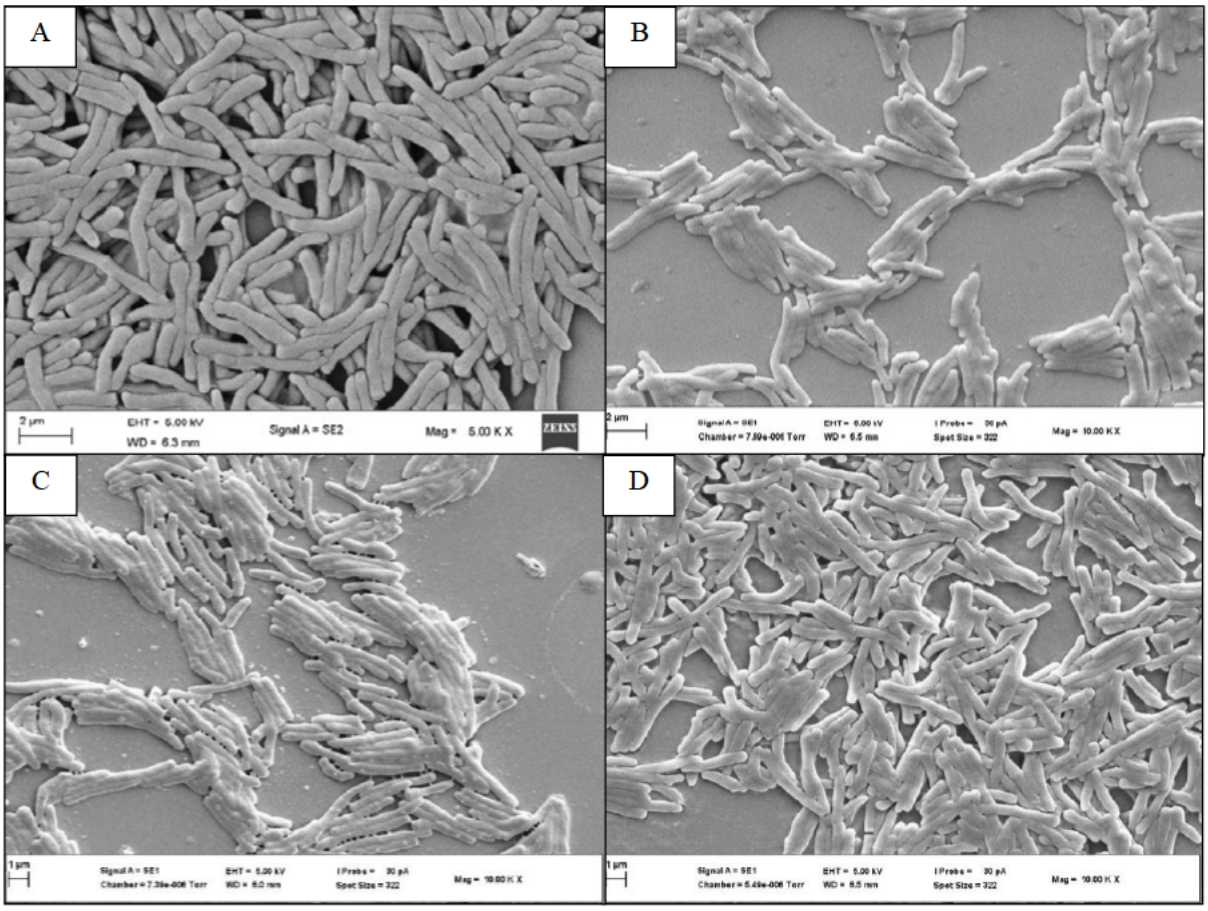

Figure 3.13. SEM images showing surface topography of cells belonging to the strains **(A)** mc^{2}155 **(B)** MΔ3019 **(C)** MComp9+6p **(D)** MComp9, viewed using the Zeiss Ultra Plus FEG SEM.

SEM analysis of the four strains showed no difference in the surface topography of mycobacterial cells. All cells displayed in figures 3.13 (A), 3.13 (B), 3.13 (C) and 3.13 (D) present the distinct rod-shaped characteristic of mycobacteria with no aberrant features. However, quantitative analysis is required to deduce if *MSMEG3019* plays a role in determining cellular size. Therefore, the length and width of 100 cells from each strain were measured and displayed as box and whisker plots in figure 3.14.

The data in figure 3.14 (A) shows that MΔ3019 displays the highest magnitude of cell length recorded. The p-value between the lengths of mc^{2}155 and MΔ3019 was < 0.01, indicating that the difference is significant. The complementation strains also differ from the wild type strain in length, however to different degrees of significance. Additionally, the cell width of mc^{2}155 is significantly larger than that of MΔ3019 and MComp9+6p with a p-value of 0.01 and 0.001 respectively. There is no significant difference in width between mc^{2}155 and MComp9.

The key finding obtained from the SEM analysis is that mycobacterial cells with a non-functional *MSMEG3019* gene exhibits increased cell length and decreased cell width, when compared to the wild type strain.

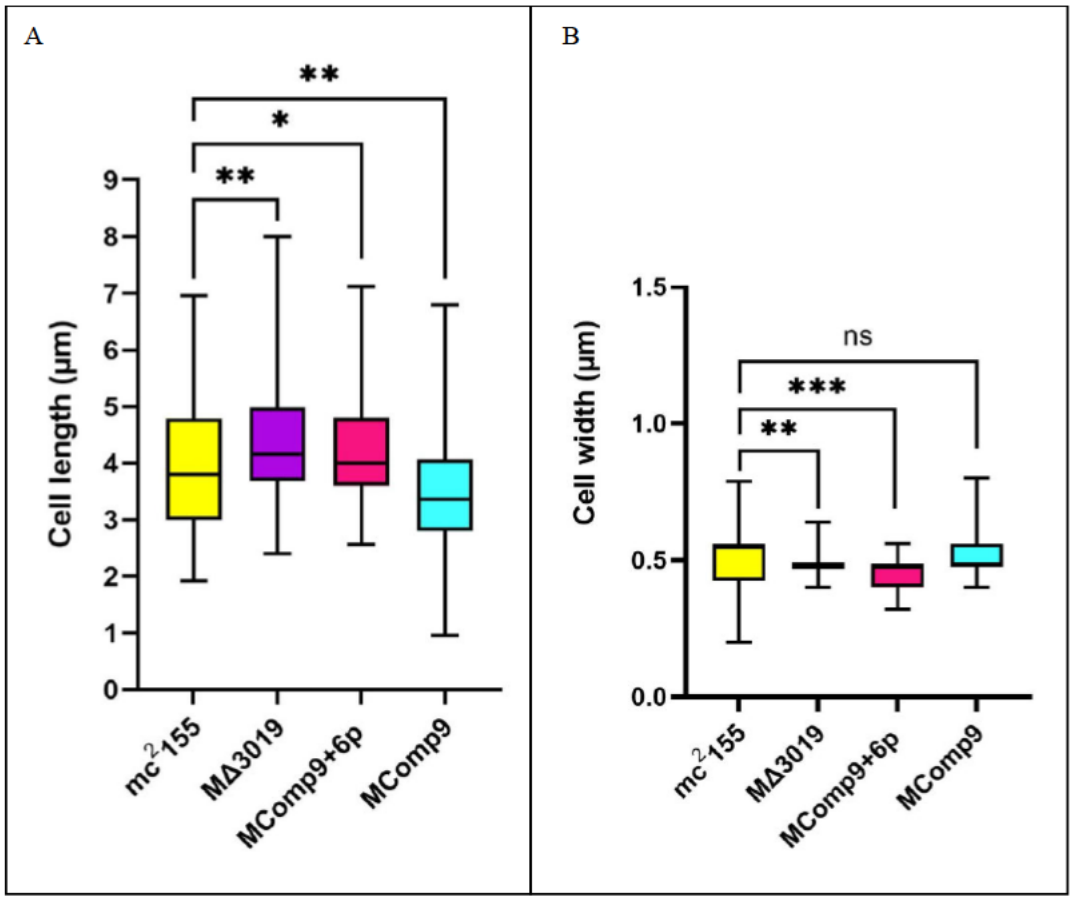

Figure 3.14. **(A)** The average length (µm) and **(B)** average width (µm) of cells belonging to mc^{2}155, MΔ3019, MComp9+6p and MComp9 respectively. p-values were obtained by use of the student's t-test and displayed as significant lines, wherein: *: $p < 0.05$, **: $p < 0.01$, ***: $p < 0.001$ and ns: $p > 0.5$ (not significant).

3.4.3. *MSMEG3019* plays a role in sliding motility

Sliding motility is the form of translocation employed by mycobacteria to facilitate dissemination and colonization of new niches. It is primarily dependent on bacterial surface proteins and cell surface properties, therefore any defects in the motility of the mutant strain could be linked to cell surface composition and regulation of biosurfactants (Martínez *et al*., 1999). Sliding motility assays were conducted as per section 2.9.4, the results of which are displayed in figure 3.15.

Initially, bacterial growth occurred at the point of inoculation on all plates shown in figure 3.15. However, after approximately 3 days, branch-like extensions appeared at the periphery of the mc^{2}155 and MΔ3019 colonies. The mc^{2}155 colony in figure 3.15 (A) has not only exhibited more branching, but also presented a greater degree of branch elongation when compared to the mutant colony in figure 3.15 (B), which displayed a decreased amount of branches, with minimal sliding. The sliding ability of strains MComp9+6p and MComp9, represented by figures 3.15 (C) and 3.15 (D) respectively, are

severely stunted. These complementation strains appear to be unable to slide via branch formation and elongation. Instead, the original colony simply grows larger in an unstructured and disoriented conformation.

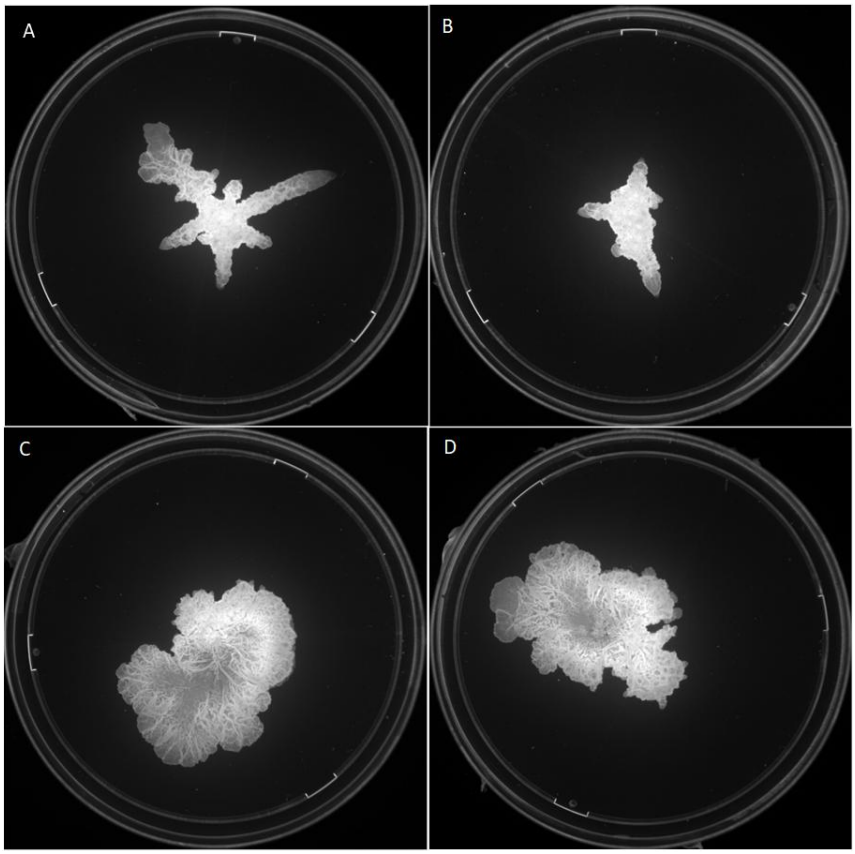

Figure 3.15. Sliding motility assay showing the movement of **(A)** mc^{2}155 **(B)** MΔ3019 **(C)** MComp9+6p and **(D)** MComp9 on solid 7H9 agar.

3.4.4. *MSMEG3019* is not involved in biofilm formation

Analysis of biofilm formation is crucial in determining the ability of a strain to respond to unfavorable conditions. Bacterial biofilms profit on the ability of the bacteria to adhere, produce exopolysaccharides (EPS) and aggregate, the result of which often confers protection of the population against environmental stressors (Mirghani *et al*., 2022). Mycobacterial biofilms *in vivo* contributes to bacterial survival, persistence and antibiotic tolerance, often increasing the duration of TB treatment (Sarangi *et al*., 2024). Analysis of biofilm formation of the mutant strain *in vitro* serves as a good indicator of the target gene's implication in bacterial resilience. Therefore, evaluation of biofilm formation was conducted to infer the role of *MSMEG3019* on the bacteria's ability to form a pellicle at the air-liquid interface using the nutrient-scarce Sauton's media. This was conducted as per section 2.9.3 and the resultant biofilms are shown in figure 3.16.

Figures 3.16 (A) and 3.16 (B) represent the biofilms of mc^{2}155 and MΔ3019 respectively. Both biofilms are equally robust when compared at all the different dilution factors. Additionally, analysis of figures

3.16 (E) and 3.16 (F) show no visible difference between the pellicles formed by them. Furthermore, the complementation strains resulted in slow and stunted growth when compared to the mutant and wild type strain. After the incubation period, wells 5 and 6 of figures 3.16 (A) and 3.16 (B) formed robust biofilms for mc^{2}155 and MΔ3019, but MComp9+6p (figure 3.16 (C)) and MComp9 (figure 3.16 (D)) contained underdeveloped biofilms, which were still in the process of forming. Additionally, it appears that MComp9 exhibits slightly slower growth of biofilms, as seen by a less dense pellicle in figure 3.16 (H) and by the formation of a weaker biofilm in well 5 of figure 3.16 (D), in contrast to the other complementation strain.

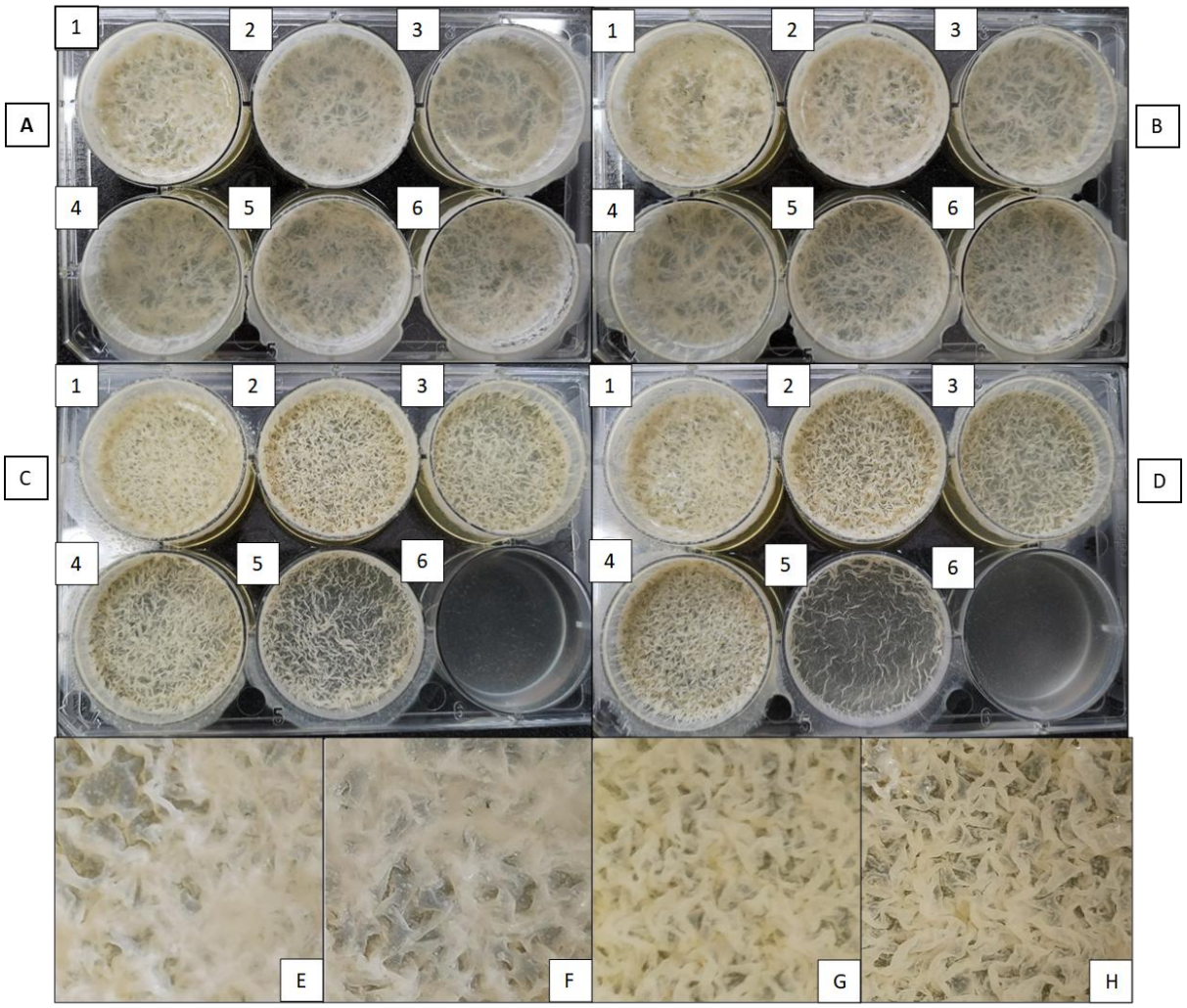

Figure 3.16. The implication of *MSMEG3019* on biofilm formation. **(A)** mc^{2}155 biofilms **(B)** MΔ3019 biofilms **(C)** MComp9+6p biofilms **(D)** MComp9 biofilms. E-F represent zoomed in images focusing on the pellicles of **(E)** mc^{2}155 **(F)** MΔ3019 **(G)** MComp9+6p and **(H)** MComp9. **[1-6]** signifies a ten-fold serial dilution of the culture used as inoculum wherein, **[1]**10^0, **[2]** 10^{-1}, **[3]** 10^{-2}, **[4]** 10^{-3}, **[5]** 10^{-4} and **[6]** 10^{-5}.

3.4.5. *MSMEG3019* does not affect colony morphology

Qualitative examination of the colonies formed by wild type and mutant strains could supplement the understanding of *MSMEG3019's* role in the physiological aspects of colony formation. Any nonconformities exhibited by the mutant strain could possibly be linked to cell wall composition/integrity, growth regulation, metabolism and response to environmental factors (such as nutrient availability) (Cooper *et al*., 1968). Figure 3.17 displays the result of the bacterial spotting assay, as outlined in section 2.9.2.

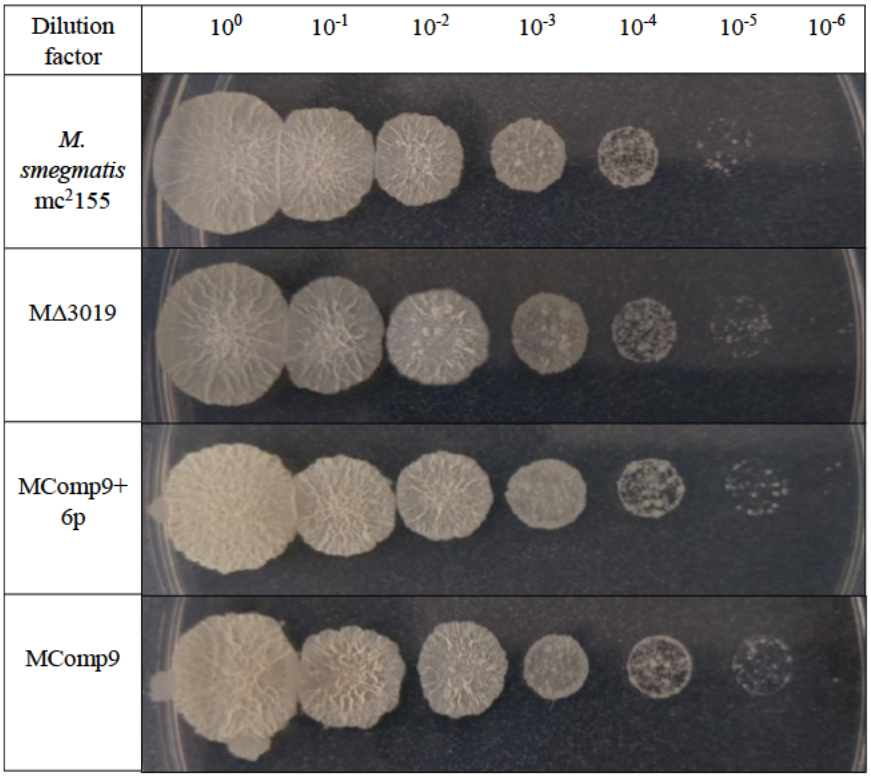

Figure 3.17. The effect of *MSMEG3019* deletion on colony morphology. The figures show decreasing dilutions of the four strains spotted onto 7H11 agar in order to establish and examine the morphology of single colonies.

No visible difference in colony morphology can be observed between either of the four strains shown in figure 3.17. The bacterial growth for all strains is consistent at all dilutions and presents buff-coloured colonies that are rough and dry, with an irregular lobate margin, that is characteristic of mycobacteria.

3.5. *MSMEG3019* contributes to antimicrobial tolerance of Vancomycin

The function of a gene involved in antibiotic tolerance could provide insight on its relevance to bacterial survival and virulence (Beceiro *et al*., 2013). Additionally, susceptibility of a knockout mutant strain to a specific antibiotic could link the deletion of the target gene to the cellular target of that antibiotic, further narrowing down the function of the unknown gene. The antimicrobial susceptibility testing was conducting using the microbroth dilution assay as per section 2.10. The results are portrayed in tables

3.3 and 3.4 as MICs; the lowest concentration of an antibiotic that inhibits bacterial growth (Butterfield *et al*., 2012).

Table 3.3 revealed that the mutant strain exhibited equal extents of susceptibility (when compared to all other strains) after exposure to all antibiotics, except one. The mutant strain displayed an increased susceptibility to Vancomycin, wherein a lower concentration of the drug was required to inhibit growth. The wild type and complementation strains all displayed a higher degree of resistance to Vancomycin; inferring possible implication of *MSMEG3019* in its tolerance.

Table 3.3. MICs of the mc^2155, MΔ3019, MComp9+6p and MComp9 strains using anti-TB drugs

Antibiotic	**MIC (mg/L)**			
	mc^2155	**MΔ3019**	**MComp9+6p**	**MComp9**
Ciprofloxacin	1	1	1	1
Amikacin	1	1	1	1
Ofloxacin	2	2	2	2
Streptomycin	0.5	0.5	0.5	0.5
Vancomycin	1.5	0.75	1.5	1.5
Clofazimine	2	2	1	1
Levofloxacin	1	1	1	1

Vancomycin's mode of action against mycobacteria is through inhibition of PG synthesis. Further examination of *MSMEG3019's* activity to other antibiotics that also target cell wall synthesis is required to supplement the understanding of *MSMEG3019's* possible role in the mycobacterial cell envelope. Thus, the MICs of Ethambutol and Ethionamide were investigated, the results of which are shown in table 3.4.

Table 3.4. MICs using antibiotics related to Vancomycin which target cell wall synthesis

Antibiotic	**MIC (mg/L)**			
	mc^2155	**MΔ3019**	**MComp9+6p**	**MComp9**
Ethambutol	8	8	8	4
Ethionamide	20	20	20	20

The additional antibiotic susceptibility testing (table 3.4) revealed no further involvement of *MSMEG3019* in the susceptibility of antibiotics targeting the mycobacterial cell wall. It is possible that *MSMEG3019* is only involved in the specific metabolic cascade behind Vancomycin's specific target. However, in keeping with the other growth kinetic assays, the complementation strains, once again, resulted in stunted growth when compared with the mutant and wild type strain. This is seen by MComp9's increased susceptibility to Ethambutol (table 3.4) and both strain's increased sensitivity to Clofazimine (table 3.3).

4. Discussion

The millennia-long battle against TB was met with humanity's centuries-spanning endurance and effort to overthrow the infectious disease. Unfortunately, nearly every attempt made by man was refuted by *Mtb*'s formidable aptitude and resilience (Alzayer & Al Nasser, 2023). The ever-strengthening virulence of *Mtb* coupled with its ability to establish LTBI has created a challenging obstacle for scientists to overcome (Behr *et al*., 2021). However, continued attempts at unravelling the bacterium has led to a better comprehension of it, which is key in eradicating it. The identification and elucidation of new molecules, molecular mechanisms and signaling cascades lays a solid foundation in the recognition of antimicrobial compounds which can aid in eliminating TB (Plotniece *et al*., 2023).

To contribute to the fight against TB, this study focused on the characterization of a novel mycobacterial zinc metalloprotease. Zinc metalloproteases act as virulence factors in multiple pathogenic microbes (Peterson, 1996). The current recognized *Mtb* zinc metalloproteases play roles in immune evasion and virulence, therefore other *Mtb* zinc metalloproteases have potential to serve as virulence factors, and by extension, new drug targets (Master *et al*., 2008).

The first stage of characterizing an unknown gene is performing bioinformatics analysis on its protein sequence. This could provide insight on its genomic architecture, functional domains, interactions with other proteins and identify other similar proteins, all of which provides information that advances the characterization process.

The layout of a gene/operon in a bacterial genome provides preparatory information regarding its regulation and expression (Alberts *et al*., 2002). Comparison of gene clusters within related species also offers evolutionary insights. In the case of related species with differing pathogenic states, assessment of gene layout also contributes to the identification of determining factors that contributes to pathogenesis (Van Rossum *et al*., 2020).

Rv2568c is part of a two-gene operon, wherein it is the second gene expressed under the control of *Rv2569c's* promoter which is located at the beginning of the operon (figure 3.1). *Rv2569c* is orthologous to *MSMEG3018*, which is directly upstream the target gene, *MSMEG3019*. Assuming the result provided by Biocyc, in figure 3.1, depicts *MSMEG3019* as part of a four-gene operon, it raises the question of how this difference in operon structure, between *Mtb* and mc^2155, affects the positioning of the promoter regions, the functional relationships between the genes within these operons and the pathogenesis of these species.

In addition to *Rv2568c* belonging to a two-gene transcriptional unit consisting of *Rv2569c*, it should be noted that the *Mtb* equivalents of *MSMEG3017* and *MSMEG3016* belong to a separate operon that includes an additional gene, *Rv2565*, which has no ortholog in *M. smegmatis* (data not shown). This

rearrangement of genes, along with the inclusion of a non-conserved gene in one of the transcriptional units, may contribute to the difference in the pathogenic status between *Mtb* and *M. smegmatis*.

The elucidation of protein-protein interactions involving an unknown gene is crucial, as it could help identify other proteins that interact with the unknown gene's product (Rao *et al*., 2014). This would allow inference of the functions/pathways/structures that the unknown gene is involved in.

Table 3.1 outlines the interactions between the target genes and their surrounding genes. The PEPPI results displayed in this table predicts interactions between the genes *MSMEG3019* and *MSMEG3018* in *M. smegmatis* and *Rv2568c* and *Rv2569c* in *Mtb*. Kegg identified *MSMEG3018* and *Rv2569c* as being transglutaminases. Mycobacterial transglutaminases are involved in protein-protein cross-linking (contributing to structural stability), glutamine deamination and insertion of amines into proteins (Fesus & Piacentini, 2002). In this way, transglutaminases contribute to post-translational modifications of proteins which could be advantageous for pathogens (Fesus & Piacentini, 2002). In *Mtb*, the transglutaminase TG2 is required for intracellular survival and replication *in vivo* (Palucci *et al*., 2018). However, *MSMEG3018* and *Rv2569c* are uncharacterized and this limits the understanding of the interaction between them and the target genes. Thus far, the interaction between bacterial zinc metalloproteases and transglutaminases are severely understudied. The only partially understood interaction between these two proteins is in *Streptomyces mobaraensis*, wherein microbial transglutaminase (MTG) is activated by the Transglutaminase-Activating Metalloprotease (TAMP), which is regulated by the inhibitor SSTI (which therefore indirectly regulates MTG as well) (Juettner *et al*., 2020). This implies that is it entirely possible for the identified mycobacterial transglutaminases in figure 3.1 and table 3.1 to be implicated in the expression/co-regulation of *MSMEG3019* and *Rv2568c*.

MSMEG3019 and *Rv2568c* contain zinc metalloprotease and zinc ribbon domains (table 3.2). Zinc ribbons, also known as zinc fingers, are domains wherein the bound zinc contributes to structural integrity and stability of the protein (Krishna *et al*., 2003). They commonly present as interaction modules which binds to compounds and thereafter aids in facilitation of a broad range of cellular processes (Krishna *et al*., 2003). This function is similar to structural zinc metalloproteases which utilize zinc ions for structural stability. However, zinc metalloproteases predominantly serve as proteolytic enzymes and catalyze the hydrolysis of proteins/peptides (McCall *et al*., 2000). Therefore, it is probable that the two domains play distinct roles in different functions of both *MSMEG3019* and *Rv2568c*. The zinc-binding metalloprotease domain of *MSMEG3019* has a lower E-value and is therefore more of a principal feature of the enzyme, possibly implying it has catalytic zinc ions instead of structural zinc ions. Therefore, the structural zinc ions, provided by the zinc ribbon present in *MSMEG3019*, could possibly function synergistically with the transglutaminase *MSMEG3018*, collectively contributing to

the structural integrity of the bacterial cell (due to their hypothesized interaction and similar cellular functions).

Characterization of the mycobacterial zinc metalloproteases, *MSMEG3019* and *Rv2568c*, thereafter progressed to bioinformatics analysis of their crystal structure, as structural similarity between genes could imply functional similarity (figure 3.2) (Ogura *et al*., 2001). Examination of the *MSMEG3019* crystal structure revealed an uncharacterized zinc metalloprotease in *B. caccae* as a structural homolog, not only to *MSMEG3019*, but also to *Rv2568c*. *B. caccae* is an opportunistic pathogen that forms part of the gut microbiota, found within the human GI tract (Shin *et al*., 2024). It is relatively understudied in comparison to other pathogenic species belonging to the genus of *Bacteroides*, such as *Bacteroides thetaiotaomicron* and *Bacteroides fragilis* (Nakjang *et al*., 2012). However, the zinc metalloproteases within these species have been studied and may provide insight on those present within *B. caccae* that contribute to its colonization of the GI tract.

B. thetaiotaomicron, *B. fragilis* and *B. caccae* contain the zinc metalloprotease domain labelled M60-like/PF13402, which is a virulence factor, conserved amongst some microbes in the human gut and is involved in cell anchorage, signal peptides, glycan binding and degradation of host mucin (Nakjang *et al*., 2012). In addition to M60-like/PF13402-induced proteolysis of mucin facilitating cellular invasion, it could also provide a source of nutrients or contribute to adaptive immunity processing in the pathogen (Nakjang *et al*., 2012). Presence of this zinc metalloprotease in the *Bacteroides* species enables it to thrive on mucosal surfaces and facilitates successful colonization of the host GI tract.

The domain M60-like/PF13402 is also related to the virulence factor M60-enhancin zinc metalloproteases in *Baculovirus*, which also targets host mucins as a mode of virulence (Nakjang *et al*., 2012). Interestingly, figure 3.2 mentions another viral constituent that *Rv2568c* shares structurally similarity with. The *orthoreovirus*, known for causing mammillary infections, contains the outer capsid protein mu1 (also known as µ1), which grants it the ability to penetrate cells and colonize the GI tract or respiratory tract of its host (Liemann *et al*., 2002). Orthoreoviral entry into host tissues begins with the attachment of σ1 to the cell surface receptors (Lee *at al*,. 1981). This results in endocytosis of the orthoreovirus, which initiates the host's gut endosomal protease activity, which degrades σ3 (a constituent of the outer capsid which coats µ1) (Chandran *et al*., 1999). This newly uncoated/exposed µ1 experiences endosomal-induced autolytic cleavage which results in the formation of a myristoylated N-terminal fragment (µ1N) and a C-terminal fragment (µ1C) (Liemann *et al*., 2002). Hydrophobic regions of µ1N interact with the lipid bilayer and cause the formation of pores in the membrane. This induced structural modification to host cells facilitates the entry of the viral genome into the cell cytoplasm (Liemann *et al*., 2002).

In addition to being responsible for skin infections, the third structural homolog of *Rv2568c*, anthrax lethal factor, is also involved in colonization of the GI or respiratory tract. Anthrax is a disease caused

by *Bacillus anthracis* which predominantly infects animals (Quinn *et al*., 2004). However, human infection is possible and may be contracted from infected animals and manifests in its method of contraction: cutaneous anthrax (skin contact leading to skin edema and eschar), inhalation anthrax (inhalation of spores which causes bacterial colonization of the respiratory tract) and gastrointestinal anthrax (ingestion of contaminated food which leads to bacterial invasion of the mucosal lining) (Lincoln *et al*., 1961). Therapeutic intervention is required immediately as anthrax results in septicemia, which is almost always fatal (Quinn *et al*., 2004).

Similar to *Mtb*, lethal factor (LF) exerts its virulence by interfering with macrophages in an attempt to disrupt and manipulate the host immune response into orchestrating its own destruction (Friedlander *et al*., 1993). Pathogens trapped within macrophages prompts the production of ROS as a mechanism of pathogen clearance (Hanna *et al*., 1994). Additionally, the ROS precursor, superoxide anion, triggers the release of proinflammatory cytokines in suitable amounts. However, exposure to lethal toxin (a toxin produced via the combination of LF and protective antigen) increases the amount of superoxide anion present, which causes the stimulation and subsequent accumulation of proinflammatory cytokines. Furthermore, this surge of superoxide anion increases ROS production to extents that cause macrophagic death (Hanna *et al*., 1994). The cytolysis of macrophages results in the release of the conglomeration of proinflammatory cytokines which causes shock and kills the host (Hanna *et al*., 1994). Additionally, LF displays selective proteolytic inhibition of the Mitogen-Activated Protein Kinase (MAPK) signal transduction pathway, which plays a crucial role in modulating host cellular activities and inflammatory responses (Duesbery *et al*., 1998). Immune suppression facilitates the unopposed spread of *B. anthracis*, whose success can be attributed to immobilizing the hosts immune response.

Furthermore, *MSMEG3019* structural homolog, the dicer hydrolases, from *Giardia intestinalis* plays a role in cellular differentiation and the transition between different stages in the giardial life cycle that affects host cell invasion (Liao *et al*., 2014). Lastly, the final structural homolog of *MSMEG3019* is the oxireductase in humans which serves to detoxify toxic compounds through redox reactions, as well as play essential roles in human metabolism and chemo-protection (Boichot *et al*., 2023).

The bioinformatics analysis provided preliminary insights which guided the wet-laboratory experimental design for this project. Laboratory-based work commenced with creation of the mutant allele, followed by testing the sensitivity of the selection markers and thereafter incorporating the plasmid construct into the mc^2155 genome using the two-step allelic exchange system (Gordhan & Parish, 2001). Figures 3.3 to 3.8 provided evidence to corroborate the successful creation of the mutant strain MΔ3019, presented in the form of restriction profiles (which visualize the genomic integrity of the plasmids), sensitivity tests (which verify optimal functioning of the selection markers and conditional lethal genes) and lastly PCR screening and southern blotting which confirm integration of

the mutant allele at the correct genomic locus. Complementation of the mutant strain was accomplished by the creation of plasmids containing functional a *MSMEG3019* gene (figures 3.9 and 3.10), this was subsequently inserted into the genome of mc^2155. PCR screening for the presence of the gene, displayed in figure 3.11, confirmed integration of the complementation plasmids and gave rise to the complementation strains, MComp9+6p and MComp9. Thereafter, characterization of the unknown zinc metalloprotease began.

The growth kinetics of mc^2155, MΔ3019, MComp9+6p and MComp9 were evaluated by a series of different assays in order to determine the effect of *MSMEG3019* deletion on mycobacterial physiology. Figure 3.12 shows the growth rates of all strains investigated in this study over a 24 h period. In this figure, it can be seen that MΔ3019 and mc^2155 grew at an almost consistent pace until 18 h, after which MΔ3019 displayed marginally restricted growth in comparison to mc^2155. Both strains reached stationary phase at the same time point (21 h), implying that maximum capacity of population growth was achieved at this point. However, MΔ3019 appears to reach stationary phase at a lower OD_{600nm} compared to mc^2155, meaning that MΔ3019 reached its maximum capacity at a lower cell density. This restricted growth suggests that MΔ3019 was unable to sustain or support the growth of a larger population due to its encounter of a limiting factor. This limiting factor could range from disrupted metabolic pathways causing dysregulation of cell cycle and proliferation, disordered nutrient uptake, response to cellular stress or accumulation of toxic byproducts (Qiu *et al*., 2022). This observation proposes that *MSMEG3019* plays a role in the latter half of mycobacterial exponential phase and transition to stationary phase. Quantification of *MSMEG3019* gene expression during the mc^2155 exponential and stationary growth phases would have accurately designated its involvement in specific phases. Unfortunately, due to time constraints, analysis of gene expression via Reverse Transcription PCR (RT-PCR) at each growth phase of mc^2155 was unable to be completed.

The exponential phase of a bacterial growth curve contains actively proliferating cells (Maier & Pepper, 2015). Characteristics of bacteria in this phase include higher metabolic activity, increased virulence, higher resistance to host immune responses and rapid spread of bacteria. It could therefore be theorized that *MSMEG3019* plays a phase-dependent role in bacterial physiology/differentiation during exponential growth (Zambrano & Kolter, 2018). This finding is in keeping with *MSMEG3019's* structural homolog, dicer hydrolases, which are involved in phase-specific cellular differentiation. This characteristic is also present in *E. coli*, wherein the adhesin Ag43 is phase-variable and is turned on during certain growth phases and turned off at others (Chekli *et al*., 2023). Ag43 is generally upregulated during the transition from exponential phase to stationary phase wherein it is responsible for the aggregation of cells (Chauhan *et al*., 2013; Chekli *et al*., 2023).

Another factor that contributes to cellular differences observed during exponential phase and stationary phase is changes to the bacterial cell wall (Zambrano & Kolter, 2018). The cell wall constituent, PG,

plays crucial roles in cell elongation and division, which generally occur during exponential phase (Garde *et al*., 2021). If *MSMEG3019* is implicated in PG synthesis, it would constrain mycobacterial cellular division and cause aberrations in cell length/width and this would most likely occur during exponential phase (Zambrano & Kolter, 2018).

The above proposition regarding *MSMEG3019's* involvement in PG synthesis is further supported by the results obtained from the SEM analysis. Figure 3.14 shows that a deletion of *MSMEG3019* can be correlated with elongated cell lengths and decreased cell widths. This result is consistent with the findings of Hirmondó *et al*., (2022), who demonstrated that interfering with PG synthesis caused alterations in the elongation and cylindrical shape produced by *M. smegmatis* (Hirmondó *et al*., 2022). This statement is further verified by the findings of Udou *et al*., (1982) and Maitra *et al*., 2019 who have successfully demonstrated PG's role in defining mycobacterial cellular elongation, division and antimicrobial tolerance (Udou *et al., 1982;* Maitra *et al*., 2022).

The correlation between PG and cellular elongation can be attributed to the mechanism employed by mycobacteria for cellular growth. In contrast to other bacteria, mycobacteria are incapable of lateral wall elongation and therefore rely on the incorporation of nascent PG at both poles of the cell for elongation to occur (Thanky *et al*., 2007; Kieser & Rubin, 2014). This is thought to occur via the MviN-mediated transportation of PG precursor subunits to the periplasm. MviN is a transmembrane protein that interacts with FhaA to localize at the correct positions at the poles, after which MviN covalently inserts the PG precursor subunits into the expanding cell wall (Kieser & Rubin, 2014).

These discoveries highlight the importance of PG on the maintenance of cell shape, size, cell wall integrity and antimicrobial tolerance and could provide an explanation for the characteristics displayed by MΔ3019. This is further corroborated by the antimicrobial tolerance testing in table 3.3, which revealed that deletion of *MSMEG3019* led to increased susceptibility to Vancomycin. Vancomycin is known to prevent PG synthesis by binding to the D-alanyl-D-alanine terminal end of PG precursors (Soetaert *et al*., 2015).

Vancomycin is generally thought of to be non-efficient in the killing of *Mtb* due to the impermeability of the bacterial cell wall (Lambert, 2002). Therefore, it was important to decipher whether the observed result directly reflects *MSMEG3019's* role in PG synthesis or if it was the indirect consequence of *MSMEG3019's* disruption of other cellular functions controlling the cell envelope, thereby synergistically facilitating antimicrobial activity of Vancomycin.

To test this theory, the susceptibility of MΔ3019 in response to antibiotics targeting the cell envelope was examined (table 3.4). Ethambutol targets the synthesis of AG and Ethionamide targets InhA which is involved in the biosynthesis of MAs (Morlock *et al*., 2003; Goude *et al*., 2009). However, exposure of these antibiotics to MΔ3019 resulted in no change to susceptibility, implying that *MSMEG3019* is not involved in the synthesis/regulation of any other cell wall constituents, except PG. Therefore, it can

be deduced that the *MSMEG3019*-induced compromised PG layer of MΔ3019 makes it more susceptible to Vancomycin, which further exacerbates impairment of the PG layer, causing cell death.

Additionally, the cellular targets of the remaining antibiotics, that resulted in no change to MΔ3019 susceptibility, are no longer candidates of *MSMEG3019* function. The antibiotics Levofloxacin, Ciprofloxacin and Ofloxacin are fluoroquinolones which targets *Mtb* DNA gyrase (Blower *et al*., 2016; Huo *et al*., 2020). Streptomycin targets RNA which codes for ribosomal proteins, whilst Amikacin targets the 30S ribosomal subunit, consequently interfering with protein synthesis (Alangaden *et al*., 1998; Shi *et al*., 2007). Lastly, Clofazimine is involved in inhibition of gene expression (Shi *et al*., 2017). Additionally, these cellular mechanisms do not correlate to any of the bioinformatics analysis or any of the phenotypic observations made and can therefore be ruled out.

Evolution has bestowed an assortment of surface translocation mechanisms upon bacteria, generally facilitated by appendages such as flagella (Henrichsen, 1972). Due to mycobacteria possessing a non-flagellated status, it was generally accepted that they are incapable of movement. However, in 1999, Martínez *et al*., discovered the ability of *M. smegmatis* to translocate by sliding across a solid surface (Martínez *et al*., 1999). The capacity of bacterial cells to migrate across surfaces are primarily due to the properties of their cell surface. Mycobacterial sliding motility can be attributed to the presence of glycopeptidolipids (GPLs) in the cell wall, however, it was theorized that this is unlikely to be the sole contributor of mycobacterial motility (Martínez *et al*., 1999). GPLs are surface exposed and could therefore lead to a more hydrophobic interaction between the cell and surface, therefore facilitating bacterial sliding/spreading (Ortalo-Magne *et al*., 1996).

Figure 3.15 shows that mc^2155 produced a higher number of branching, in different directions and to a lengthier extent, when compared to MΔ3019, which displayed decreased sliding. Bacterial growth phases also influence the translocation/spread and infectivity of mycobacteria (Hett & Rubin, 2008). The interference of bacterial spreading observed in the sliding motility assays of this project could therefore also be associated to the restricted exponential growth observed in MΔ3019 during analysis of growth rates.

Bacterial motility is considered to play a crucial role in bacterial dissemination and host cell invasion, thereby facilitating spread of infection (Martínez *et al*., 1999). The sliding motility of mc^2155 *in vitro* represents the ability of *Mtb* to spread and colonize new surfaces of host tissue (Martínez *et al*., 1999). Taking into consideration the altered sliding capacity of MΔ3019, in conjunction with the invasive-nature of the identified structural homologs of *MSMEG3019* and *Rv2568c*, it can be suggested that *Rv2568c* is implicated in bacterial dissemination, and as a result host cell invasion.

Further experimental analysis of MΔ3019 is required to determine the specific mode of action employed by *MSMEG3019* to facilitate sliding. *MSMEG3019* could either directly or indirectly contribute to altered production of GPLs and the extracellular matrix, modified secretion systems or impaired cell

envelope integrity: all of which could play roles in bacterial dispersion and adherence (Martínez *et al*., 1999). It is probable that weakened cell envelope integrity affects the translocation capacity of MΔ3019, as PG is one of the principal constituents of the cell envelope. The induced PG-damage facilitated by the *MSMEG3019* deletion may cause the observed abnormalities in the sliding ability of the mutant.

The alteration of phenotypes displayed by MΔ3019 during the sliding motility, growth curve and cell size examinations but not during analysis of biofilm formation (figure 3.16) and colony morphology (figure 3.17) could be attributed to a few things. Firstly, these results could implicate *MSMEG3019's* non-involvement in cell-cell aggregation, despite being implicated in growth. Secondly, the differences could be a reflection of mc^2155's favorable media (and by extension preferred supplementation). Sliding motility and growth curves were conducted in 7H9 media, whereas analysis of colony morphology and biofilm formation were conducted in 7H11 and Sauton's media respectively. 7H9 media and Sauton's media both consist of low quantities of zinc sulphate, whereas 7H11 agar does not (Merck, Germany). Presence of the additional zinc ions in the zinc sulphate may enhance the activity of the zinc metalloprotease *MSMEG3019*, leading to optimal expression of it in mc^2155 during sliding motility and growth curve analysis and therefore highlighting the stark difference caused by its absence in MΔ3019 colony formation (Hussain *et al*., 2022).

Thirdly, it is difficult to directly compare biofilm formation to sliding motility and bacterial growth curves, as biofilm formation is the result of the onset of very distinct pathways (Beloin & Ghigo, 2005). The results could simply imply that *MSMEG3019* is not associated with any pathway that specifically affects biofilm formation.

The complementation of knockout strains is a method of verifying that the mutant was created correctly. Reinstating the function of the target gene in the complementation strain should result in the display of phenotypic attributes that are observed in the wild type strain (Arras *et al*., 2015). In this study, the complementation strains were unable to be successfully created. The complementation strains exhibited distinct physiological differences when compared to MΔ3019 and mc^2155. This could be attributed to two reasons or the simultaneous combination of both: (i) the hypothesized promoter regions were incorrect, resulting in the creation of a non-functional *MSMEG3019* gene, or (ii) the complementation plasmids did not integrate at the correct genomic locus on the mycobacterial genome.

The complementation aspect of this project was at a disadvantage due to the lack of data available on the mc^2155 gene sequences. It is possible that the hypothesized promoter regions (upstream *MSMEG3019* and *MSMEG3016*) were incorrect. This uncertainty is reasonable as the layout of genes surrounding *MSMEG3019* is different compared to those surrounding *Rv2568c* in *Mtb*, making it difficult to deduce the location of the correct promoter region (figure 3.1).

Integration of the incorrect promoter sequence upstream the target gene could result in the creation of unanticipated mutations which would produce an altered phenotype, as seen in the results generated by

this study (de Vooght *et al*., 2009). In the analysis of cell size, antimicrobial testing and biofilm formation assays (figures 3.14 and 3.16 and table 3.4), it can be seen that MComp9 displays a higher degree of defect (exhibited as decreased cell length, increased susceptibility to Ethambutol and the formation of less dense biofilms) compared to MComp9+6p. This highlights the significant effect of the different promoter regions on the phenotypic expression of the complementation strains, further proving that the incorrect promoter regions were used

Mutations resulting in unintended phenotypic attributes could also be due to integration of the complementation plasmids into the incorrect locus within the genome (de Vooght *et al*., 2009). This could, not only, misregulate expression of the complement allele but also cause unwanted genomic alteration at the site of integration (Parsons *et al*., 2021). This could possibly disrupt essential genes and interfere with important cellular processes and impair the bacteria's ability to grow normally.

Considering the observed defects of the complementation strains during sliding motility, growth curve analysis, biofilm formation, cell size investigation and antimicrobial susceptibility testing, it could be suggested that integration of the complementation plasmids interfered with essential genes. A limitation of the PCR screening used in this study to verify presence of *MSMEG3019* in the complementation strains (figure 3.11), is that it only reflects the presence/absence status of the target gene. In order to validate integration at the correct genomic locus, Southern blotting should have been conducted in order to provide genomic mapping of the integration region.

The failed attempts at creating a successful complementation strain in conjunction with the interpretation of *Mtb's* annotated genomic layout in figure 3.1, leads to the theory that *MSMEG3019's* promoter region could be directly upstream *MSMEG3018*. This would also validate the results shown in table 3.1 which states that there is a probability of *MSMEG3019* interacting with *MSMEG3018* in order to facilitate expression.

It is important to note that unsuccessful complementation of a knockout strain does not necessarily invalidate the mutant phenotype (Hawley & Gilliland, 2006). However, further justification provided by the correct complementation of MΔ3019 would eliminate any uncertainty surrounding the results. In this specific study, two types of screening were conducted (figures 3.7 and 3.8) to ensure genomic validity of the mutant strain. The results of this screening guaranteed the presence of the correct mutant allele at the correct genomic locus. These screening results coupled with the absence of genes downstream *MSMEG3019* and the reliability of the two-step allelic exchange system, endorses the assumption that all the phenotypic characteristics displayed by MΔ3019 can be attributed solely to the deletion of *MSMEG3019*.

5. Conclusion

This study revealed the role of the novel zinc metalloprotease, *MSMEG3019*, in the synthesis and/or regulation of PG. This is supported by the mutant strain's increased sensitivity to Vancomycin in combination with its role in exponential growth, as exhibited by decreased capacity for population sustenance and the incidence of increased lengths and decreased widths of individual cells. Additionally, *MSMEG3019* was discovered to be involved in the ability of *M. smegmatis* to translocate. These results collectively imply that *MSMEG3019* contributes to mycobacterial growth, proliferation and dissemination, which is a reflection of its contribution to pathogenesis in *Mtb*. This study was limited by the failure to successfully create a complementation strain, which would have provided additional validation of the observed results.

6. Future work

The initial set of results generated by this MMedSci research project suffices to prove *MSMEG3019's* involvement in mycobacterial physiology. Therefore, the subsequent phase is to investigate the zinc metalloprotease *Rv2568c* in *Mtb*. An *Mtb* mutant strain harboring a deletion of *Rv2568c* should be created using the two-step allelic exchange system. All experiments conducted in this project should be repeated on the *Mtb* mutant to assess the consistency between *MSMEG3019* and *Rv2568c*. Thereafter, further analysis of *Rv2568c's* role in mycobacterial physiology is required, in addition to examining its contribution to virulence. Due to bioinformatics analysis accentuating host-cell invasion as a possible function, macrophage infection assays should be conducted using the mutant strain to elucidate the interactions between the strain and the host, as well as to establish the infection/invasion efficacy conferred by *Rv2568c*. Mycobacterial dissemination of the strains should be studied in zebrafish models to determine *Rv2568c's* contribution to mycobacterial motility/dissemination. A static adhesion assay should be conducted to assess the adherence ability of the mutant to host cells. The gene *Rv2569c* should be studied in conjunction with *Rv2568c* to determine the phenotypic byproduct as a result of the protein-protein interaction. Additionally, RT-PCR should be conducted on the mutant and wild type strains at different time points of the bacterial growth curve to quantify the expression of *Rv2568c* at different phases of growth. This could help specify phase-dependent functions of *Rv2568c*, in addition to PG synthesis. Furthermore, fluorescence microscopy (in combination with specific staining) should be conducted to evaluate any modification to intracellular structure (e.g. cell envelope) as a result of *Rv2568c* deletion. Provided the results yield substantial contribution of *Rv2568c* to *Mtb* physiology and virulence, thereafter the pathways involved in its function can be deciphered and antimicrobial compounds which inhibit this pathway can be discovered; thus creating a new TB drug for a new TB drug target.

7. References

Abdallah, A.M., Gey van Pittius, N.C., DiGiuseppe Champion, P.A., Cox, J., Luirink, J., Vandenbroucke-Grauls, C.M., Appelmelk, B.J. and Bitter, W., 2007. Type VII secretion—mycobacteria show the way. Nature reviews microbiology, 5(11), pp.883-891.

Abdallah, A.M., Verboom, T., Hannes, F., Safi, M., Strong, M., Eisenberg, D., Musters, R.J., Vandenbroucke-Grauls, C.M., Appelmelk, B.J., Luirink, J. and Bitter, W., 2006. A specific secretion system mediates PPE41 transport in pathogenic mycobacteria. Molecular microbiology, 62(3), pp.667-679.

Agyeman, A.A. and Ofori-Asenso, R., 2017. Tuberculosis—an overview. Journal of Public Health and Emergency, 1(1).

Alangaden, G.J., Kreiswirth, B.N., Aouad, A., Khetarpal, M., Igno, F.R., Moghazeh, S.L., Manavathu, E.K. and Lerner, S.A., 1998. Mechanism of resistance to amikacin and kanamycin in *Mycobacterium tuberculosis*. Antimicrobial agents and chemotherapy, 42(5), pp.1295-1297.

Alberts, B., Johnson, A., Lewis, J., Raff, M., Roberts, K. and Walter, P., 2002. Studying gene expression and function. In Molecular Biology of the Cell. 4th edition. Garland Science.

Alzayer, Z. and Al Nasser, Y., 2023. Primary Lung Tuberculosis. In StatPearls. StatPearls Publishing. [Updated 2023 Jan 2]. Available from: https://www.ncbi.nlm.nih.gov/books/NBK567737/

Amar, C. and Vilkas, E., 1973. Isolation of arabinose phosphate from the walls of *Mycobacterium tuberculosis* H3 Ra. Comptes rendus hebdomadaires des seances de l'Academie des sciences. Serie D: Sciences naturelles, 277(18), pp.1949-1951.

Andries, K., Verhasselt, P., Guillemont, J., Göhlmann, H.W., Neefs, J.M., Winkler, H., Van Gestel, J., Timmerman, P., Zhu, M., Lee, E. and Williams, P., 2005. A diarylquinoline drug active on the ATP synthase of *Mycobacterium tuberculosis*. Science, 307(5707), pp.223-227.

Angel, C.Y., Worrall, L.J. and Strynadka, N.C., 2012. Structural insight into the bacterial mucinase StcE essential to adhesion and immune evasion during enterohemorrhagic *E. coli* infection. Structure, 20(4), pp.707-717.

Arras, S.D., Chitty, J.L., Blake, K.L., Schulz, B.L. and Fraser, J.A., 2015. A genomic safe haven for mutant complementation in *Cryptococcus neoformans*. PloS one, 10(4), p.e0122916.

Asano, M., Nakane, A. and Minagawa, T., 1993. Endogenous gamma interferon is essential in granuloma formation induced by glycolipid-containing mycolic acid in mice. Infection and immunity, 61(7), pp.2872-2878.

Ates, L.S., Ummels, R., Commandeur, S., van der Weerd, R., Sparrius, M., Weerdenburg, E., Alber, M., Kalscheuer, R., Piersma, S.R., Abdallah, A.M. and Abd El Ghany, M., 2015. Essential role of the ESX-5 secretion system in outer membrane permeability of pathogenic mycobacteria. PLoS genetics, 11(5), p.e1005190.

Balloux, F. and van Dorp, L., 2017. Q&A: What are pathogens, and what have they done to and for us?. BMC biology, 15, pp.1-6.

Beceiro, A., Tomás, M. and Bou, G., 2013. Antimicrobial resistance and virulence: a successful or deleterious association in the bacterial world?. Clinical microbiology reviews, 26(2), pp.185-230.

Behr, M.A., Kaufmann, E., Duffin, J., Edelstein, P.H. and Ramakrishnan, L., 2021. Latent tuberculosis: two centuries of confusion. American journal of respiratory and critical care medicine, 204(2), pp.142-148.

Bell, E.W., Schwartz, J.H., Freddolino, P.L. and Zhang, Y., 2022. PEPPI: whole-proteome protein-protein interaction prediction through structure and sequence similarity, functional association, and machine learning. Journal of molecular biology, 434(11), p.167530.

Beloin, C. and Ghigo, J.M., 2005. Finding gene-expression patterns in bacterial biofilms. Trends in microbiology, 13(1), pp.16-19.

Bento, C.M., Gomes, M.S. and Silva, T., 2021. Evolution of antibacterial drug screening methods: current prospects for mycobacteria. Microorganisms, 9(12), p.2562.

Berthet, F.X., Lagranderie, M., Gounon, P., Laurent-Winter, C., Ensergueix, D., Chavarot, P., Thouron, F., Maranghi, E., Pelicic, V., Portnoï, D. and Marchal, G., 1998. Attenuation of virulence by disruption of the *Mycobacterium tuberculosis erp* gene. Science, 282(5389), pp.759-762.

Bhamidi, S., Scherman, M.S., Jones, V., Crick, D.C., Belisle, J.T., Brennan, P.J. and McNeil, M.R., 2011. Detailed structural and quantitative analysis reveals the spatial organization of the cell walls of in vivo grown *Mycobacterium leprae* and in vitro grown *Mycobacterium tuberculosis*. Journal of Biological Chemistry, 286(26), pp.23168-23177.

Bhatt, A., Fujiwara, N., Bhatt, K., Gurcha, S.S., Kremer, L., Chen, B., Chan, J., Porcelli, S.A., Kobayashi, K., Besra, G.S. and Jacobs Jr, W.R., 2007. Deletion of *kasB* in *Mycobacterium tuberculosis* causes loss of acid-fastness and subclinical latent tuberculosis in immunocompetent mice. Proceedings of the National Academy of Sciences, 104(12), pp.5157-5162.

Birnboim, H. and Doly, J., 1979. A rapid alkaline extraction procedure for screening recombinant plasmid DNA. Nucleic acids research, 7(6), pp.1513-1523.

Bloom, B.R., Atun, R., Cohen. T., Dye, C., Fraser, H., Gomez, G.B., Knight, G., Murray, M., Nardell, E., Rubin, E., Salomon, J., Vassall, A., Volchenkov, G., White, R., Wilson, D. and Yadav P., 2017. Tuberculosis. In: Holmes KK, Bertozzi S, Bloom BR, et al., editors. Major Infectious Diseases. 3rd edition. Washington (DC): The International Bank for Reconstruction and Development / The World Bank; 2017 Nov 3. Chapter 11. Available from: https://www.ncbi.nlm.nih.gov/books/NBK525174/ doi: 10.1596/978-1-4648-0524-0_ch11

Blower, T.R., Williamson, B.H., Kerns, R.J. and Berger, J.M., 2016. Crystal structure and stability of gyrase–fluoroquinolone cleaved complexes from *Mycobacterium tuberculosis*. Proceedings of the National Academy of Sciences, 113(7), pp.1706-1713.

Boichot, V., Menetrier, F., Saliou, J.M., Lirussi, F., Canon, F., Folia, M., Heydel, J.M., Hummel, T., Menzel, S., Steinke, M. and Hackenberg, S., 2023. Characterization of human oxidoreductases involved in aldehyde odorant metabolism. Scientific Reports, 13(1), p.4876.

Bottai, D., Di Luca, M., Majlessi, L., Frigui, W., Simeone, R., Sayes, F., Bitter, W., Brennan, M.J., Leclerc, C., Batoni, G. and Campa, M., 2012. Disruption of the ESX-5 system of *Mycobacterium tuberculosis* causes loss of PPE protein secretion, reduction of cell wall integrity and strong attenuation. Molecular microbiology, 83(6), pp.1195-1209.

Brennan, P.J. and Nikaido, H., 1995. The envelope of mycobacteria. Annual review of biochemistry, 64(1), pp.29-63.

Brennan, P.J., 2003. Structure, function, and biogenesis of the cell wall of *Mycobacterium tuberculosis*. Tuberculosis, 83(1-3), pp.91-97.

Britannica, T., 2020. Editors of Encyclopaedia. "proteolytic enzyme." Encyclopedia Britannica, May 18, 2020. https://www.britannica.com/science/proteolytic-enzyme.

Butler, A., 1998. Acquisition and utilization of transition metal ions by marine organisms. Science, 281(5374), pp.207-209.

Butterfield, J., Lodise Jr, T.P. and Pai, M.P., 2012. Applications of Pharmacokinetic and Pharmacodynamic Principles to Optimize Drug Dosage Selection: Example of Antibiotic Therapy Management. Therapeutic Drug Monitoring, pp.175-196.

Calamita, H., Ko, C., Tyagi, S., Yoshimatsu, T., Morrison, N.E. and Bishai, W.R., 2005. The *Mycobacterium tuberculosis* SigD sigma factor controls the expression of ribosome-associated gene products in stationary phase and is required for full virulence. Cellular microbiology, 7(2), pp.233-244.

Catalão, M.J., Filipe, S.R. and Pimentel, M., 2019. Revisiting anti-tuberculosis therapeutic strategies that target the peptidoglycan structure and synthesis. Frontiers in microbiology, 10, p.190.

Cave, A.J.E. and Demonstrator, A., 1939. The evidence for the incidence of tuberculosis in ancient Egypt. British Journal of Tuberculosis, 33(3), pp.142-152.

Chai, Q., Zhang, Y. and Liu, C.H., 2018. *Mycobacterium tuberculosis*: an adaptable pathogen associated with multiple human diseases. Frontiers in cellular and infection microbiology, 8, p.158.

Chakraborty, S. and Rhee, K.Y., 2015. Tuberculosis drug development: history and evolution of the mechanism-based paradigm. Cold Spring Harbor perspectives in medicine, 5(8), p.a021147.

Chandran, K., Walker, S.B., Chen, Y.A., Contreras, C.M., Schiff, L.A., Baker, T.S. and Nibert, M.L., 1999. In vitro recoating of reovirus cores with baculovirus-expressed outer-capsid proteins μ1 and ς3. Journal of virology, 73(5), pp.3941-3950.

Chang, A.Y., Chau, V., Landas, J.A. and Pang, Y., 2017. Preparation of calcium competent *Escherichia coli* and heat-shock transformation. JEMI methods, 1(22-25).

Chatterjee, D., Bozic, C.M., McNeil, M. and Brennan, P.J., 1991. Structural features of the arabinan component of the lipoarabinomannan of *Mycobacterium tuberculosis*. Journal of Biological Chemistry, 266(15), pp.9652-9660.

Chauhan, A., Sakamoto, C., Ghigo, J.M. and Beloin, C., 2013. Did I pick the right colony? Pitfalls in the study of regulation of the phase variable antigen 43 adhesin. PloS one, 8(9), p.e73568.

Chekli, Y., Stevick, R.J., Kornobis, E., Briolat, V., Ghigo, J.M. and Beloin, C., 2023. *Escherichia coli* aggregates mediated by native or synthetic adhesins exhibit both core and adhesin-specific transcriptional responses. Microbiology Spectrum, 11(3), pp.e00690-23.

Chen, A.Y., Adamek, R.N., Dick, B.L., Credille, C.V., Morrison, C.N. and Cohen, S.M., 2018. Targeting metalloenzymes for therapeutic intervention. Chemical reviews, 119(2), pp.1323-1455.

Churchyard, G., Kim, P., Shah, N.S., Rustomjee, R., Gandhi, N., Mathema, B., Dowdy, D., Kasmar, A. and Cardenas, V., 2017. What we know about tuberculosis transmission: an overview. The Journal of infectious diseases, 216(suppl_6), pp.S629-S635.

Clemmensen, H.S., Knudsen, N.P.H., Rasmussen, E.M., Winkler, J., Rosenkrands, I., Ahmad, A., Lillebaek, T., Sherman, D.R., Andersen, P.L. and Aagaard, C., 2017. An attenuated *Mycobacterium tuberculosis* clinical strain with a defect in ESX-1 secretion induces minimal host immune responses and pathology. Scientific Reports, 7(1), p.46666.

Cole, S.T., Brosch, R., Parkhill, J., Garnier, T., Churcher, C., Harris, D., Gordon, S.V., Eiglmeier, K. and Gas, S., 1998. Barry 3rd. CE, Tekaia, F., Badcock, K., Basham, D., Brown, D., Chillingworth, T., Connor, R., Davies, R., Devlin, K., Feltwell, T., Gentles, S., Hamlin, N., Holroyd, S., Hornsby, T., Jagels, K., Krogh, A., McLean, J., Moule, S., Murphy, L., Oliver, K., Osborne, J., Quail, MA, Rajandream, MA, Rogers, J., Rutter, S., Seeger, K., Skelton, J., Squares, R., Squares, S., Sulston, JE, Taylor, K., Whitehead, S., Barrell, BG, pp.537-544.

Comstock, G.W., Baum, C. and Snider Jr, D.E., 1979. Isoniazid prophylaxis among Alaskan Eskimos: a final report of the bethel isoniazid studies. American Review of Respiratory Disease, 119(5), pp.827-830.

Cooper, A.L., Dean, A.C.R. and Hinshelwood, C.N., 1968. Factors affecting the growth of bacterial colonies on agar plates. Proceedings of the Royal Society of London. Series B. Biological Sciences, 171(1023), pp.175-199.

Countries of the world. 2022. How many countries are in the world? https://www.countries-ofthe-world.com/how-many-countries.html

Crichton, R.R., 2012. Biological inorganic chemistry: a new introduction to molecular structure and function. Elsevier.

Crubézy, E., Ludes, B., Poveda, J.D., Clayton, J., Crouau-Roy, B. and Montagnon, D., 1998. Identification of *Mycobacterium* DNA in an Egyptian Pott's disease of 5400 years old. Comptes Rendus de l'Académie des Sciences-Series III-Sciences de la Vie, 321(11), pp.941-951.

Cunliffe, J., 2008. A proliferation of pathogens through the 20th century. Scandinavian journal of immunology, 68(2), pp.120-128.

Daffé, M. and Marrakchi, H., 2019. Unraveling the structure of the mycobacterial envelope. Microbiology spectrum, 7(4), pp.10-1128.

Daniel, T.M., 1997. Captain of death: the story of tuberculosis. Rochester, NY: University of Rochester Press.

Daniel, T.M., 2004. René Théophile Hyacinthe Laënnec and the founding of pulmonary medicine [Founders of Our Knowledge]. The International Journal of Tuberculosis and Lung Disease, 8(5), pp.517-518.

Daniel, T.M., 2006. The history of tuberculosis. Respiratory medicine, 100(11), pp.1862-1870.

Dartois, V.A. and Rubin, E.J., 2022. Anti-tuberculosis treatment strategies and drug development: challenges and priorities. Nature Reviews Microbiology, 20(11), pp.685-701.

Deb, C., Lee, C.M., Dubey, V.S., Daniel, J., Abomoelak, B., Sirakova, T.D., Pawar, S., Rogers, L. and Kolattukudy, P.E., 2009. A novel *in vitro* multiple-stress dormancy model for *Mycobacterium tuberculosis* generates a lipid-loaded, drug-tolerant, dormant pathogen. PloS one, 4(6), p.e6077.

DeJesus, M.A., Gerrick, E.R., Xu, W., Park, S.W., Long, J.E., Boutte, C.C., Rubin, E.J., Schnappinger, D., Ehrt, S., Fortune, S.M. and Sassetti, C.M., 2017. Comprehensive essentiality analysis of the *Mycobacterium tuberculosis* genome via saturating transposon mutagenesis. MBio, 8(1), pp.10-1128.

de Vooght, K.M., van Wijk, R. and van Solinge, W.W., 2009. Management of gene promoter mutations in molecular diagnostics. Clinical chemistry, 55(4), pp.698-708.

Dinarello, C.A., 2005. An IL-1 family member requires caspase-1 processing and signals through the ST2 receptor. *Immunity*, *23*(5), pp.461-462.

Dookie, N., Rambaran, S., Padayatchi, N., Mahomed, S. and Naidoo, K., 2018. Evolution of drug resistance in *Mycobacterium tuberculosis*: a review on the molecular determinants of resistance and implications for personalized care. Journal of Antimicrobial Chemotherapy, 73(5), pp.1138-1151.

Dorman, S.E., Nahid, P., Kurbatova, E.V., Phillips, P.P., Bryant, K., Dooley, K.E., Engle, M., Goldberg, S.V., Phan, H.T., Hakim, J. and Johnson, J.L., 2021. Four-month rifapentine regimens with or without moxifloxacin for tuberculosis. New England Journal of Medicine, 384(18), pp.1705-1718.

Doron, S. and Gorbach, S.L., 2008. Bacterial infections: overview. International Encyclopedia of Public Health, p.273.

Dragset, M.S., Ioerger, T.R., Zhang, Y.J., Mærk, M., Ginbot, Z., Sacchettini, J.C., Flo, T.H., Rubin, E.J. and Steigedal, M., 2019. Genome-wide phenotypic profiling identifies and categorizes genes required for mycobacterial low iron fitness. Scientific reports, 9(1), p.11394.

Duesbery, N.S., Webb, C.P., Leppla, S.H., Gordon, V.M., Klimpel, K.R., Copeland, T.D., Ahn, N.G., Oskarsson, M.K., Fukasawa, K., Paull, K.D. and Vande Woude, G.F., 1998. Proteolytic inactivation of MAP-kinase-kinase by anthrax lethal factor. Science, 280(5364), pp.734-737.

Dutta, A. and Bahar, I., 2010. Metal-binding sites are designed to achieve optimal mechanical and signaling properties. Structure, 18(9), pp.1140-1148.

Ehlers, S. and Schaible, U.E., 2013. The granuloma in tuberculosis: dynamics of a host–pathogen collusion. Frontiers in immunology, 3, p.411.

Ehrt, S. and Schnappinger, D., 2007. *Mycobacterium tuberculosis* virulence: lipids inside and out. Nature medicine, 13(3), pp.284-285.

Falzon, D., Jaramillo, E., Schünemann, H.J., Arentz, M., Bauer, M., Bayona, J., Blanc, L., Caminero, J.A., Daley, C.L., Duncombe, C. and Fitzpatrick, C., 2011. WHO guidelines for the programmatic management of drug-resistant tuberculosis: 2011 update.

Feltcher, M.E., Sullivan, J.T. and Braunstein, M., 2010. Protein export systems of *Mycobacterium tuberculosis*: novel targets for drug development?. Future microbiology, 5(10), pp.1581-1597.

Ferraris, D.M., Sbardella, D., Petrera, A., Marini, S., Amstutz, B., Coletta, M., Sander, P. and Rizzi, M., 2011. Crystal structure of *Mycobacterium tuberculosis* zinc-dependent metalloprotease-1 (Zmp1), a metalloprotease involved in pathogenicity. Journal of Biological Chemistry, 286(37), pp.32475-32482.

Fesus, L. and Piacentini, M., 2002. Transglutaminase 2: an enigmatic enzyme with diverse functions. Trends in biochemical sciences, 27(10), pp.534-539.

Finlay, B.B. and Falkow, S., 1997. Common themes in microbial pathogenicity revisited. Microbiology and molecular biology reviews, 61(2), pp.136-169.

Fiol, F.D.S.D., Barberato-Filho, S., Lopes, L.C. and Toledo, M.I.D., 2010. Level of patient information on antibiotic use. Brazilian Journal of Pharmaceutical Sciences, 46, pp.437-444.

Forbes, M., Kuck, N.A. and Peets, E.A., 1965. Effect of ethambutol on nucleic acid metabolism in *Mycobacterium smegmatis* and its reversal by polyamines and divalent cations. Journal of bacteriology, 89(5), pp.1299-1305.

Forrellad, M. A., Klepp, L. I., Gioffré, A., Sabio y García, J., Morbidoni, H. R., de la Paz Santangelo, M., Cataldi, A. A., and Bigi, F. 2013. Virulence factors of the *Mycobacterium tuberculosis* complex. Virulence, 4(1), 3–66

Fortune, S.M., Jaeger, A., Sarracino, D.A., Chase, M.R., Sassetti, C.M., Sherman, D.R., Bloom, B.R. and Rubin, E.J., 2005. Mutually dependent secretion of proteins required for mycobacterial virulence. Proceedings of the National Academy of Sciences, 102(30), pp.10676-10681.

Friedlander, A.M., Bhatnagar, R., Leppla, S.H., Johnson, L. and Singh, Y., 1993. Characterization of macrophage sensitivity and resistance to anthrax lethal toxin. Infection and immunity, 61(1), pp.245-252.

Fu, L.M. and Fu-Liu, C.S., 2002. Is *Mycobacterium tuberculosis* a closer relative to Gram-positive or Gram–negative bacterial pathogens?. Tuberculosis, 82(2-3), pp.85-90.

Furin, J., Cox, H., and Pai, M. 2019. Tuberculosis. Lancet (London, England), 393(10181), pp.1642–1656.

Garde, S., Chodisetti, P.K. and Reddy, M., 2021. Peptidoglycan: structure, synthesis, and regulation. EcoSal Plus, 9(2).

Gordhan, B.G. and Parish, T., 2001. Gene replacement using pre-treated DNA. Methods in Molecular Medicine. 54, 77-92.

Gordon, S.V. and Parish, T., 2018. Microbe Profile: *Mycobacterium tuberculosis*: Humanity's deadly microbial foe. Microbiology. 164(4):437-9.

Goude, R., Amin, A.G., Chatterjee, D. and Parish, T., 2009. The arabinosyltransferase EmbC is inhibited by ethambutol in *Mycobacterium tuberculosis*. Antimicrobial agents and chemotherapy, 53(10), pp.4138-4146.

Guinn, K.M., Hickey, M.J., Mathur, S.K., Zakel, K.L., Grotzke, J.E., Lewinsohn, D.M., Smith, S. and Sherman, D.R., 2004. Individual RD1-region genes are required for export of ESAT-6/CFP-10 and for virulence of *Mycobacterium tuberculosis*. Molecular microbiology, 51(2), pp.359-370.

Guinn, K.M. and Rubin, E.J. 2017. Tuberculosis: just the FAQs. MBio. 8(6):e01910-17.

Gygli, S.M., Borrell, S., Trauner, A. and Gagneux, S., 2017. Antimicrobial resistance in *Mycobacterium tuberculosis*: mechanistic and evolutionary perspectives. FEMS microbiology reviews, 41(3), pp.354-373.

Hall, B.G., Acar, H., Nandipati, A. and Barlow, M., 2014. Growth rates made easy. Molecular biology and evolution, 31(1), pp.232-238.

Hanna, P.C., Kruskal, B.A., Ezekowitz, R.A.B., Bloom, B.R. and Collier, R.J., 1994. Role of macrophage oxidative burst in the action of anthrax lethal toxin. Molecular Medicine, 1, pp.7-18.

Harding, E., 2020. WHO global progress report on tuberculosis elimination. The Lancet Respiratory Medicine, 8(1), p.19.

Hawley, R.S. and Gilliland, W.D., 2006. Sometimes the result is not the answer: the truths and the lies that come from using the complementation test. Genetics, 174(1), pp.5-15.

Heinemann, P.M., Armbruster, D. and Hauer, B., 2021. Active-site loop variations adjust activity and selectivity of the cumene dioxygenase. Nature Communications, 12(1), p.1095.

Henrichsen, J., 1972. Bacterial surface translocation: a survey and a classification. Bacteriological reviews, 36(4), pp.478-503.

Hett, E.C. and Rubin, E.J., 2008. Bacterial growth and cell division: a mycobacterial perspective. Microbiology and Molecular Biology Reviews, 72(1), pp.126-156.

Hirmondó, R., Horváth, Á., Molnár, D., Török, G., Nguyen, L. and Tóth, J., 2022. The effects of mycobacterial *RmlA* perturbation on cellular dNTP pool, cell morphology, and replication stress in *Mycobacterium smegmatis*. Plos one, 17(2), p.e0263975.

Hmelo, L.R., Borlee, B.R., Almblad, H., Love, M.E., Randall, T.E., Tseng, B.S., Lin, C., Irie, Y., Storek, K.M., Yang, J.J. and Siehnel, R.J., 2015. Precision-engineering the *Pseudomonas aeruginosa* genome with two-step allelic exchange. Nature protocols, 10(11), pp.1820-1841.

Houben, R.M. and Dodd, P.J., 2016. The global burden of latent tuberculosis infection: a re-estimation using mathematical modelling. PLoS medicine, 13(10), p.e1002152.

Huheey, J.E., Keiter, E.A., Keiter, R.L. and Medhi, O.K., 2006. Inorganic chemistry: principles of structure and reactivity. Pearson Education India; 2006.

Humann, J. and Lenz, L.L., 2009. Bacterial peptidoglycan-degrading enzymes and their impact on host muropeptide detection. Journal of innate immunity, 1(2), pp.88-97.

Hunter, R.L., Olsen, M.R., Jagannath, C. and Actor, J.K., 2006. Multiple roles of cord factor in the pathogenesis of primary, secondary, and cavitary tuberculosis, including a revised description of the pathology of secondary disease. Annals of Clinical & Laboratory Science, 36(4), pp.371-386.

Huo, F., Zhang, F., Xue, Y., Shang, Y., Liang, Q., Ma, Y., Li, Y., Zhao, L. and Pang, Y., 2020. Increased prevalence of levofloxacin-resistant *Mycobacterium tuberculosis* in China is associated with specific mutations within the *gyrA* gene. International Journal of Infectious Diseases, 92, pp.241-246.

Hussain, S., Khan, M., Sheikh, T.M.M., Mumtaz, M.Z., Chohan, T.A., Shamim, S. and Liu, Y., 2022. Zinc essentiality, toxicity, and its bacterial bioremediation: A comprehensive insight. Frontiers in microbiology, 13, p.900740.

Ilic, M., Bjelic, D., Javorac, J., Veres, K.T., Zivanovic, D., Kovačevic, D., Maric, N., Lalic, N., Colic, N. and Stjepanovic, M., 2023. Knowledge is the most powerful tool in the fight against tuberculosis. The Journal of Infection in Developing Countries, 17(08), pp.1099-1106.

Indrigo, J., Hunter Jr, R.L. and Actor, J.K., 2002. Influence of trehalose 6, 6′-dimycolate (TDM) during mycobacterial infection of bone marrow macrophages. Microbiology, 148(7), pp.1991-1998.

Johansen, P., Fettelschoss, A., Amstutz, B., Selchow, P., Waeckerle-Men, Y., Keller, P., Deretic, V., Held, L., Kündig, T.M., Böttger, E.C. and Sander, P., 2011. Relief from Zmp1-mediated arrest of phagosome maturation is associated with facilitated presentation and enhanced immunogenicity of mycobacterial antigens. Clinical and Vaccine Immunology, 18(6), pp.907-913.

Judd, J.A., Canestrari, J., Clark, R., Joseph, A., Lapierre, P., Lasek-Nesselquist, E., Mir, M., Palumbo, M., Smith, C., Stone, M. and Upadhyay, A., 2021. A mycobacterial systems resource for the research community. MBio, 12(2), pp.10-1128.

Juettner, N.E., Schmelz, S., Anderl, A., Colin, F., Classen, M., Pfeifer, F., Scrima, A. and Fuchsbauer, H.L., 2020. The N-terminal peptide of the transglutaminase-activating metalloprotease inhibitor from Streptomyces mobaraensis accommodates both inhibition and glutamine cross-linking sites. The FEBS Journal, 287(4), pp.708-720.

Justen, A.M., Hodges, H.L., Kim, L.M., Sadecki, P.W., Porfirio, S., Ultee, E., Black, I., Chung, G.S., Briegel, A., Azadi, P. and Kiessling, L.L., 2020. Polysaccharide length affects mycobacterial cell shape and antibiotic susceptibility. Science Advances, 6(38), p.eaba4015.

Kalscheuer, R., Palacios, A., Anso, I., Cifuente, J., Anguita, J., Jacobs Jr, W.R., Guerin, M.E. and Prados-Rosales, R., 2019. The *Mycobacterium tuberculosis* capsule: a cell structure with key implications in pathogenesis. Biochemical Journal, 476(14), pp.1995-2016.

Kana, B.D., Mizrahi, V. and Gordhan, B.G., 2010. Depletion of resuscitation-promoting factors has limited impact on the drug susceptibility of *Mycobacterium tuberculosis*. Journal of antimicrobial chemotherapy, 65(8), pp.1583-1585.

Kanetsuna, F., Imaeda, T. and Cunto, G., 1969. On the linkage between mycolic acid and arabinogalactan in phenol-treated mycobacterial cell walls. Biochimica et Biophysica Acta (BBA)-Biomembranes, 173(2), pp.341-344.

Kaufmann, S.H., 2001. How can immunology contribute to the control of tuberculosis?. Nat Rev Immunol. 1(1):20-30.

Kearns, D.B., Bonner, P.J., Smith, D.R. and Shimkets, L.J., 2002. An extracellular matrix-associated zinc metalloprotease is required for dilauroyl phosphatidylethanolamine chemotactic excitation in *Myxococcus xanthus*. Journal of bacteriology, 184(6), pp.1678-1684.

Kieser, K.J. and Rubin, E.J., 2014. How sisters grow apart: mycobacterial growth and division. Nature Reviews Microbiology, 12(8), pp.550-562.

Kieswetter, N.S., Ozturk, M., Jones, S.S., Senzani, S., Chengalroyen, M.D., Brombacher, F., Kana, B. and Guler, R., 2021. Deletion of N-acetylmuramyl-L-alanine amidases alters the host immune response to *Mycobacterium tuberculosis* infection. Virulence, 12(1), pp.1227-1238.

Knutson, K.L., Hmama, Z., Herrera-Velit, P., Rochford, R. and Reiner, N.E., 1998. Lipoarabinomannan of *Mycobacterium tuberculosis* promotes protein tyrosine dephosphorylation and inhibition of Mitogen-activated Protein Kinase in human mononuclear phagocytes: Role of the *src* homology 2 containing tyrosine phosphatase 1. Journal of Biological Chemistry, 273(1), pp.645-652.

Koul, A., Arnoult, E., Lounis, N., Guillemont, J. and Andries, K., 2011. The challenge of new drug discovery for tuberculosis. Nature, 469(7331), pp.483-490.

Krishna, S.S., Majumdar, I. and Grishin, N.V., 2003. Structural classification of zinc fingers: survey and summary. Nucleic acids research, 31(2), pp.532-550.

Krishnamurthi, V.R., Niyonshuti, I.I., Chen, J. and Wang, Y., 2021. A new analysis method for evaluating bacterial growth with microplate readers. PLoS One, 16(1), p.e0245205.

Kulka, K., Hatfull, G. and Ojha, A.K., 2012. Growth of *Mycobacterium tuberculosis* biofilms. Journal of visualized experiments: JoVE, (60), p.3820.

Lambert, P.A., 2002. Cellular impermeability and uptake of biocides and antibiotics in Gram-positive bacteria and mycobacteria. Journal of applied microbiology, 92(s1), pp.46S-54S.

Lederer, E., Adam, A., Ciorbaru, R., Petit, J.F. and Wietzerbin, J., 1975. Cell walls of mycobacteria and related organisms; chemistry and immunostimulant properties. Molecular and cellular biochemistry, 7(2), pp.87-104.

Lee, P.W., Hayes, E.C. and Joklik, W.K., 1981. Protein σ1 is the reovirus cell attachment protein. Virology, 108(1), pp.156-163.

Lee, W.H., Loo, C.Y., Traini, D. and Young, P.M., 2015. Nano-and micro-based inhaled drug delivery systems for targeting alveolar macrophages. Expert opinion on drug delivery, 12(6), pp.1009-1026.

Lepp, D., Roxas, B., Parreira, V.R., Marri, P.R., Rosey, E.L., Gong, J., Songer, J.G., Vedantam, G. and Prescott, J.F., 2010. Identification of novel pathogenicity loci in *Clostridium perfringens* strains that cause avian necrotic enteritis. PLoS One, 5(5), p.e10795.

Leseigneur, C., Lê-Bury, P., Pizarro-Cerdá, J. and Dussurget, O., 2020. Emerging evasion mechanisms of macrophage defenses by pathogenic bacteria. Frontiers in Cellular and Infection Microbiology, 10, p.577559.

Li, Y.Y., Liu, H.M., Wang, D., Lu, Y., Ding, C., Zhou, L.S., Wu, X.Y., Zhou, Z.W., Xu, S.Q., Lin, C. and Qin, L.H., 2022. Arabinogalactan enhances *Mycobacterium marinum* virulence by suppressing host innate immune responses. Frontiers in Immunology, 13, p.879775.

Liao, J.Y., Guo, Y.H., Zheng, L.L., Li, Y., Xu, W.L., Zhang, Y.C., Zhou, H., Lun, Z.R., Ayala, F.J. and Qu, L.H., 2014. Both endo-siRNAs and tRNA-derived small RNAs are involved in the differentiation of primitive eukaryote *Giardia lamblia*. Proceedings of the National Academy of Sciences, 111(39), pp.14159-14164.

Liemann, S., Chandran, K., Baker, T.S., Nibert, M.L. and Harrison, S.C., 2002. Structure of the reovirus membrane-penetration protein, μ1, in a complex with its protector protein, σ3. Cell, 108(2), pp.283-295.

Lin, H., Andersen, G.R. and Yatime, L., 2016. Crystal structure of human S100A8 in complex with zinc and calcium. BMC structural biology, 16, pp.1-10.

Lincoln, R.E., Rhian, M.A., Klein, F. and Fernelius, A., 1961. Pathogenesis as related to physiological state of anthrax spore and cell. Spores, 11, pp.255-73.

Liu, L., White, M.J. and MacRae, T.H., 1999. Transcription factors and their genes in higher plants: functional domains, evolution and regulation. European Journal of Biochemistry, 262(2), pp.247-257.

López-Otín, C. and Bond, J.S., 2008. Proteases: multifunctional enzymes in life and disease. Journal of Biological Chemistry, 283(45), pp.30433-30437.

Lou, Y., Rybniker, J., Sala, C. and Cole, S.T., 2017. *EspC* forms a filamentous structure in the cell envelope of *Mycobacterium tuberculosis* and impacts ESX-1 secretion. Molecular microbiology, 103(1), pp.26-38.

Ly, A. and Liu, J., 2020. Mycobacterial virulence factors: Surface-exposed lipids and secreted proteins. International Journal of Molecular Sciences, 21(11), p.3985.

Magombedze, G., Dowdy, D. and Mulder, N., 2013. Latent tuberculosis: models, computational efforts and the pathogen's regulatory mechanisms during dormancy. Frontiers in bioengineering and biotechnology, 1, p.4.

Mahapatra, S., Scherman, H., Brennan, P.J. and Crick, D.C., 2005. N Glycolylation of the nucleotide precursors of peptidoglycan biosynthesis of Mycobacterium spp. is altered by drug treatment. Journal of bacteriology, 187(7), pp.2341-2347.

Maier, R.M. and Pepper, I.L., 2015. Bacterial growth. In Environmental microbiology (pp. 37-56). Academic Press.

Maitra, A., Munshi, T., Healy, J., Martin, L.T., Vollmer, W., Keep, N.H. and Bhakta, S., 2019. Cell wall peptidoglycan in *Mycobacterium tuberculosis*: An Achilles' heel for the TB-causing pathogen. FEMS microbiology reviews, 43(5), pp.548-575.

Major, R.H., 1945. Classic descriptions of disease: with biographical sketches of the authors. (No Title).

Makinoshima, H. and Glickman, M.S., 2005. Regulation of *Mycobacterium tuberculosis* cell envelope composition and virulence by intramembrane proteolysis. Nature, 436(7049), pp.406-409.

Malhotra, S., Vedithi, S.C. and Blundell, T.L., 2017. Decoding the similarities and differences among mycobacterial species. PLoS neglected tropical diseases, 11(8), p.e0005883.

Maphasa, R.E., Meyer, M. and Dube, A., 2021. The macrophage response to *Mycobacterium tuberculosis* and opportunities for autophagy inducing nanomedicines for tuberculosis therapy. Frontiers in Cellular and Infection Microbiology, 10, p.618414.

Martínez, A., Torello, S. and Kolter, R., 1999. Sliding motility in mycobacteria. Journal of bacteriology. 181(23):7331-8.

Master, S.S., Rampini, S.K., Davis, A.S., Keller, C., Ehlers, S., Springer, B., Timmins, G.S., Sander, P. and Deretic, V., 2008. *Mycobacterium tuberculosis* prevents inflammasome activation. Cell host & microbe, 3(4), pp.224-232.

Mawuenyega, K.G., Forst, C.V., Dobos, K.M., Belisle, J.T., Chen, J., Bradbury, E.M., Bradbury, A.R. and Chen, X., 2005. *Mycobacterium tuberculosis* functional network analysis by global subcellular protein profiling. Molecular Biology of the cell, 16(1), pp.396-404.

McCall, K.A., Huang, C.C. and Fierke, C.A., 2000. Function and mechanism of zinc metalloenzymes. The Journal of nutrition, 130(5), pp.1437S-1446S.

Middlebrook, G., Dubos, R.J. and Pierce, C., 1947. Virulence and morphological characteristics of mammalian tubercle bacilli. The Journal of experimental medicine, 86(2), pp.175-184.

Mirghani, R., Saba, T., Khaliq, H., Mitchell, J., Do, L., Chambi, L., Diaz, K., Kennedy, T., Alkassab, K., Huynh, T. and Elmi, M., 2022. Biofilms: Formation, drug resistance and alternatives to conventional approaches. AIMS microbiology, 8(3), p.239.

Miyoshi, S.I. and Shinoda, S., 2000. Microbial metalloproteases and pathogenesis. Microbes and infection, 2(1), pp.91-98.

Moianos, D., Prifti, G.M., Makri, M. and Zoidis, G., 2023. Targeting Metalloenzymes: The "Achilles' Heel" of Viruses and Parasites. Pharmaceuticals, 16(6), p.901.

Morlock, G.P., Metchock, B., Sikes, D., Crawford, J.T. and Cooksey, R.C., 2003. ethA, inhA, and katG loci of ethionamide-resistant clinical *Mycobacterium tuberculosis* isolates. Antimicrobial agents and chemotherapy, 47(12), pp.3799-3805.

Morse, D., 1967. Tuberculosis. In: Brothwell D, Sandison AT, editors. Diseases in antiquity. A survey of the diseases, injuries and surgery of early populations. Springfield, IL: Charles C. Thomas.

Müller, B. and Grossniklaus, U., 2010. Model organisms—a historical perspective. Journal of proteomics, 73(11), pp.2054-2063.

Nakjang, S., Ndeh, D.A., Wipat, A., Bolam, D.N. and Hirt, R.P., 2012. A novel extracellular metallopeptidase domain shared by animal host-associated mutualistic and pathogenic microbes. PloS one, 7(1), p.e30287.

Nikitushkin, V.D., Demina, G.R., Shleeva, M.O. and Kaprelyants, A.S., 2013. Peptidoglycan fragments stimulate resuscitation of "non-culturable" mycobacteria. Antonie Van Leeuwenhoek, 103, pp.37-46.

Oddo, M., Renno, T., Attinger, A., Bakker, T., MacDonald, H.R. and Meylan, P.R., 1998. Fas ligand-induced apoptosis of infected human macrophages reduces the viability of intracellular *Mycobacterium tuberculosis*. The Journal of Immunology, 160(11), pp.5448-5454.

Ogura, Y., Inohara, N., Benito, A., Chen, F.F., Yamaoka, S. and Nunez, G., 2001. Nod2, a Nod1/Apaf-1 family member that is restricted to monocytes and activates NF-κB. Journal of Biological Chemistry, 276(7), pp.4812-4818.

Ortalo-Magne, A., Dupont, M.A., Lemassu, A., Andersen, A.B., Gounon, P. and Mamadou, D., 1995. Molecular composition of the outermost capsular material of the tubercle bacillus. Microbiology, 141(7), pp.1609-1620.

Ortalo-Magne, A., Lemassu, A., Laneelle, M.A., Bardou, F., Silve, G., Gounon, P., Marchal, G. and Daffé, M., 1996. Identification of the surface-exposed lipids on the cell envelopes of *Mycobacterium tuberculosis* and other mycobacterial species. Journal of bacteriology, 178(2), pp.456-461.

Palucci, I., Matic, I., Falasca, L., Minerva, M., Maulucci, G., De Spirito, M., Petruccioli, E., Goletti, D., Rossin, F., Piacentini, M. and Delogu, G., 2018. Transglutaminase type 2 plays a key role in the pathogenesis of *Mycobacterium tuberculosis* infection. Journal of internal medicine, 283(3), pp.303-313.

Parish, T., Gordhan, B.G., McAdam, R.A., Duncan, K., Mizrahi, V. and Stoker, N.G., 1999. Production of mutants in amino acid biosynthesis genes of *Mycobacterium tuberculosis* by homologous recombination. Microbiology, 145(12), pp.3497-3503.

Parish, T. and Stoker, N.G., 2000. Use of a flexible cassette method to generate a double unmarked *Mycobacterium tuberculosis tlyA plcABC* mutant by gene replacement. Microbiology, 146(8), pp.1969-1975.

Parsons, C., Azizoglu, R., Elhanafi, D. and Kathariou, S., 2021. Mutant Construction and Integration Vector-Mediated Genetic Complementation in *Listeria monocytogenes*. *Listeria Monocytogenes*: Methods and Protocols, pp.177-185.

Peterson, J.W., 1996. Bacterial Pathogenesis. In: Baron S, editor. Medical Microbiology. 4th edition. Galveston (TX): University of Texas Medical Branch at Galveston; 1996. Chapter 7. Available from: https://www.ncbi.nlm.nih.gov/books/NBK8526/

Pieters, J., 2008. *Mycobacterium tuberculosis* and the macrophage: maintaining a balance. Cell host & microbe. 3(6):399-407.

Plotniece, A., Sobolev, A., Supuran, C.T., Carta, F., Björkling, F., Franzyk, H., Yli-Kauhaluoma, J., Augustyns, K., Cos, P., De Vooght, L. and Govaerts, M., 2023. Selected strategies to fight pathogenic bacteria. Journal of enzyme inhibition and medicinal chemistry, 38(1), p.2155816.

Pope, W.H., Ferreira, C.M., Jacobs-Sera, D., Benjamin, R.C., Davis, A.J., DeJong, R.J., Elgin, S.C., Guilfoile, F.R., Forsyth, M.H., Harris, A.D. and Harvey, S.E., 2011. Cluster K mycobacteriophages: insights into the evolutionary origins of mycobacteriophage TM4. PLoS One, 6(10), p.e26750.

Portal-Celhay, C., Tufariello, J.M., Srivastava, S., Zahra, A., Klevorn, T., Grace, P.S., Mehra, A., Park, H.S., Ernst, J.D., Jacobs, W.R. and Philips, J.A., 2016. *Mycobacterium tuberculosis EsxH* inhibits ESCRT-dependent CD4+ T-cell activation. Nature microbiology, 2(2), pp.1-9.

Puri, R.V., Reddy, P.V. and Tyagi, A.K., 2013. Secreted acid phosphatase (SapM) of *Mycobacterium tuberculosis* is indispensable for arresting phagosomal maturation and growth of the pathogen in guinea pig tissues. PloS one, 8(7), p.e70514.

Qiagen. 2024. How do I perform a DNA precipitation to concentrate my sample? https://www.qiagen.com/us/resources/faq?id=5d591b8b-968a-4a17-849f-9d0f719b40af&lang=en

Qiu, Y., Zhou, Y., Chang, Y., Liang, X., Zhang, H., Lin, X., Qing, K., Zhou, X. and Luo, Z., 2022. The effects of ventilation, humidity, and temperature on bacterial growth and bacterial genera distribution. International Journal of Environmental Research and Public Health, 19(22), p.15345.

Quémard, A., Lanéelle, G. and Lacave, C., 1992. Mycolic acid synthesis: a target for ethionamide in mycobacteria?. Antimicrobial agents and chemotherapy, 36(6), pp.1316-1321.

Quinn, C.P., Dull, P.M., Semenova, V., Li, H., Crotty, S., Taylor, T.H., Steward-Clark, E., Stamey, K.L., Schmidt, D.S., Stinson, K.W. and Freeman, A.E., 2004. Immune responses to *Bacillus anthracis* protective antigen in patients with bioterrorism-related cutaneous or inhalation anthrax. The Journal of infectious diseases, 190(7), pp.1228-1236.

Rahman, F., Wushur, I., Malla, N., Åstrand, O.A.H., Rongved, P., Winberg, J.O. and Sylte, I., 2021. Zinc-chelating compounds as inhibitors of human and bacterial zinc metalloproteases. Molecules, 27(1), p.56.

Rajni, Rao N, Meena LS. 2011. Biosynthesis and virulent behavior of lipids produced by *Mycobacterium tuberculosis*: LAM and cord factor: an overview. Biotechnology research international. 2011(1):274693.

Raman, S., Hazra, R., Dascher, C.C. and Husson, R.N., 2004. Transcription regulation by the *Mycobacterium tuberculosis* alternative sigma factor SigD and its role in virulence. Journal of bacteriology, 186(19), pp.6605-6616.

Randall, P.J., Hsu, N.J., Quesniaux, V., Ryffel, B. and Jacobs, M., 2015. *Mycobacterium tuberculosis* infection of the 'non-classical immune cell'. Immunology and cell biology, 93(9), pp.789-795.

Ranjitha, J., Rajan, A. and Shankar, V., 2020. Features of the biochemistry of *Mycobacterium smegmatis*, as a possible model for *Mycobacterium tuberculosis*. Journal of infection and public health, 13(9), pp.1255-1264.

Rao, M.B., Tanksale, A.M., Ghatge, M.S. and Deshpande, V.V., 1998. Molecular and biotechnological aspects of microbial proteases. Microbiology and molecular biology reviews, 62(3), pp.597-635.

Rao, V.S., Srinivas, K., Sujini, G.N. and Kumar, G.S., 2014. Protein-protein interaction detection: methods and analysis. International journal of proteomics, 2014(1), p.147648.

Rawlings, N.D., Barrett, A.J., Thomas, P.D., Huang, X., Bateman, A. and Finn, R.D., 2018. The MEROPS database of proteolytic enzymes, their substrates and inhibitors in 2017 and a comparison with peptidases in the PANTHER database. Nucleic acids research, 46(D1), pp.D624-D632.

Raymond, J.B., Mahapatra, S., Crick, D.C. and Pavelka, M.S., 2005. Identification of the *namH* gene, encoding the hydroxylase responsible for the N-glycolylation of the mycobacterial peptidoglycan. Journal of Biological Chemistry, 280(1), pp.326-333.

Roelens, M., Battista Migliori, G., Rozanova, L., Estill, J., Campbell, J.R., Cegielski, J.P., Tiberi, S., Palmero, D., Fox, G.J., Guglielmetti, L. and Sotgiu, G., 2021. Evidence-based definition for extensively drug-resistant tuberculosis. American journal of respiratory and critical care medicine, 204(6), pp.713-722.

Romero, M.M., Balboa, L., Basile, J.I., Lopez, B., Ritacco, V., De la Barrera, S.S., Sasiain, M.C., Barrera, L. and Alemán, M., 2012. Clinical isolates of *Mycobacterium tuberculosis* differ in their ability to induce respiratory burst and apoptosis in neutrophils as a possible mechanism of immune escape. Journal of Immunology Research, 2012(1), p.152546.

Roy, S., Ghatak, D., Das, P. and BoseDasgupta, S., 2020. ESX secretion system: The gatekeepers of mycobacterial survivability and pathogenesis. European Journal of Microbiology and Immunology, 10(4), pp.202-209.

Ruiz-Barba, J.L., Maldonado-Barragán, A. and Jiménez Díaz, R., 2005. Small-scale total DNA extraction from bacteria and yeast for PCR applications.

Salton, M.R.J. and Kim, K.S., 1996. Structure In: Baron S, editor. Galveston (TX), University of Texas Medical Branch at Galveston.

Sani, M., Houben, E.N., Geurtsen, J., Pierson, J., de Punder, K., van Zon, M., Wever, B., Piersma, S.R., Jiménez, C.R., Daffé, M. and Appelmelk, B.J., 2010. Direct visualization by cryo-EM of the mycobacterial capsular layer: a labile structure containing ESX-1-secreted proteins. PLoS pathogens, 6(3), p.e1000794.

Sarangi, A., Singh, S.P., Das, B.S., Rajput, S., Fatima, S. and Bhattacharya, D., 2024. Mycobacterial biofilms: A therapeutic target against bacterial persistence and generation of antibiotic resistance. Heliyon.

Schaberg, T., Bauer, T., Brinkmann, F., Diel, R., Feiterna-Sperling, C., Haas, W., Hartmann, P., Hauer, B., Heyckendorf, J., Lange, C. and Nienhaus, A., 2017. Tuberculosis guideline for adults-guideline for diagnosis and treatment of tuberculosis including LTBI testing and treatment of the German central committee (DZK) and the German respiratory society (DGP). Pneumologie (Stuttgart, Germany), 71(6), pp.325-397.

Schenk, M., Mahapatra, S., Le, P., Kim, H.J., Choi, A.W., Brennan, P.J., Belisle, J.T. and Modlin, R.L., 2016. Human NOD2 recognizes structurally unique muramyl dipeptides from *Mycobacterium leprae*. Infection and immunity, 84(9), pp.2429-2438.

Seid, M.A., Ayalew, M.B., Muche, E.A., Gebreyohannes, E.A. and Abegaz, T.M., 2018. Drug-susceptible tuberculosis treatment success and associated factors in Ethiopia from 2005 to 2017: a systematic review and meta-analysis. BMJ open, 8(9), p.e022111.

Senzani, S., Li, D., Bhaskar, A., Ealand, C., Chang, J., Rimal, B., Liu, C., Joon Kim, S., Dhar, N. and Kana, B., 2017. An Amidase_3 domain-containing N-acetylmuramyl-L-alanine amidase is required for mycobacterial cell division. Scientific reports, 7(1), p.1140.

Seung, K.J., Keshavjee, S. and Rich, M.L., 2015. Multidrug-resistant tuberculosis and extensively drug-resistant tuberculosis. Cold Spring Harbor perspectives in medicine, 5(9), p.a017863.

Shah, M. and Chida, N., 2017. Extrapulmonary tuberculosis. Handbook of Tuberculosis. 91-118.

Shi, R., Zhang, J., Li, C., Kazumi, Y. and Sugawara, I., 2007. Detection of streptomycin resistance in *Mycobacterium tuberculosis* clinical isolates from China as determined by denaturing HPLC analysis and DNA sequencing. Microbes and infection, 9(14-15), pp.1538-1544.

Shi, W., Zhang, S., Feng, J., Cui, P., Zhang, W. and Zhang, Y., 2017. Clofazimine targets essential nucleoid associated protein, mycobacterial integration host factor (*mIHF*), in *Mycobacterium tuberculosis*. bioRxiv, p.192161.

Shin, J.H., Tillotson, G., MacKenzie, T.N., Warren, C.A., Wexler, H.M. and Goldstein, E.J., 2024. Bacteroides and related species: The keystone taxa of the human gut microbiota. Anaerobe, 85, p.102819.

Siegrist, M.S., Unnikrishnan, M., McConnell, M.J., Borowsky, M., Cheng, T.Y., Siddiqi, N., Fortune, S.M., Moody, D.B. and Rubin, E.J., 2009. Mycobacterial Esx-3 is required for mycobactin-mediated iron acquisition. Proceedings of the National Academy of Sciences, 106(44), pp.18792-18797.

Singh, G., Kumar, A., Maan, P. and Kaur, J., 2017. Cell wall associated factors of *Mycobacterium tuberculosis* as major virulence determinants: current perspectives in drugs discovery and design. Current drug targets, 18(16), pp.1904-1918.

Sklar, J.G., Makinoshima, H., Schneider, J.S. and Glickman, M.S., 2010. *M. tuberculosis* intramembrane protease Rip1 controls transcription through three anti-sigma factor substrates. Molecular microbiology, 77(3), pp.605-617.

Smieja, M., Marchetti, C., Cook, D., Smaill, F.M. and Cochrane Infectious Diseases Group, 1996. Isoniazid for preventing tuberculosis in non-HIV infected persons. Cochrane database of systematic reviews, 2019(5).

Smith, I., 2003. *Mycobacterium tuberculosis* pathogenesis and molecular determinants of virulence. Clin Microbiol Rev. 16(3):463-96

Smith, S.A. and Pease, J.B., 2017. Heterogeneous molecular processes among the causes of how sequence similarity scores can fail to recapitulate phylogeny. Briefings in bioinformatics, 18(3), pp.451-457.

Snapper, S.B., Melton, R.E., Mustafa, S., Kieser, T. and Jr, W.J., 1990. Isolation and characterization of efficient plasmid transformation mutants of *Mycobacterium smegmatis*. Molecular microbiology, 4(11), pp.1911-1919.

Soetaert, K., Rens, C., Wang, X.M., De Bruyn, J., Lanéelle, M.A., Laval, F., Lemassu, A., Daffé, M., Bifani, P., Fontaine, V. and Lefèvre, P., 2015. Increased vancomycin susceptibility in mycobacteria: a new approach to identify synergistic activity against multidrug-resistant mycobacteria. Antimicrobial Agents and Chemotherapy, 59(8), pp.5057-5060.

Solomonson, M., Setiaputra, D., Makepeace, K.A., Lameignere, E., Petrotchenko, E.V., Conrady, D.G., Bergeron, J.R., Vuckovic, M., DiMaio, F., Borchers, C.H. and Yip, C.K., 2015. Structure of *EspB* from the ESX-1 type VII secretion system and insights into its export mechanism. Structure, 23(3), pp.571-583.

Somerville, W., Thibert, L., Schwartzman, K. and Behr, M.A., 2005. Extraction of *Mycobacterium tuberculosis* DNA: a question of containment. Journal of clinical microbiology, 43(6), pp.2996-2997.

Song, H., Sandie, R., Wang, Y., Andrade-Navarro, M.A. and Niederweis, M., 2008. Identification of outer membrane proteins of *Mycobacterium tuberculosis*. Tuberculosis, 88(6), pp.526-544.

Sparks, I.L., Derbyshire, K.M., Jacobs Jr, W.R. and Morita, Y.S., 2023. *Mycobacterium smegmatis*: the vanguard of mycobacterial research. Journal of bacteriology, 205(1), pp.e00337-22.

Stats SA. 2021. TB tops leading causes of death in Sa in 2018. http://www.statssa.gov.za/?p=14435

Stover, C.K., De La Cruz, V.F., Fuerst, T.R., Burlein, J.E., Benson, L.A., Bennett, L.T., Bansal, G.P., Young, J.F., Lee, M.H., Hatfull, G.F. and Snapper, S.B., 1991. New use of BCG for recombinant vaccines. Nature, 351(6326), pp.456-460.

Thanky, N.R., Young, D.B. and Robertson, B.D., 2007. Unusual features of the cell cycle in mycobacteria: polar-restricted growth and the snapping-model of cell division. Tuberculosis, 87(3), pp.231-236.

Thermofisher Scientific. "Competent cell genotypes and genetic markers". Thermofisher Scentific. Available on: https://www.thermofisher.com/za/en/home/life-science/cloning/cloning-learning-center/invitrogen-school-of-molecular-biology/molecular-cloning/transformation/competent-cell-genotypes-genetic-markers.html. Accessed on 15/12/2024

Theron, L.W. and Divol, B., 2014. Microbial aspartic proteases: current and potential applications in industry. Applied microbiology and biotechnology. 98:8853-68.

Thompson, M.W., 2022. Regulation of zinc-dependent enzymes by metal carrier proteins. Biometals. 35(2):187-213.

Tseng, S.T., Tai, C.H., Li, C.R., Lin, C.F. and Shi, Z.Y., 2015. The mutations of *katG* and *inhA* genes of isoniazid-resistant *Mycobacterium tuberculosis* isolates in Taiwan. Journal of Microbiology, Immunology and Infection, 48(3), pp.249-255.

Udou, T., Ogawa. and Mizuguchi, Y., 1982. Spheroplast formation of *Mycobacterium smegmatis* and morphological aspects of their reversion to the bacillary form. Journal of Bacteriology, 151(2), pp.1035-1039.

Vallee, B.L. and Auld, D.S., 1990. Zinc coordination, function, and structure of zinc enzymes and other proteins. Biochemistry. 29(24):5647-59.

Van Rossum, T., Ferretti, P., Maistrenko, O.M. and Bork, P., 2020. Diversity within species: interpreting strains in microbiomes. Nature Reviews Microbiology, 18(9), pp.491-506.

Vemula, M.H., Medisetti, R., Ganji, R., Jakkala, K., Sankati, S., Chatti, K. and Banerjee, S., 2016. *Mycobacterium tuberculosis* zinc metalloprotease-1 assists mycobacterial dissemination in zebrafish. Frontiers in Microbiology, 7, p.1347.

Vergne, I., Chua, J. and Deretic, V., 2003. Tuberculosis toxin blocking phagosome maturation inhibits a novel Ca2+/calmodulin-PI3K hVPS34 cascade. The Journal of experimental medicine, 198(4), pp.653-659.

Viljoen, A., Gutiérrez, A.V., Dupont, C., Ghigo, E. and Kremer, L., 2018. A simple and rapid gene disruption strategy in *Mycobacterium abscessus*: on the design and application of glycopeptidolipid mutants. Frontiers in cellular and infection microbiology, 8, p.69.

Wade, B., Keyburn, A.L., Haring, V., Ford, M., Rood, J.I. and Moore, R.J., 2020. Two putative zinc metalloproteases contribute to the virulence of *Clostridium perfringens* strains that cause avian necrotic enteritis. Journal of Veterinary Diagnostic Investigation, 32(2), pp.259-267.

Wang, Q., Boshoff, H.I., Harrison, J.R., Ray, P.C., Green, S.R., Wyatt, P.G. and Barry III, C.E., 2020. PE/PPE proteins mediate nutrient transport across the outer membrane of *Mycobacterium tuberculosis*. Science, 367(6482), pp.1147-1151.

Wang, Y., Yue, X.J., Yuan, S.F., Hong, Y., Hu, W.F. and Li, Y.Z., 2021. Internal promoters and their effects on the transcription of operon genes for epothilone production in *Myxococcus xanthus*. Frontiers in bioengineering and biotechnology, 9, p.758561.

Wiker, H.G. and Harboe, M., 1992. The antigen 85 complex: a major secretion product of *Mycobacterium tuberculosis*. Microbiological reviews, 56(4), pp.648-661.

Williams, R.J., 1987. The biochemistry of zinc. Polyhedron. 6(1):61-9.

Wivagg, C.N. and Hung, D.T., 2012. Resuscitation-promoting factors are required for β-lactam tolerance and the permeability barrier in *Mycobacterium tuberculosis*. Antimicrobial agents and chemotherapy, 56(3), pp.1591-1594.

WHO. 2020. Global Tuberculosis Report 2020. Geneva, Switzerland

WHO. 2022. Global Tuberculosis Report 2022. Geneva, Switzerland.

WHO. 2024. Global tuberculosis report 2024. Geneva, Switzerland

Wright, P.E. and Dyson, H.J., 2009. Linking folding and binding. Current opinion in structural biology, 19(1), pp.31-38.

Wu, H.J., Wang, A.H. and Jennings, M.P., 2008. Discovery of virulence factors of pathogenic bacteria. Current opinion in chemical biology, 12(1), pp.93-101.

Wu, Y., Xiong, D.C., Chen, S.C., Wang, Y.S. and Ye, X.S., 2017. Total synthesis of mycobacterial arabinogalactan containing 92 monosaccharide units. Nature communications, 8(1), p.14851.

Yamazaki, Y., Danelishvili, L., Wu, M., MacNab, M. and Bermudez, L.E., 2006. *Mycobacterium avium* genes associated with the ability to form a biofilm. Applied and environmental microbiology, 72(1), pp.819-825.

Yang, J. and Zhang, Y., 2015. I-TASSER server: new development for protein structure and function predictions. Nucleic acids research, 43(W1), pp.W174-W181.

Yee, D., Valiquette, C., Pelletier, M., Parisien, I., Rocher, I. and Menzies, D., 2003. Incidence of serious side effects from first-line antituberculosis drugs among patients treated for active tuberculosis. American journal of respiratory and critical care medicine, 167(11), pp.1472-1477.

Zambrano, M.M. and Kolter, R., 2018. Changes in bacterial cell properties in going from exponential growth to stationary phase. In Microbiological Quality Assurance (pp. 21-30). CRC Press.

Zastrow, M.L. and Pecoraro, V.L., 2014. Designing hydrolytic zinc metalloenzymes. Biochemistry, 53(6), pp.957-978.

Zhai, W., Wu, F., Zhang, Y., Fu, Y. and Liu, Z., 2019. The immune escape mechanisms of *Mycobacterium tuberculosis*. International journal of molecular sciences, 20(2), p.340.

Zhang Y, Heym B, Allen B, Young D, Cole S. The catalase—peroxidase gene and isoniazid resistance of *Mycobacterium tuberculosis*. Nature. 1992 Aug 13;358(6387):591-3.

Zhao, Y., Xu, S., Wang, L., Chin, D.P., Wang, S., Jiang, G., Xia, H., Zhou, Y., Li, Q., Ou, X. and Pang, Y., 2012. National survey of drug-resistant tuberculosis in China. New England Journal of Medicine, 366(23), pp.2161-2170.

8. Appendices

8.1. Appendix A: Culture media

- Nutrient Broth (NB)

1 g D (+)-glucose, 15 g peptone, 6 g NaCl, 3 g yeast extract, 1 000 mL dH_20, autoclaved

- Nutrient agar (NA)

15 g agar, 1 g meat extract, 5 g peptone, 5 g NaCl, 2 g yeast extract, 1 000 mL dH_20, autoclaved

- Luria-Bertani Broth (LB)

5 g yeast extract, 10 g tryptone, 10 g NaCl, 1 000 mL dH_2O, autoclaved

- Luria-Bertani Agar (LA)

5 g yeast extract, 10 g tryptone, 10 g NaCl, 15 g agar, 1 000 mL dH_2O, autoclaved

- 2 × TY broth

10 g yeast extract, 16 g tryptone, 5 g NaCl, 1 000 mL dH_2O, autoclaved

- 7H9 broth

2.35 g Difco Middlebrook 7H9 broth powder, 1 mL of 100% glycerol, 1.25 mL of 20% tyloxapol, 5 mL of 100 × glucose-salt, 500 mL dH_2O, autoclave

- 7H11 agar

9.5 g Difco Middlebrook 7H11 agar powder, 2.5 mL of 100% glycerol, 5 mL of 100 × glucose-salt, 500 mL dH_2O, autoclave

- 100 × glucose-salt

10 g glucose, 4.25 g NaCl, 500 ml dH_2O

- Sauton's Media (pH 7.2)

0.1 g Ammonium ferric citrate, 4 g L-asparagine, 2 g citric acid, 0.5 g magnesium sulphate, 0.5 g potassium dihydrogenorthophosphate, 60 mL glycerol, 1 000 mL dH_2O, 100 µL of 1% Zinc sulphate heptahydrate, pH using ammonium hydroxide and autoclave.

8.2. Appendix B: Solutions

8.2.1. DNA manipulation solutions

- 0.8% agarose gel

0.4 g agarose, 50 mL 1 × Sodium borate buffer, microwave until dissolved

- Loading dye

0.2 g bromophenol blue, 6 mL of 50% glycerol, 4 mL autoclaved dH_2O and supplemented with 0.01% gel red

- 10% Glycerol

10 mL glycerol, 90 mL dH_2O, autoclave

- 30% Glycerol

30 mL glycerol, 70 mL dH_2O, autoclaved

- Solution I

50 mM Glucose, 25 mM Tris-HCl, 10 mM Ethylenediaminetetraacetic acid disodium salt dihydrate (EDTA) (pH 8.0)

- Solution II

1 mL 10% SDS, 1 mL 2 M Sodium hydroxide (NaOH), 8 mL dH_2O

- Solution III

49 g potassium acetate, 11.5 mL glacial acetic acid, dH_2O up to 100 mL, autoclave

- 50 mM $CaCl_2$

2.20 g $CaCl_2$, 300 mL dH_2O, filter sterilize

- 50 mM $CaCl_2$ with 15% glycerol

2.20 g $CaCl_2$, 45 mL glycerol, make up to 300 mL dH_2O, autoclave

- 10 mg/mL RNase A

100 mg RNase, 10 mL dH_2O, boil at 100°C for 10 min

- 20 × sodium borate buffer

8 g NaOH, 47 g boric acid, 1 000 mL dH_2O, autoclave

- CTAB

4.1% NaCl, 10% N-cetyl-N, N, N-trimethyl ammonium bromide dissolved in dH_2O, filter sterilized

- 10 × TE Buffer

1 mL of 1 M Tris-HCl (pH 10-11), 2 mL 0.5 M EDTA, 100 mL dH_2O, autoclave

- 10 mg/mL Lysozyme

100 mg lysozyme, 10 mL dH_2O

- 10% SDS

10 g SDS, 100 mL dH_2O, autoclave

- 10 mg/mL Proteinase K

100 mg Proteinase K, 10 mL dH_2O

- Chloroform: isoamyl alcohol (24:1)

24 mL chloroform, 1 mL isoamyl alcohol

- 5 M NaCl

11.688 g NaCl, 40 mL dH_2O, filter sterilize

- 3 M Sodium acetate

24.61 g sodium acetate, 100 mL dH_2O, filter sterilize

- 40 mg/mL X-gal

400 mg X-gal, 10 mL Dimethylformamide, filter sterilize

- 75% sucrose

75 g sucrose, 100 mL dH_2O, autoclave

- 0.2 M EDTA

7,44 g EDTA, 100 ml dH_2O, autoclave

- 2 M NaOH

23.99 g NaOH, 300 mL dH_2O, filter sterilize

- PBS

Dissolve 1 PBS tablet in 100 mL dH_2O, autoclave

8.2.2. Southern blotting solutions

- Denaturation solution

0.5 M NaOH, 1.5 M NaCl, dissolve in dH_2O

- Depurination solution

0.2 M HCl diluted in dH_2O

- 5 × TBE buffer

27 g Tris Base, 13,75 g boric acid, make up to 500 mL dH_2O, autoclave

- 20 × saline-sodium citrate (SSC) buffer

3 M NaCl, 0.3 M trisodium citrate, dissolve in dH_2O, autoclave

- 2 × SSC and 0.1% SDS solution

10 mL 20 × SSC buffer, 1 mL 10% SDS, 89 mL dH_2O

- 0.5 × SSC and 0.1% SDS solution

2.5 mL 20 × SSC buffer, 1 mL 10% SDS, 96.5 mL dH_2O

- 1 M maleic acid buffer (pH 7.5)

116.1 g maleic acid powder, 87.66 g NaCl, 1 000 mL dH_2O, autoclave

- Wash buffer

0.1 M maleic acid buffer, 0.3% Tween 20

- 1 × blocking solution

45 mL of 0.1 M maleic acid buffer, 5 mL of 10 × blocking solution (Merck)

- Antibody solution

20 mL blocking solution, 2 µL antibody solution (Merck)

8.2.3. Antibiotic solvents

Table B1. Solvents utilized to create antibiotics

Antibiotic	**Solvent**
Kanamycin	dH_2O
Ampicillin	dH_2O
Hygromycin	PBS
Ciprofloxacin	1% HCl
Streptomycin	dH_2O
Ofloxacin	1 M NaOH
Vancomycin	dH_2O
Ethambutol	dH_2O
Ethionamide	DMSO
Clofazimine	Dimethylformamide
Amikacin	dH_2O
Levofloxacin	dH_2O

8.3. Appendix C: Molecular weight markers

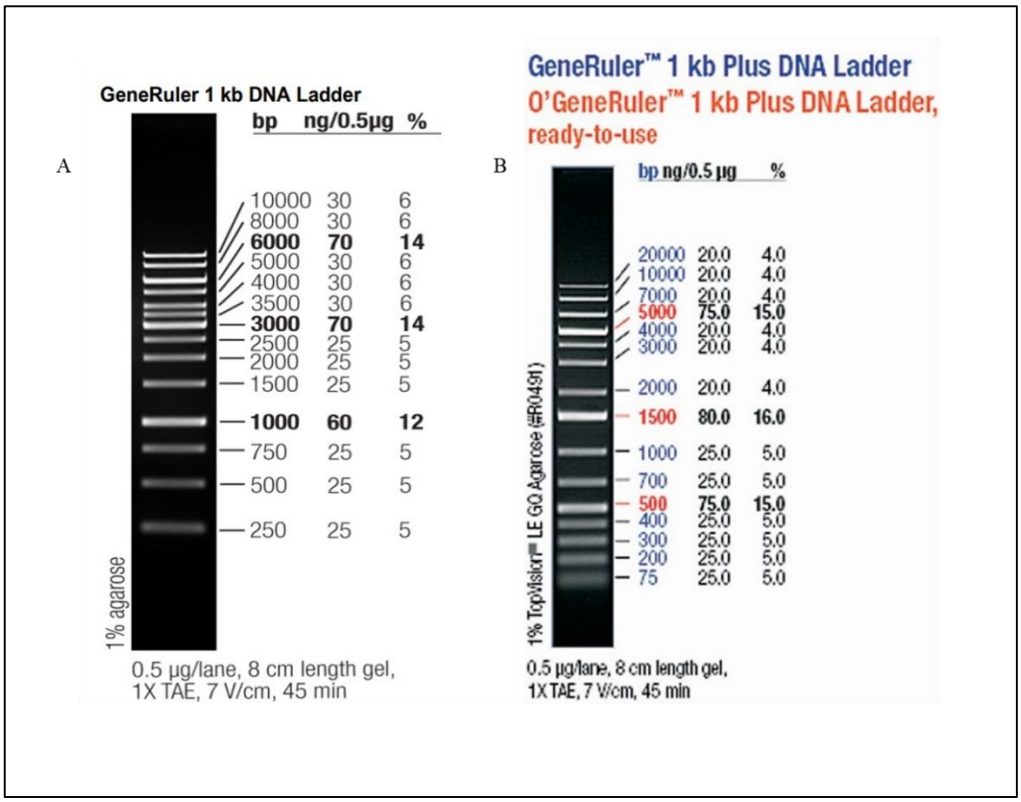

Figure C1. Molecular weight markers **(A)** GeneRuler 1 kb **(B)** GeneRuler 1 kb plus.

8.4. Appendix D: Ethics approval

UNIVERSITY OF KWAZULU-NATAL
INYUVESI YAKWAZULU-NATALI

08 August 2022

Miss Kiara Ramchunder (218005852)
School of Lab Med & Medical Sc
Medical School

Dear Miss Ramchunder,

Protocol reference number: BREC/00004387/2022
Project title: Characterizing an essential Mycobacterium tuberculosis zinc metalloprotease Rv2017 as a potential novel target for drug discovery.
Degree: MMedSc

EXPEDITED APPLICATION: APPROVAL LETTER

A sub-committee of the Biomedical Research Ethics Committee has considered and noted your application.

The conditions have been met and the study is given full ethics approval and may begin as from 08 August 2022. Please ensure that any outstanding site permissions are obtained and forwarded to BREC for approval before commencing research at a site.

This approval is valid for one year from 08 August 2022. To ensure uninterrupted approval of this study beyond the approval expiry date, an application for recertification must be submitted to BREC on the appropriate BREC form 2-3 months before the expiry date.

Any amendments to this study, unless urgently required to ensure safety of participants, must be approved by BREC prior to implementation.

Your acceptance of this approval denotes your compliance with South African National Research Ethics Guidelines (2015), South African National Good Clinical Practice Guidelines (2020) (if applicable) and with UKZN BREC ethics requirements as contained in the UKZN BREC Terms of Reference and Standard Operating Procedures, all available at http://research.ukzn.ac.za/Research-Ethics/Biomedical-Research-Ethics.aspx.

BREC is registered with the South African National Health Research Ethics Council (REC-290408-009). BREC has US Office for Human Research Protections (OHRP) Federal-wide Assurance (FWA 678).

The sub-committee's decision will be noted by a full Committee at its next meeting taking place on 13 September 2022.

Yours sincerely,

[redacted]

Prof D Wassenaar
Chair: Biomedical Research Ethics Committee

Biomedical Research Ethics Committee
Chair: Professor D R Wassenaar
UKZN Research Ethics Office Westville Campus, Govan Mbeki Building
Postal Address: Private Bag X54001, Durban 4000
Email: BREC@ukzn.ac.za
Website: http://research.ukzn.ac.za/Research-Ethics/Biomedical-Research-Ethics.aspx

8.5. Appendix E: Turnitin report

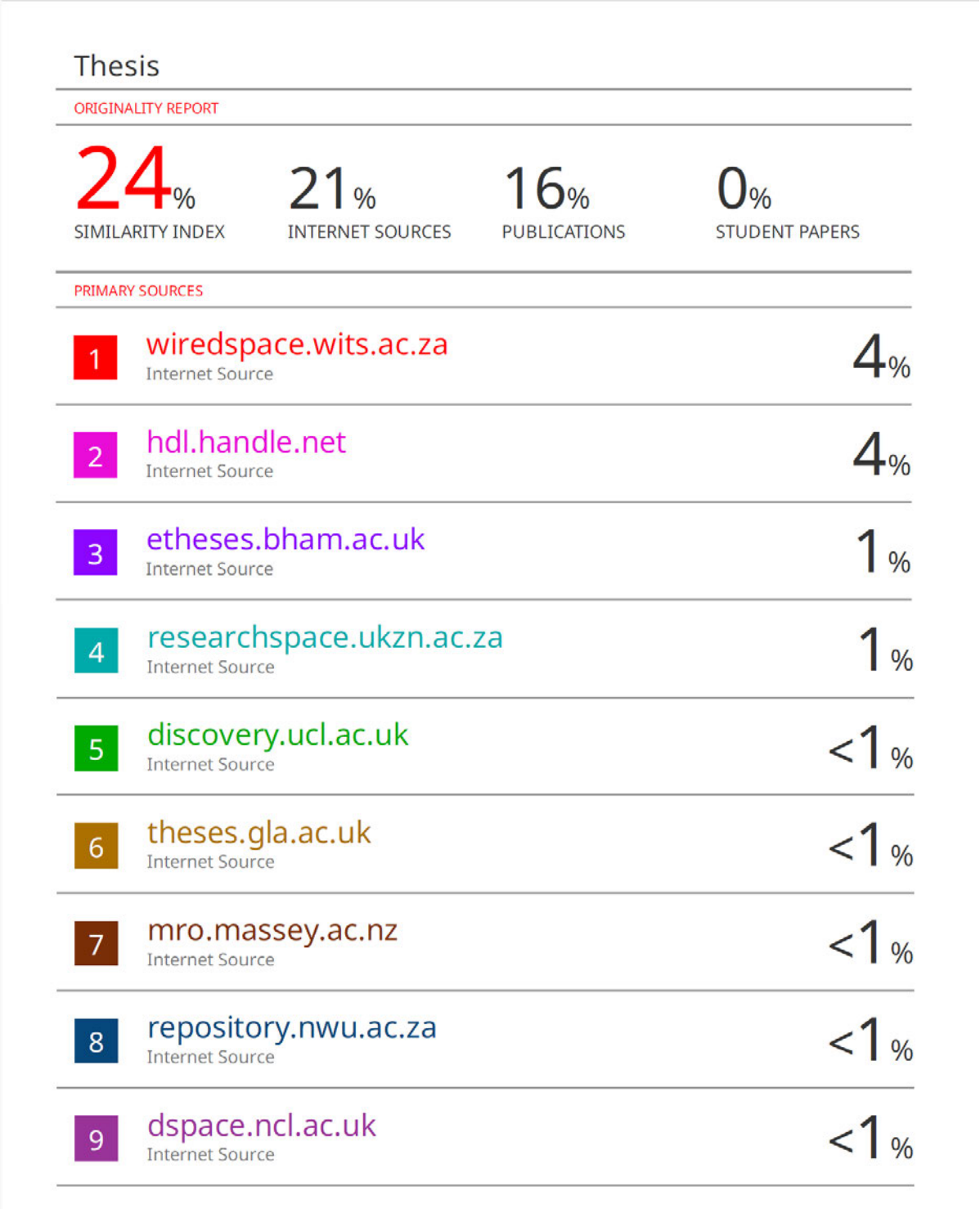

Thesis

ORIGINALITY REPORT

24%	21%	16%	0%
SIMILARITY INDEX	INTERNET SOURCES	PUBLICATIONS	STUDENT PAPERS

PRIMARY SOURCES

1	wiredspace.wits.ac.za Internet Source	4%
2	hdl.handle.net Internet Source	4%
3	etheses.bham.ac.uk Internet Source	1%
4	researchspace.ukzn.ac.za Internet Source	1%
5	discovery.ucl.ac.uk Internet Source	<1%
6	theses.gla.ac.uk Internet Source	<1%
7	mro.massey.ac.nz Internet Source	<1%
8	repository.nwu.ac.za Internet Source	<1%
9	dspace.ncl.ac.uk Internet Source	<1%